SELF–ASSOCIATION AND CHAPERON ACTIVITY OF THE SMALL HEAT SHOCK PROTEIN 27

by

BARBARA LELJ GAROLLA DI BARD
Laurea in Chimica, Univerista' degli Studi di Napoli "Federico II", 2001

A THESIS SUBMITTED IN PARTIAL FULFILLMENT OF THE REQUIREMENTS FOR THE DEGREE OF

DOCTOR OF PHILOSOPHY

in

THE FACULTY OF GRADUATE STUDIES

(BIOCHEMISTRY AND MOLECULAR BIOLOGY)

THE UNIVERISTY OF BRITISH COLUMBIA

August 2007

ABSTRACT

Human Hsp27 is a member of the small heat shock protein family that is over–expressed during cellular stress and that is involved in biological functions ranging from inhibition of apoptosis to regulation of cellular glutathione levels. In addition, Hsp27 is an ATP–independent molecular chaperon that binds to unfolding peptides and inhibits their precipitation. Roles for Hsp27 in several human diseases have also been proposed. For example, the expression of Hsp27 by several human tumors has been noted as a potential diagnostic feature or a therapeutic target. Increasing evidence indicates that the biological functions of Hsp27 are linked to the reversible self–association of the protein to form large oligomers in a process that is at least in part regulated by reversible phosphorylation of three Ser residues. The three–dimensional structure of Hsp27 is not available, and relatively few rigorous physical studies of the protein have been reported.

In the present study, analytical ultracentrifugation has been used to define self–association of Hsp27 and selected variants as a function of protein concentration, pH, temperature, and ionic strength to evaluate the role of structural domains believed to be functionally significant. These results are correlated with the chaperon activity, as determined by monitoring the inhibition of insulin unfolding, and with the kinetics of subunit exchange, monitored by fluorescence resonance energy transfer.

The results establish that wild–type Hsp27 forms a distribution of oligomers that ranges from dimers to at least 32–mers and that oligomerization is highly regulated by temperature but not ionic strength or pH. Moreover, the oligomeric size of Hsp27 increases with increased temperature in a manner that correlates well with increased chaperon activity and rate of subunit exchange. Comparison of results from all three types of

experiments obtained for the wild–type protein to those obtained with Hsp27 variants has led to the development of a model for Hsp27 self–association and chaperon activity.

TABLE OF CONTENTS

LIST OF TABLES

LIST OF FIGURES

LIST OF ABBREVIATIONS

AIAS	4-aceto-4'-((iodoacetyl)amino) stilbene-2,2'-disulfonate
AUC	Analytical ultracentrifugation
Cryo–EM	Cryo electron microscopy
CD	Circular dichroism
FRET	Fluorescence Resonance Energy Transfer
Hsp27	Heat shock protein 27
Ins	Insulin
IPTG	(Isopropyl β–D–1–thiogalactopyranoside)
LYI	Luciferase yellow iodoacetamide
SDS–PAGE	Sodium dodecyl sulfate polyacrylamide gel Electrophoresis
sHsp	Small heat shock protein
TRIS	Tris(hydroxymethyl)aminomethane

ACKNOWLEDGEMENTS

I will never be able to fully acknowledge all the people that have been part of my life and have influenced my work during the years spent working on this thesis, this is just an attempt.

My greatest appreciation goes to my supervisor Prof. Grant Mauk for his support, directions and teachings. His way of thinking, precision and excitement for discovery have perfused the way I do science and will stay with me for ever. A special thank to my committee members Prof. Charles Haynes and Prof. Ed Pryzdial, who have been present for every step of this work and have challenged me in a very constructive way. I would like to thank with deep gratitude Dr. Peter Schuck at the National Institute of Health, Bethesda, for having me taught almost all I know about the data analysis for analytical ultracentrifugation and for being always available and willing to help with my many questions despite the distance. Moreover, I would have been lost without the support of all the AUC community, who is always fighting to get the best answer to any question published on the mailing list at the fastest possible speed.

There are a number of other people that have made this work possible, Dr. Louise Creagh who helped my with the analytical ultracentrifugation, current and past members of the Mauk lab and in particular, Dr. Sung-Hye Hong for useful advice regarding fluorescence experiments and Dr. Fred Rosell for help with the numerous instruments in our lab. Prof. Natalie Srynadka for help with crystallography; Prof. Lawrence McIntosh and Dr. Mark Okon for help with the NMR, Prof. Michel Roberge and Lianne for the attempted IP experiments and Dunja in Prof. Les Burtnick lab for setting up screens with the Hsp27–actin complex.

The University of British Columbia and the Faculty of Medicine are acknowledged for provision of Studentships, in particular for the University Graduate Fellowship, the Cordula and Günter Paetzold Fellowship and the Roman M. Babicki Fellowship for Medical Research.

I need to thank my fellow students and in particular (and strictly in alphabetical order) I would like to acknowledge Chantal Levesque, Kaley Wilson, Lianne McHardy, Mike Krisinger

and Sonya Cressman for their friendship and constant support, I am sure you will always be part of my life no matter where we will all end up, this Ph.D. experience would not have been nearly has much fun and constructive without you. My life in Canada and my enjoyment of research would have not been the same without the support of the UBC Women's Rugby team, my coach and all the girls who have made this past 5 years unforgettable, in particular I would like to thank Rosie and Merns for also having shared my apartment and many adventures! A special thank goes to Paul and Margaret–Ann for being my Canadian family. My greatest and deepest appreciation is for my invaluable family, in particular to my parents who always give me the freedom to do what I believe it is right for me. They have supported all my life choices and have always been present when I needed them most. This work is dedicated to you.

To my family who is far away but never far from my heart:

My parents, Francesco and Maria Laura

My brother, Andrea

My grandparents, nonna Baby, nonna Giuliana, nonno Goffredo and nonno Leo.

1. INTRODUCTION

1.1 Heat shock proteins

Stress or heat shock proteins (Hsps) were discovered in 1962 as a class of conserved proteins the expression of which is induced by various types of stress (Ritossa, 1962), Hsps are ubiquitous and have been identified in archaea, bacteria, and eukarya (Caspers *et al.*, 1995).

Five major classes of Hsps have been identified that differ in size, structure and function: Hsp100, Hsp90, Hsp70, Hsp60 and the small heat shock proteins, sHsps. One of the main biological roles of the heat shock proteins is to act as chaperones to stabilize partially unfolded proteins, but it has also been shown that Hsps have several additional functions that account for their cytoprotective effects. Each family is comprised of members that are expressed either constitutively or transcriptional regulated and that are targeted to different subcellular compartments. For instance, although Hsp90 is abundantly expressed constitutively in cells (Bedard & Brandhorst, 1986; Darmon & Paulin, 1985a; Darmon & Paulin, 1985b; Farrelly & Finkelstein, 1984), Hsp70 and Hsp27 are highly induced by various stresses such as heat, oxidative stress or anticancer drugs (Bienz & Pelham, 1982; Corces *et al.*, 1981; Pelham & Bienz, 1982). Even though the heat shock promoter regions of Hsp27 and Hsp70 seem to be organized quite differently (Hoffman & Corces, 1986), in normal non–stressed cells, these proteins are either not expressed or expressed at low levels. On the other hand in a wide range of tumors, in particular tissues and during specific phases of development and differentiation, the basal level of Hsp27 and/or Hsp70 is unusually high (Pauli *et al.*, 1990). Once induced, these Hsps, can modulate the execution of the apoptotic signaling pathway directly.

1.2 Small Heat Shock Proteins

Small heat shock proteins are one class of stress proteins and are characterized by a low monomeric molecular weight, a conserved domain near the C–terminus – the α–crystallin domain – and ATP–independent chaperon activity.

Ten human small heat shock proteins are known: Hsp27 (HspB1; also called Hsp25 in rodents and birds), myotonic dystrophy protein kinase–binding protein (MKBP/HspB2), HspB3, αA–crystallin (HspB4), αB–crystallin (HspB5), Hsp20 (p20, HspB6), cardiovascular heat shock protein (cvHsp/HspB7), Hsp22 (HspB8), HspB9 and most recently the sperm outer dense fiber protein (ODFP/HspB10) (Arrigo & Welch, 1987; Boelens *et al.*, 1998; Fontaine *et al.*, 2003; Ingolia & Craig, 1982; Iwaki *et al.*, 1997; Kappe *et al.*, 2001; Kato *et al.*, 1994a; Klemenz *et al.*, 1991; Krief *et al.*, 1999). The best studied and first known (Mörner, 1894) are the two α–crystallins with the polypeptides αA– and αB–crystallin. While the first is mainly expressed in the ocular lens, αB–crystallin is expressed in significant amounts in cardiac, skeletal, and smooth muscle and in varying amount in a number of other tissues such as kidney and brain (Bhat & Nagineni, 1989). Interestingly, it was not until 2000 that αB–crystallin was recognized to belong to the small heat shock protein family (MacRae, 2000). In fact, the first protein that was described as being a heat inducible small heat shock protein was Hsp27 (HspB1). Induction of over–production of Hsp27 in response to hyperthermia was first described in *Drosophila* in the 70s ((Peterson *et al.*, 1979), for a review (Ashburner & Bonner, 1979)), in 1978 in chicken embryos (Kelley & Schlesinger, 1978) and in 1982 in HeLa cells (Hickey & Weber, 1982). Even though it has a molecular weight of 22,651 Da, Hsp27 was

name as such because it migrates with an apparent molecular weight of 27 kDa during SDS–PAGE.

Small heat shock proteins exhibit molecular weights of 9–40 kDa and share a number of structural features. In addition to a relatively low monomeric molecular weight, most sHsps form large oligomeric complexes in a process that is regulated by phosphorylation of key seryl residues. The sHsp monomers are comprised of several domains. The most conserved domain is the α–crystallin domain that occurs near the C–terminal region, and is named after the lens protein α–crystallin (de Jong *et al.*, 1988). This consists of a β–sandwich comprised of two β–sheets, each formed by 3 β–strands in a fold similar to that of immunoglobulins. A somewhat less conserved domain that occurs near the N–terminus is referred to as the WDPF domain owing to the presence of this sequence of amino acid residues (Lambert *et al.*, 1999). The WDPF domain is followed by a short sequence with the reasonably conserved amino acids: PSRLFDQXFGEXLL (Sugiyama *et al.*, 2000). The variability in the monomeric size of sHsps results primarily from the highly variable N–terminal sequence and from the length of the C–terminal tail, which is highly flexible (Carver *et al.*, 1995). The only conserved sequence near the C–terminus is an IXI motif characterized by two isoleucines with any amino acids in between. In all cases X represents any amino acid.

The focus of this dissertation will be the human small Hsp27. The amino acid sequence and the conserved domains of this protein are shown in Figure 1.1

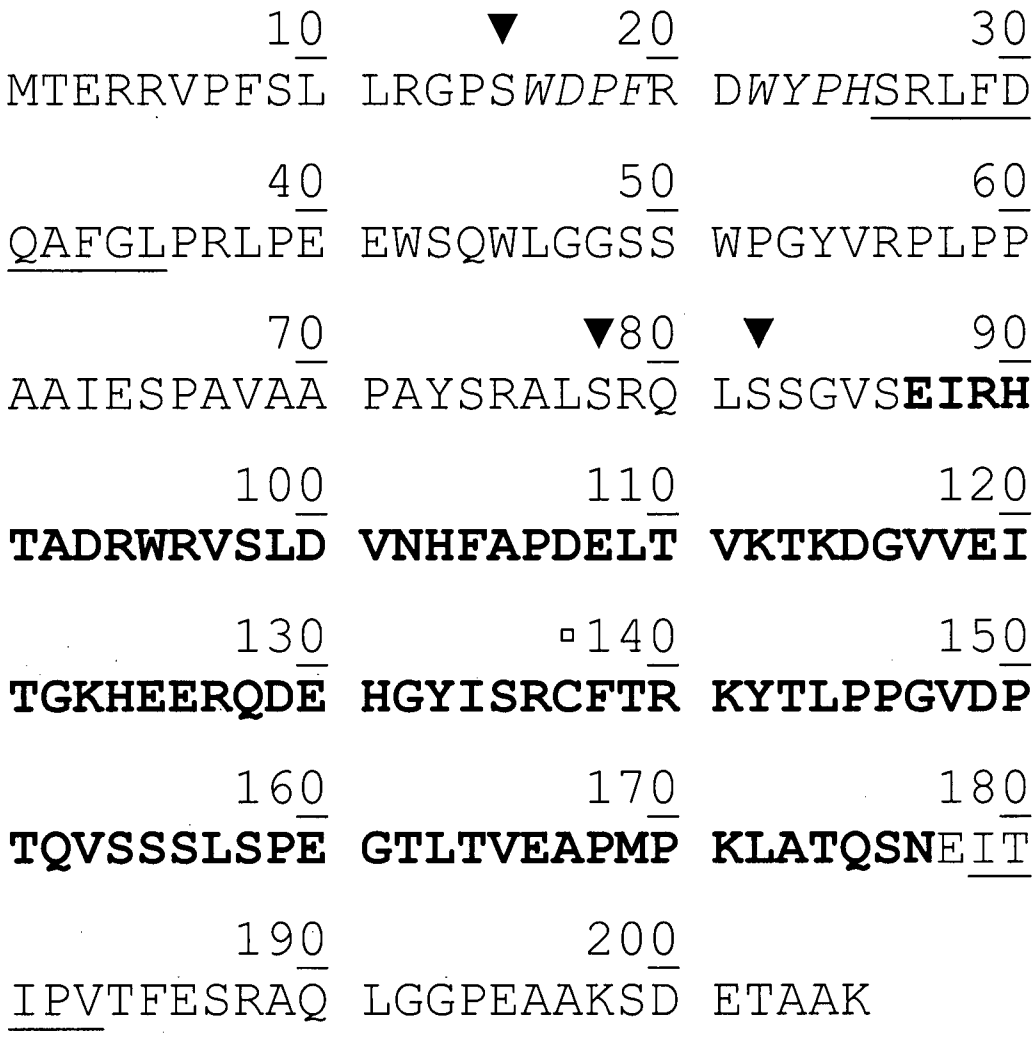

Figure 1.1. Amino acid sequence of the small Hsp27. Italics denotes the WDPF conserved sequences. The two conserved sequences near the N– and C–terminal tails are underlined. Bold residues correspond to the α–crystallin domain. Arrowheads indicate the seryl residues that are phosphorylated *in vivo*, and the open square indicates the position of the only cysteinyl residue.

1.2.1 Structures and Activity

At present, detailed structural characterization of sHsps has been limited to crystallographic structure determination of two, non–mammalian sHsps. Specifically, MjHsp16.5 from the thermophile *Methanococcus jannaschii* crystallizes as a 24–mer (Kim *et al.*, 1998), and wHsp16.9 from wheat forms a 12–mer (van Montfort *et al.*, 2001). Both of these proteins have much shorter N– and C–terminal regions than does Hsp27. Although both MjHsp16.5 and wHsp16.9 have chaperon activity, neither exhibits all of the cytoprotective functions attributed to Hsp27.

MjHsp16.5 crystallized as an apparently hollow sphere with outer diameter of ~120 Å and inner diameter of ~65 Å (Figure 1.2A). No electron density was observed in the cavity of the sphere, but the first 32 amino acids at the N–terminus of the protein were not visible, and the most N–terminal residue that is observed points towards the inside of the sphere. It is, therefore, plausible that the inside of the sphere would be at least partially occupied by the missing N–terminal sequences. Each of the 24 subunits is composed of nine β–strands in two sheets, two short 3_{10}–helices, and one short β–strand. The two β–sheets are packed as parallel layers with one of the β–strands (β6) in one β–sheet coming from a neighboring subunit as shown in Figure 1.2B (Kim *et al.*, 1998).

The other crystallized small Hsp, wHsp16.9, assembles as a dodecamer consisting of two disks, each comprising six α–crystallin domains organized in a trimer of dimers as shown in Figure 1.3 (van Montfort *et al.*, 2001).

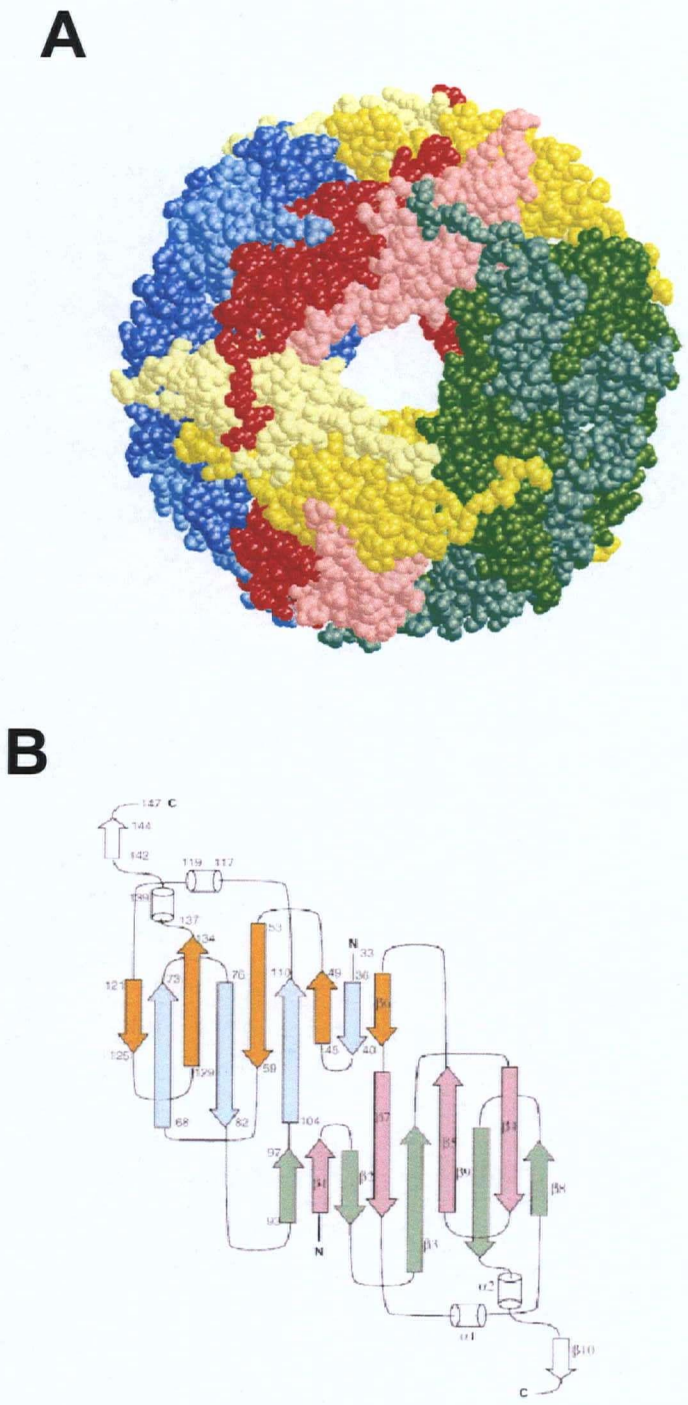

Figure 1.2. Crystal structure of the small Hsp 16.5 from *Methanococcus jannaschii.* **A**. the 24–mer structure. **B**. Topology of the secondary structure of a MjHsp16.5 dimer (modified from (Kim *et al.*, 1998))

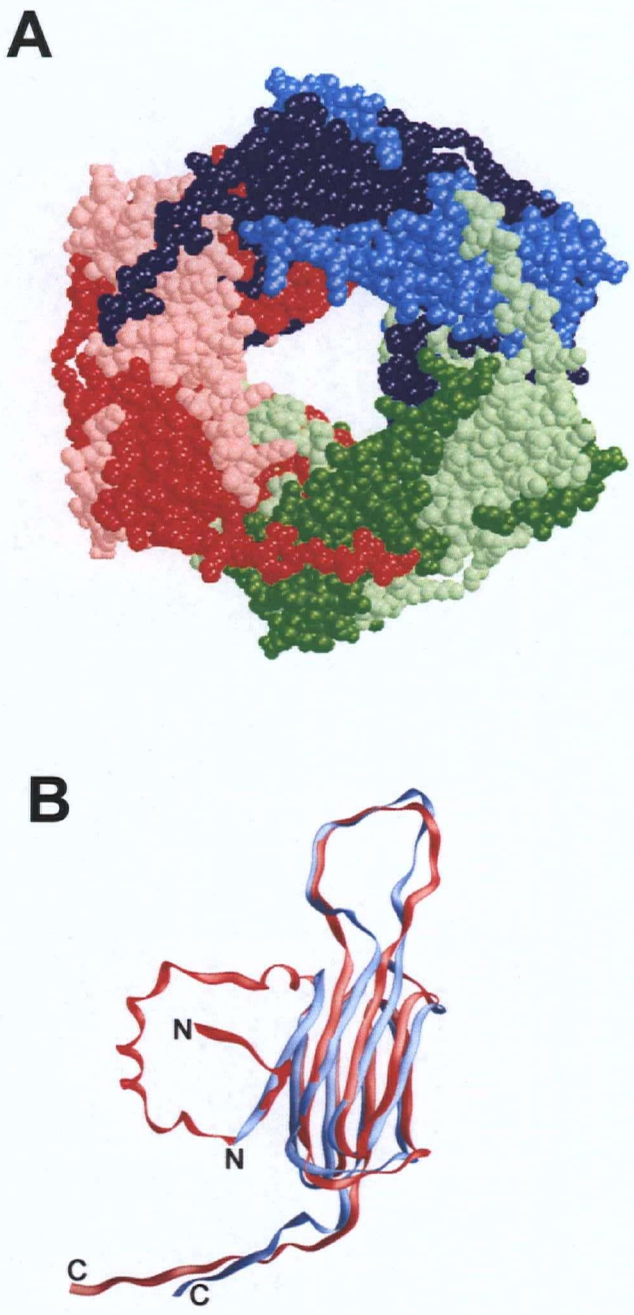

Figure 1.3. Crystal structure of wheat Hsp16.9. **A.** 12–mer assembly from wheat Hsp 16.9 **B**. Superposition of the monomer of M. jannaschi Hsp16.5 (blue) and wheat Hsp16.9 (red). Residues close to the N–terminus of Hsp16.9 coincide with the β1 strand of Hsp16.5 but run in the opposite direction (modified from (van Montfort *et al.*, 2001)).

In contrast to the Hsp16.5 structure, only one N–terminal sequence per dimer pair is disordered while the other forms helices connected by a coil. Moreover, in the α–crystallin domain, the two β–sheets are in an antiparallel orientation. Similarly to the thermophilic protein, the β strand 6 of the wheat sHsp forms inter–molecular interactions with a neighboring subunit. A superposition of the monomers of Hsp16.5 and Hsp16.9 is shown in Figure 1.3B.

Based on theses two crystal structures, Theriault *et al.* proposed a model for the folding of hamster Hsp27 (Theriault *et al.*, 2004). The sequence alignment of human and hamster Hsp27 and wheat Hsp16.9 on which the model is based is shown in Figure 1.4, while the model is presented in Figure 1.5. All software used to predict Hsp27 secondary structure, JNET (Cuff & Barton, 2000), PROFsec and PHDsec (Rost & Sander, 1993) indicate that the α–crystallin domain of Hsp27 is composed primarily of β–strands. Moreover, the program Superfamily (Gough *et al.*, 2001) used for sequence alignment indicates that the α–crystallin domain of Hsp27 aligns well with the known secondary structure of Hsp16.9. The position of the β–strand in Hsp27 is also predicted to match the equivalent structural element of the sHsp from *Methanococcus jannaschii* quite well. However, Hsp27 as well as the Hsp16.9 wheat protein appear to lack the β1 strand present in Hsp16.5. The NH_2–terminal SXXFDPF motif of Hsp16.9, which meditates essential inter– and intramolecular contacts in the oligomeric assembly, thus mimicking the function of the β1–strand of Hsp16.5, aligns with a high degree of homology with the sequences around the Trp^{16}–Glu–Pro–Phe motif of Hsp27.

Two major differences between the model of Hsp27 and the experimentally determined structure of Hsp16.9 are noteworthy. First, the loop between the β5 and β7

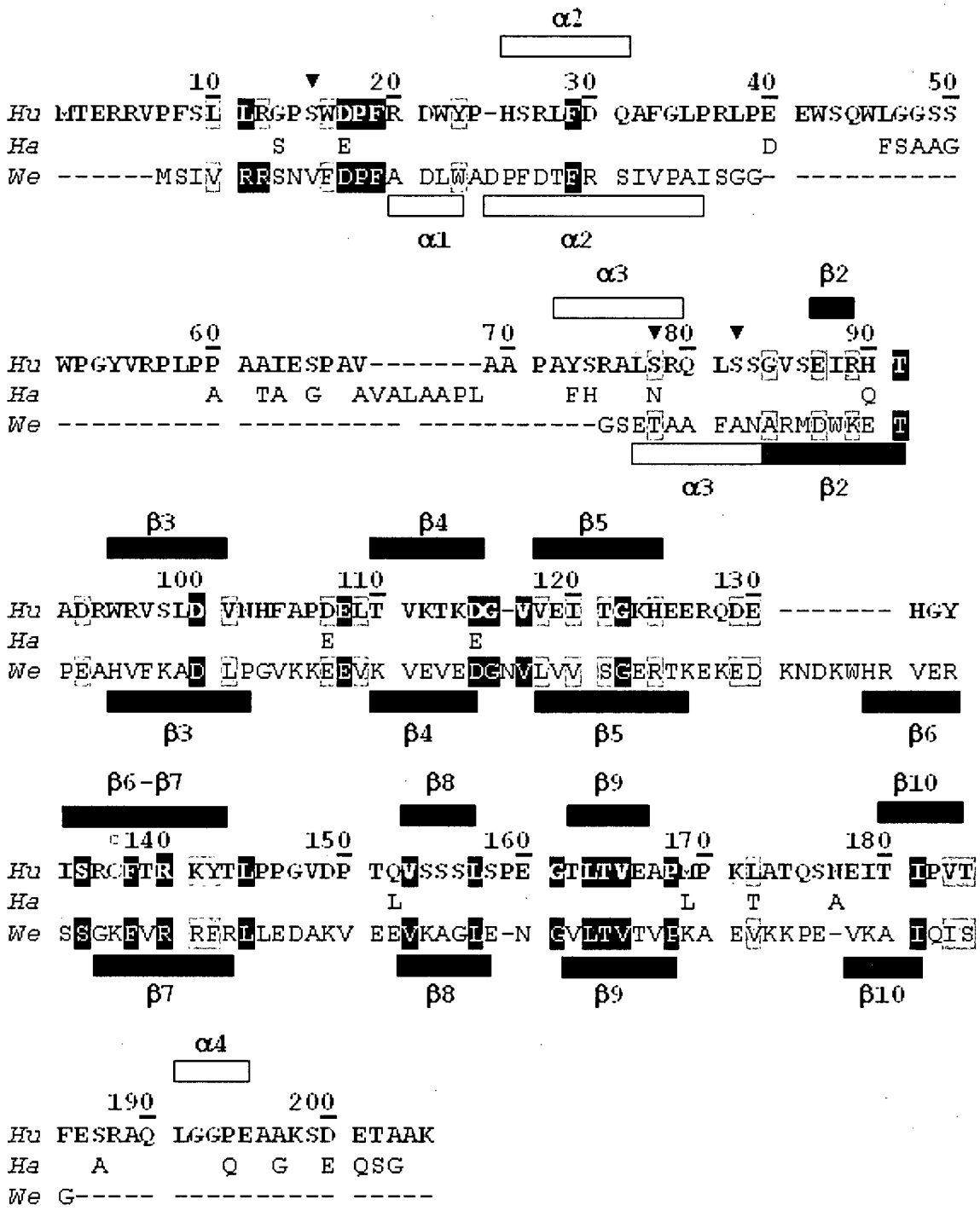

Figure 1.4. Sequence alignment of human (Hu) and hamster (Hm) Hsp27, and wheat (We) Hsp16.5. β–strands (black bars) and α–helices (white bars) are indicated at the top for human Hsp27 and bottom for wheat Hsp16.5. Residues that are homologous (grey highlight) or identical (black highlight) between the sequences are indicated. Residue numbers are kept for the human Hsp27. Only the residues that differ between the human and the hamster protein are shown (modified from (Theriault et al., 2004)).

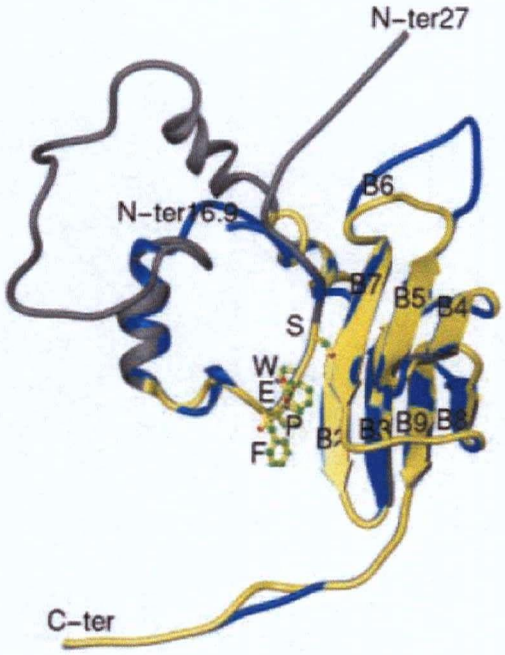

Figure 1.5. Model of hamster Hsp27 (yellow and grey) and wheat Hsp16.5 (blue). Grey areas represent regions of Hsp27 that have no correspondence to the wheat protein (modified from (Theriault *et al.*, 2004)).

strands is 7 residues longer in Hsp16.9. Second, the connecting sequence between the NH_2– terminal and α–crystallin region is 42 residues longer in Hsp27. The model predicts that as in Hsp16.9, the strands (β2–β8) of the crystallin domain of Hsp27 are organized as sandwich of two antiparallel β–sheets formed by strands β2, β3, β9 and β8 on one side of the sandwich and β7, β5 and β4 on the other.

The model also predicts that the sequence Trp^{16}–Glu–Pro–Phe plays an important structural role by participating in intramolecular interactions and patching a hydrophobic pocket formed by residues Ile^{96}, Gln^{98}, Tyr^{150}, Thr^{151} and Pro^{153} at the interface of strands β2 and β7 in the hamster sequence that corresponds to residues Ile^{88}, His^{90}, Tyr^{142}, Thr^{143} and Pro^{145} in the human protein. Moreover, Hsp27 lacks the β–strand 6 which is involved in dimer association in the wheat and the thermophilic proteins.

The structure of Tsp36 from a flatworm is the first protein structure of a small heat shock protein from a metazoan. Interestingly, the monomer of Tsp36 has two α–crystallin domains, each preceded by a short N–terminal region (Stamler *et al.*, 2005). The crystallin domains are separated by a linker region, and the protein has a long N–terminal tail. A schematic comparison of Tsp36 with the other two crystallized small heat shock proteins is provided in Figure 1.6.

Tsp36 is a dimeric protein that can form tetramers under oxidizing conditions (Kappe *et al.*, 2004). The dimerization interface is very different from that observed for the non–metazoan proteins. In fact, Tsp36 lacks the long β5–β7 loop and β6 and a conserved proline residue at the end of β3 in both of its α–crystallin domains. These features are involved in maintaining the dimeric strand by strand exchange and ring stacking in the non–metazoan sHsp, respectively. On the other hand, Tsp36 has a conserved phenylalanine

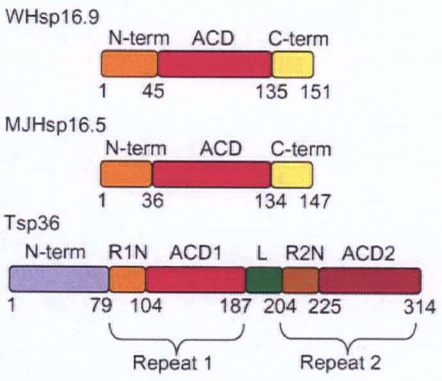

Figure 1.6 Domain boundaries for wheat Hsp16.9, thermophilic Hsp16.5 and flatworm Tsp36. ACD is α–crystallin domain, R1N and R2N are the N–terminal regions preceding the α–crystallin domain. Modified from (Stamler *et al.*, 2005).

residue between β3 and β4 that displaces the shorter β5–β7 loop from the strand exchanged position.

Moreover, Tsp36 has only one cysteine residue in the β5–β7 loop that is probably involved in the formation of disulfide bonds to form tetramers under oxidizing conditions. Hsp27 is also a metazoan protein, and its α–crystallin domain has the same features as those of Tsp36: a shorter β5–β7 loop with one cysteine in position 137 and no proline but with the conserved phenylalanine residue at the end of β3.

The N–terminus of Tsp36 is characterized by a series of helices with sharp turns marked by proline residues. The main interaction between dimers occurs through this region, where α–helices of one monomer cross over the dimeric interface. Moreover, residues Ile^3 and Pro^5 bury hydrophobic residues at the edges of the first α–crystallin domain in a manner similar to the one observed for the IXI region of the C–terminus of Hsp16.5 and Hsp16.9. In fact, Tsp36 lacks the C–terminal flexible tail and the conserved

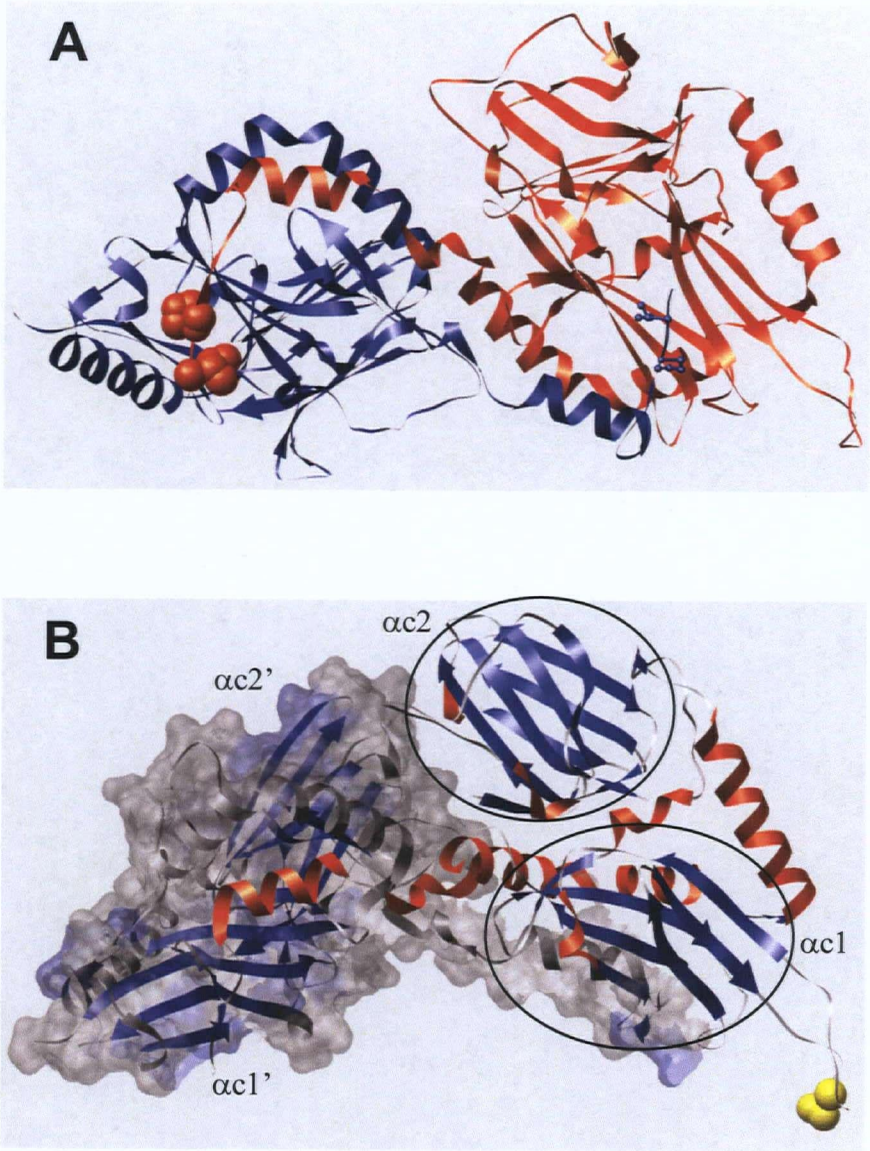

Figure 1.7 Structure of Tsp36. **A.** Each monomer is highlighted in a different color; Ile^3 and Pro^5 are represented as ball & stick in one monomer and as space–filling in the other. **B**. The strands and helices of monomer one are highlighted as well as the only cysteine residue in the β5–β7 loop (space–filling representation), the other monomer is with surface representation. The four α–crystallin domains are indicated for the first (αc1, αc2) and second monomer (αc1', αc2'). Structure coordinates have been obtained from the protein data bank (2bol) and figures were prepared with the program CHIMERA (Pettersen *et al.*, 2004)

IXI sequence. A representation of the dimer showing the special arrangement of each monomer is presented in Figure 1.7A–B.

1.2.2 Thermal dependence of oligomerization and activity

One interesting aspect of heat shock protein self–association is the effect of temperature. Oligomerization behavior varies greatly from protein to protein, and this variation extends to the effect of temperature. Gel filtration studies show that the Hsp16.9 dodecamer undergoes a reversible temperature–dependent dissociation into smaller species by increasing the temperature from 25 to 40 °C (van Montfort *et al.*, 2001). Similarly yeast Hsp 26, which normally forms large and highly symmetrical assembly of 24 subunits, dissociates at temperature above 35 °C and, above 43 °C, is present only in a dimeric form (Haslbeck *et al.*, 1999).

At one time it was thought that dissociation into dimers seemed to be required for chaperon activity of Hsp26, because dimers were initially reported to be the form of the protein that binds to the substrate (Haslbeck *et al.*, 1999; Stromer *et al.*, 2004b). Upon binding of its substrate in a 2:1 ratio (Hsp26:substrate), Hsp26 re–assembles into a chaperon–substrate complex that is not based on the original shell–like structure indicated by electron microscopy (Haslbeck *et al.*, 1999). A variant of Hsp26 lacking the first 95 residues (ΔN–Hsp26) forms only a dimeric structure that lacks chaperon activity, indicating that the regions important for both assembly of the 24–mer and interaction with non–native proteins reside in the N–terminal domain (Stromer *et al.*, 2004b). However, recently, an Hsp26 variant with unaffected chaperon activity was reported. This variant

(Hsp26 S4C) is locked into a large oligomer form by a disulfide bond at the N–terminus (Franzmann *et al.*, 2005), implying oligomerization is not the only regulator of function.

Hsp16.3 from *Mycobacterium tuberculosis* exhibits a significantly increased chaperon activity after heating to >60 °C (Fu *et al.*, 2003). The oligomeric size of the heated protein, however, is the same as that of the untreated protein when examined at 4 °C by non–denaturing pore–gradient gel electrophoresis or at 25 °C by size exclusion chromatography. This increased chaperon activity has been attributed to an increased rate of subunit exchange and not to a change in quaternary structure (Fu *et al.*, 2003; Hartl & Hayer-Hartl, 2002).

Gel filtration analysis of murine Hsp25 shows that this protein occurs as a hexadecamer in equilibrium with smaller species and that by increasing the temperature above 65 °C, large oligomers called "heat shock granules" form that are visible by electron microscopy. Purification of these granules revealed an activity similar to that of the untreated protein (Ehrnsperger *et al.*, 1999).

The sHsp14 from *Sulfolobus tododaii* exists as a stable 24–mer, but subunit exchange between the oligomers was observed at elevated temperature. This result correlates well with the observation that the chaperon activity of this protein also increases at elevated temperatures (Usui *et al.*, 2004a; Usui *et al.*, 2004b). Interestingly an N–terminal deletion variant of this protein lacking the first 21 amino acids exhibits unaltered oligomeric structure but exhibits reduced subunit exchange and chaperon activity at high temperature (Usui *et al.*, 2004a).

The sHsp from *Escherichia coli*, IbpB (inclusion–body binding protein B), exhibits enhanced chaperon activity at high temperatures with no activity observed below 30 °C

and maximum activity between 45 and 60 °C. Moreover, upon an increase from physiologically optimal to heat shock temperatures, IbpB dissociates. Interestingly, while the quaternary structure of this protein changes, very minor changes are observed in the β–sheet dominated secondary structure as detected by circular dichroism. Formation of the polydisperse oligomers depends on both of the highly flexible N– and C–termini, with the dimeric forms appearing to be the basic structural unit of such polydisperse oligomers (Jiao *et al.*, 2005). In fact, deletion of the first and last 11 amino acids leads to variants that are inactive and mainly dimeric.

The rhizobial bacterium *Bradyrhizobium japonicum* has two classes of sHsps. Class A consists of proteins that show similarity to *E. coli* IbpB, and class B, whose members show greater similarity to other sHsps from prokaryotes and eukaryotes (Munchbach *et al.*, 1999; Nocker *et al.*, 2001). Members of both classes form large complexes and have chaperon activity *in vivo* (Studer & Narberhaus, 2000). Gel filtration chromatography and electrospray mass spectrometry show that members of both classes, HspH and HspB (class A), and HspF (class B) undergo temperature–induced dissociation (Lentze *et al.*, 2004).

The oligomerization behavior of α–crystallin is controversial in that the protein changes tertiary and quaternary structure with increased temperature, but the nature of these changes is unclear. The chaperon–like activity of α–crystallin increases above 30 °C with two distinctive transitions, one at 30 °C and one above 55 °C. Upon incubation of the protein at 37 °C for 1 or 20 h, the observed sedimentation coefficient decreases from 18 S to 16.2 S to 14 S, indicating a decrease in oligomer size (Raman & Rao, 1997). On the other hand, electron microscopy indicates that the mean diameter of the temperature (37 °C)–modified α–crystallin is within experimental error of that observed for the native

protein (Siezen *et al.*, 1980). Finally, Vanhoudt *et al.* have observed that α–crystallin can be represented by a distribution of expanded particles with a weight average molar mass of 550,000 g/mol and that on decreasing (4 °C) or increasing (up to 50 °C) the temperature, the size distribution shifts to larger particles as observed by light scattering and sedimentation equilibrium experiments (Thomson & Augusteyn, 1983; Vanhoudt *et al.*, 1998).

Hsp33 is unusual in that the reduced protein is monomeric and the oxidized protein is a disulfide–linked dimer (at 25 °C) that forms tetramers or octamers at elevated temperature (Akhtar *et al.*, 2004). The dimeric form of this protein with an exchanged domain has been characterized by X–ray crystallography (Kim *et al.*, 2001; Vijayalakshmi *et al.*, 2001). Notably, however, Hsp33 lacks an α–crystallin domain and, thus, is not a small heat shock protein by definition.

It is evident that chaperon activity and oligomerization are highly conserved features of all the small heat shock proteins. On the other hand, it appears that there is no consistent pattern that describes the oligomerization, the role of conserved domain and the effect of temperature on activity and self–association of these proteins. In fact, similarity in structure and function of these proteins that is implied in the similarity in their name is misleading. Consequently, each member of the sHsp family must be characterized individually.

1.3 Hsp27

1.3.1 Domains and their role in self–association

Some sHsps have well–defined oligomeric structures that appear to be monodisperse while Hsp27 forms large oligomers *in vivo* and exhibits a dynamic distribution of oligomeric forms *in vitro* and *in vivo*. The distribution of Hsp27 oligomers in solution and the roles of the various domains in Hsp27 self–assembly have not been characterized rigorously. Nevertheless, a large body of experimental evidence indicates that Hsp27 oligomerization is controlled by phosphorylation of three key seryl residues at position 15, 78 and 82 which are phosphorylated *in vivo* by MAPKAP kinase2 (Kato *et al.*, 1994b; Stokoe *et al.*, 1992). Hsp27 from human glioma cells has been resolved into two forms by sucrose gradient centrifugation: a large aggregated form and a small dissociated form (Kato *et al.*, 1994b). Moreover, the amount of dissociated form could be increased chemically by addition of compounds like arsenite, which induce phosphorylation and, thereby, indicates that the shift in oligomer formation is controlled by phosphorylation.

Hsp27 oligomerization is a dynamic process, and the WDPF domain is crucial for oligomerization (Bova *et al.*, 2000; Jakob *et al.*, 1993). Bova *et al.* showed that a variant of Hsp27 lacking the first 55 residues does not undergo subunit exchange. Lambert *et al.*, showed that a chimeric protein comprised of amino acids 5–109 of hamster Hsp27 fused to luciferase, a monomeric protein of 62 kDa, formed multimers >350 kDa in NIH–3T3 cells (Lambert *et al.*, 1999) and that oligomer formation can be reversed by treatment with arsenite, again suggesting a phosphorylation–induced dissociation of Hsp27–luciferase multimers into monomers. These observations support the idea that the N–terminal domain

is fundamentally important for oligomerization and that dissociation is phosphorylation–dependent. On the other hand, deletion of the 33 N–terminal residues from the closely related murine Hsp25 has been reported not to affect oligomerization or function of this protein (Guo & Cooper, 2000). Notably, the two variants reported in this latter work were purified and analyzed with a histidine tag at the N–terminus of the protein.

Circular dichroism measured as a function of temperature to obtain thermal denaturation curves of mouse Hsp25 shows that the greatest change in ellipticity (T_m) occurs at ~ 69 °C and that this transition is highly cooperative. Moreover, micro calorimetric measurements of Hsp25 denaturation are best described by assuming a molecular mass of 50 kDa, which corresponds to the dimeric unit, indicating that the basic structural unit of Hsp25 is indeed a dimer (Dudich *et al.*, 1995).

As both α–crystallin and mouse Hsp25 form large oligomers in solution, it was expected that neither would be amenable to analysis by NMR spectroscopy owing to the very long relaxation times that large complexes exhibit. Nevertheless, ^{1}H NMR studies of α–crystallin show that the C–terminus extension is very flexible compared to the bulk of the protein and that it does not adopt a preferred conformation (Carver *et al.*, 1992; Carver & Lindner, 1998). Similarly, two–dimensional ^{1}H NMR spectroscopy of mouse Hsp25 reveals that the 18 C–terminal residues exhibit great flexibility that is essentially independent of the core domain of the protein (Carver *et al.*, 1995).

Several physical methods have been used to study the self–association of Hsp27. For example, analytical ultracentrifugation analysis was used to establish that the mean molecular weight is 730 kDa (Behlke *et al.*, 1991), and pore exclusion limit electrophoresis

was used to demonstrate that Hsp27 forms oligomers of 200–800 kDa (Lavoie *et al.*, 1995). Gel filtration chromatography indicated that Hsp27 forms 24–mers in the non–phosphorylated state, that the phosphorylated protein is primarily tetrameric, and that the triple variant S15D/S78D/S82D behaves as the phosphorylated protein *in vitro* (Rogalla *et al.*, 1999). Electron microscopy has been used to show that, while Hsp16.5 particle images show clear symmetry, none of the α–crystallin or Hsp27 particle images were clearly symmetrical. In particular, the Hsp27 particles were the most variable, with diameters of 90 to 220 Å and no single, dominant diameter (Haley *et al.*, 2000).

1.3.2 Activity

Most sHsps bind to non–native proteins during cellular stress (Jakob & Buchner, 1994; Jakob *et al.*, 1993). Though the mechanism by which sHsps bind to unfolding polypeptides is unknown, there is evidence that each oligomer binds to several non–native proteins, and binding and release of substrates requires neither binding nor hydrolysis of ATP (Jakob *et al.*, 1993). Release of unfolded proteins bound by sHsps alone is, in fact, highly inefficient though both, protein release and refolding, can be achieved with the assistance of larger heat shock proteins (e.g., Hsp70) in an ATP–dependent reaction (Ehrnsperger *et al.*, 1997; Wang & Spector, 2001). A variety of unfolded substrate proteins can be bound by small heat shock proteins, and the size and stoichiometry of the resulting complexes vary with the nature of the unfolded protein (Stromer *et al.*, 2003). In fact, size exclusion chromatography profiles of mixtures of Hsp25 or Hsp26 with unfolding protein, (*i.e.*, citrate synthase, rhodanase, α–glucosidase and insulin) vary substantially with substrates.

Over–expression of Hsp27 in tumor cells increases their tumorigenicity and protects against cell death triggered by a number of stimuli, *e.g.*, hyperthermia, oxidative stress, staurosporine, ligation of the Fas/Apo–1/CD95 death receptor and cytotoxic drugs (Garrido *et al.*, 1998). Hsp27 cytoprotective activity has been attributed to a number of roles that this small Hsp plays during cellular stress. In addition to chaperon activity, Hsp27 interferes with the mechanism of caspase activation, modulates oxidative stress and regulates the cytoskeleton (for recent reviews see (Garrido, 2002; Garrido *et al.*, 2001; Gusev *et al.*, 2002; Schmitt *et al.*, 2007)). Notably, Hsp27 is reported to modulate the intrinsic pathway of apoptosis by interacting with cytosolic cytochrome *c* (Bruey *et al.*, 2000a) or with caspase–3 (Pandey *et al.*, 2000) and to inhibit the extrinsic pathway through interaction with Daxx (Charette *et al.*, 2000). Hsp27 can also enhance the oxidative defense of the cell by increasing cellular glutathione (GSSG) content (Mehlen *et al.*, 1996), and it is recognized as a potent regulator of cytoskeletal dynamics, in particular, actin microfilament polymerization (Benndorf *et al.*, 1994). Hsp27 facilitates activation of the ubiquitin–proteosome pathway by direct interaction with the proteosomal apparatus, demonstrating that Hsp27 can act as a chaperon to target different ubiquitinated substrates to the proteolytic apparatus (Parcellier *et al.*, 2003).

Mutations in the Hsp27 gene have been linked to the formation of human neuromuscular disorders like axonal Charcot–Marie–Tooth disease and distal hereditary motor neuropathy. Five mutations were identified in conserved residues of Hsp27 that seem to be linked to premature axonal degeneration. Four out of five are residues in the α–crystallin domain (Arg^{127}, Ser^{135}, Arg^{136}, Thr^{151}) while the fifth is the conserved Pro^{182} near the flexible C–terminal tail (Evgrafov *et al.*, 2004). Moreover, a genetic deletion of

the Hsp27 gene has also been linked to Williams syndrome (Stock *et al.*, 2003), a congenital developmental disorder involving the vascular, connective tissue, and central nervous system (Ewart *et al.*, 1993). αB–crystallin as well as Hsp27 accumulate in individuals with various neurodegenerative disorders that include Alzheimer's, Parkinson, Alexander diseases, Creutzfeldt–Jakob disease and multiple sclerosis (Aquino *et al.*, 1997; Head *et al.*, 1993; Iwaki *et al.*, 1993; Kato *et al.*, 1992; Renkawek *et al.*, 1999; Stege *et al.*, 1999).

Interestingly, the functional properties of Hsp27 are dependent on the quaternary structure of the protein. For example, Hsp27 acts as chaperon and binds to cytochrome *c* as a large, non–phosphorylated oligomer (Bruey *et al.*, 2000b) while it binds to Daxx (Charette *et al.*, 2000) and transiently deteriorates actin stress fibers (Lavoie *et al.*, 1995) as a small, phosphorylated or non–phosphorylated oligomer, respectively.

1.4 Methods to characterize assembly of protein oligomers

1.4.1 Analytical ultracentrifugation

1.4.1a Overview

The characterization of oligomeric size distribution is a major challenge to understanding the properties of small heat shock proteins. Of the physical and chemical techniques that can be employed to study macromolecular oligomerization, analytical ultracentrifugation (AUC) has been used in the present work because it affords several advantages over alternative methods e.g. high resolution mass spectrometry, dynamic light scattering, size–exclusion chromatography and gel electrophoresis. Although, analytical

ultracentrifugation is the oldest of these techniques, a vast computational development has been done in the last few years that has improved the quality and quantities for experiments. Moreover, experiments provide a large quantity of data with relatively high precision.

Analytical ultracentrifugation is attractive for its theoretical simplicity and firm basis on first principles. Hydrodynamic theory and thermodynamics can be directly applied, and no interaction with matrices, surfaces or bulk flow is required in the separation of subpopulations of different size. Analytical ultracentrifugation can be applied to a very large range of macromolecular sizes simply by adjusting the rotor speed and to a large range of concentrations by using different optics. The instrument employed in this work, a Beckman XL–I, is equipped with both absorbance (Giebeler, 1992; Hanlon *et al.*, 1962; Schachman *et al.*, 1962) and interference (Schachman, 1959; Yphantis *et al.*, 1994) optics.

Although analytical ultracentrifugation is not a high throughput technique, it is the most precise technique for characterizing the hydrodynamic and thermodynamic properties of proteins and protein complexes, including molecular mass, sedimentation coefficients and binding–constant determinations, because, as previously mentioned, it is based on equilibrium and non–equilibrium thermodynamics only.

Analytical ultracentrifugation affords several advantages for the study of small heat shock proteins over other techniques. Size exclusion chromatography (SEC), for example, requires the use of calibration curves. Often monomeric proteins are used for calibrating the column, and the behavior of monomers may differ from that of a self–associating protein. Moreover, separation in SEC is effected by the interactions between the solute and

the matrix, and sedimentation coefficient distributions may be evaluated over a much wider dynamic range. An advantage of gel filtration is that the diffusional broadening in the raw data is lower compared to analytical ultracentrifugation experiments, but in an sedimentation experiment the amount of data collected is very large and allows for diffusional deconvolution (Lebowitz *et al.*, 2002; Schuck *et al.*, 2002).

Dynamic light scattering (DLS) is an appealing technique because, like AUC, DLS can be performed in batch mode without interaction with a matrix. One of the main disadvantages of DLS is that the scattering intensity for any species is proportional to the product of the concentration times the molecular mass of that scattering species. This characteristic makes DLS extremely appealing for detection of small percentages of large aggregates because such species produce very strong scattering signals. However, it is a poor tool for studying small oligomers. Moreover, DLS has low resolution; normally two species by DLS are not resolved as separate peaks unless their radii differ by a factor of approximately 2 (*i.e.*, a factor of ~8 in molecular mass). Moreover, the conversion of the intensity distribution into fraction by weight is subject to many assumptions and sources of error (Philo, 2006). Finally, the primary advantage of analytical ultracentrifugation compared to electrospray mass spectrometry is that measurements for the latter are done in the gas phase while analytical ultracentrifugation evaluates the self–association in solution. Classically, two types of analytical ultracentrifugation experiments are considered: sedimentation velocity and sedimentation equilibrium experiments.

1.4.1b Sedimentation Velocity

A sedimentation velocity experiment, produces radial concentration profiles as a function of time as shown in Figure 1.8.

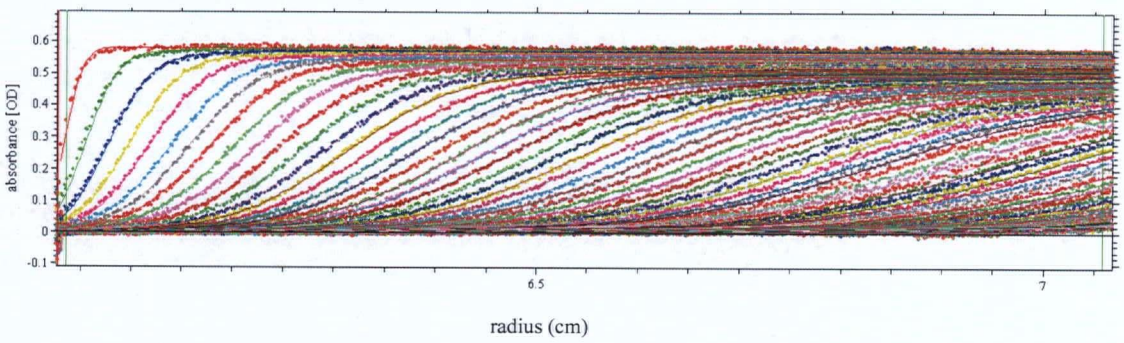

Figure 1.8 Example of sedimentation velocity run. Shown are the concentrations versus radius distributions at different times after start of the sedimentation at 50,000 rpm. Concentration are in absorbance units.

Upon application of a centrifugal force to a protein solution, the macromolecules are depleted at the meniscus, and a concentration boundary is formed that moves toward the bottom of the centrifuge cell as a function of time. The Svedberg equation (Equation 1.1) describes the sedimentation coefficient s of a macromolecule and the molecular parameters that determine the s–value (Svedberg & Pedersen, 1940):

$$s = \frac{u}{\omega^2 r} = \frac{M(1-\bar{\nu}\rho)}{N_A f} = \frac{MD(1-\bar{\nu}\rho)}{RT} \qquad \text{[Eq.1.1]}$$

where s is the sedimentation coefficient, u is the observed radial velocity of the macromolecules, ω is the angular velocity of the rotor, r is the radial position, $\omega^2 r$ is the centrifugal field, M is the molar mass, $\bar{\nu}$ is the partial specific volume, ρ is the buffer density, N_A is Avogadro's number, f the frictional coefficient, D is diffusion coefficient, R is gas constant and T is the temperature. The relation $D = \frac{RT}{N_A f}$ was used to obtain the

right side of Equation 1. The sedimentation coefficient is expressed in Svedberg (S) units, which corresponds to 10^{-13} sec.

The evolution of the concentration distribution of macromolecular species throughout the sector–shaped cell and the fit of such data can be achieved by modeling the data directly with the underlying transport function known as the Lamm equation (Equation 1.2), which is a form of the more general Navier–Stokes equation:

$$\frac{\partial \chi(r,t)}{\partial t} = \frac{1}{r}\frac{\partial}{\partial r}\left[rD\frac{\partial \chi(r,t)}{\partial r} - s\omega^2 r^2 \chi(r,t)\right] \qquad \text{[Eq.1.2]}$$

which describes the evolution of the concentration χ as a function of time and radial position under the influence of sedimentation and diffusion (Lamm, 1929).

The programs SEDFIT (Schuck, 1998) and SEDPHAT (Schuck, 2003), which are the principal programs used in this thesis to analyze velocity experiments, use different numerical finite element solutions to the Lamm equation. In particular, the numerical analysis known as *c(s)* distribution provided by the program SEDFIT does not require initial guesses or information concerning the system under analysis other than the standard physical parameters (*e.g.*, temperature, buffer viscosity and density, and the protein amino acid sequence) and the assumption of a non-interacting mixture of species with the same frictional coefficient. This program uses a differential sedimentation coefficient distribution that deconvolutes diffusion effects based on direct boundary modeling with a distribution of Lamm equation solutions. In brief, a sedimentation coefficient distribution *c(s)* can be defined as (Equation 1.3):

$$a(r,t) = \int c(s)\chi(s, D(s), r, t)ds + \varepsilon \qquad \text{[Eq.1.3]}$$

with *a(r,t)* denoting the observed sedimentation data, *c(s)* the concentration of species with sedimentation coefficients between s and $s + ds$, and $\chi(s,D(s),r,t)$ the Lamm equation solution described before (Schuck & Rossmanith, 2000).

1.4.1c Sedimentation Equilibrium

In equilibrium experiments, sedimentation is balanced by diffusional transport, and equilibrium is achieved when the net transport disappears throughout the solution. The concentration distribution generally approaches an exponential, and for a mixture of non–interacting ideal sedimenting molecules, the signal measured as a function of radial position, *a(r)*, can be described with the following equation (Equation 1.4):

$$a(r) = \sum_n c_{n,0}\varepsilon_n d \exp\left[\frac{M_n(1-\bar{\nu}\rho)\omega^2}{2RT}(r^2 - r_0^2)\right] + \delta \qquad \text{[Eq. 1.4]}$$

where the summation is overall n species; $c_{n,0}$ denotes the molar concentration of species n at a reference position r_0; M_n, $\overline{\nu_n}$, and ε_n, denote the molar mass, partial specific volume and the molar extinction coefficient, respectively; d is the optical path length and δ is a baseline offset.

For self–associating systems, Equation 4 can be modified by relating the molar concentration at the reference point of all oligomeric species via $c_{n,0} = K_n(c_{1,0})^n$ (where the

subscript 1 denotes the monomer). In addition, for M_n, nM_1 can be substituted in each exponential term to obtain Equation 1.5:

$$a(r) = \sum_n n\varepsilon_1 K_n (c_{1,0})^n \exp\left[\frac{nM_1(1-\bar{\nu}\rho)\omega^2}{2RT}(r^2 - r_0^2)\right] + \delta \text{ with } K_1=1 \qquad \text{[Eq. 1.5]}$$

The association constants K_n are defined from monomer to the n–mer.

More extensive reviews of analytical ultracentrifugation and related data analysis are available (Howlett *et al.*, 2006; Lebowitz *et al.*, 2002; Minton, 2000; Schuster & Toedt, 1996).

1.4.2 Förster Resonance Energy Transfer

1.4.2a Application to small heat shock protein subunit exchange.

Small heat shock proteins undergo subunit exchange. The biological consequences for this remain uncertain but in some cases, increased chaperon activity has been correlated with increased subunit exchange. Interestingly, heterogeneous complexes have been observed to form as the result of subunit exchange between various small heat shock proteins *in vivo* as well as *in vitro*. Complexes of phosphorylated Hsp27 and Hsp22 have been reported among proteins expressed from a human heart cDNA library (Benndorf *et al.*, 2001), and, although Hsp22 is believed to be primarily monomeric *in vitro* (Chowdary *et al.*, 2004), this protein has been reported to occur *in vivo* as a 25–670 kDa oligomer, probably in complexes with other sHsps (Sun *et al.*, 2004). α–crystallin is known to be an oligomeric protein comprised primarily of 4 peptides: αA_1, αA_2, αB_1 and αB_2–crystallin

(Bloemendal, 1981; Sun & Liang, 1998). Mouse Hsp25, αA–crystallin and αB–crystallin can form mixed oligomers, both *in vitro* and *in vivo,* that dissociate upon heat treatment (Merck *et al.*, 1993; Zantema *et al.*, 1992). Understanding subunit exchange of small Hsps is, therefore, important to an understanding of the fundamental properties of such proteins.

1.4.2b Theory

The technique used in this thesis to analyze subunit exchange is Förster resonance energy transfer or FRET (Förster, 1948). This phenomenon occurs when the emission spectrum of a fluorophore, called the donor, overlaps with the absorption spectrum of another molecule, called the acceptor. When two such fluorophores are in proximity of each other, energy can transfer directly from one to the other. This process does not involve emission of light by the donor, but the donor and acceptor are coupled by a dipole–dipole interaction. The extent of energy transfer depends on the distance between the two fluorophore and the extent of spectroscopic overlap as well as the orientation of the donor and acceptor, the dielectric constant of the intervening medium and the quantum yield. The efficiency of energy transfer (E) is described by the Förster equation (Equation 1.6):

$$E = \frac{R_0^6}{R_0^6 + r^6} \qquad \text{[Eq. 1.6]}$$

Where R_0 is the Förster distance and r is the distance between the centers of the fluorophores. The Förster distance (R_0) is defined as in the Equation 1.7:

$$R_0^6 \equiv \frac{9\ln(10)}{128\pi^5 n^4 N} \kappa^2 \int \frac{f_D(\bar{\nu})\varepsilon_A(\bar{\nu})}{\bar{\nu}^4} d\bar{\nu} \qquad \text{[Eq. 1.7]}$$

where $\bar{\nu}$ is the wavenumber in cm^{-1}, $f_D(\bar{\nu})$ is the emission spectrum in units such that its integral is unity : $\int f_D(\bar{\nu})d\bar{\nu}=1$, $\varepsilon_A(\bar{\nu})$ is the molar decadic extinction coefficient in L/(mol cm) at wavenumber $\bar{\nu}$, N' is Avogadro's constant divided by 1000, and k^2 is a factor depending on the relative orientations of the transition dipole moments of the donor and acceptor and their orientations relative to the separation vector. The parameter n is the index of refraction.

The rate of energy transfer $k_T(r)$ is given by (Equation 1.8):

$$k_T(r)=\frac{1}{\tau_D}\left(\frac{R_0}{r}\right)^6 \qquad \text{[Eq. 1.8]}$$

where r is the same distance between the donor and the acceptor, and τ_D is the lifetime of the donor in the absence of energy transfer.

In summary, the extent of energy transfer is determined by the distance between the donor and the acceptor and the extent of spectroscopic overlap.

1.5 Scope of this thesis

One of the most intriguing and fundamental characteristics of small heat shock proteins is the mechanism of their self–association and how self–association affects activity. The present study focuses on these aspects of Hsp27 because of its numerous biological roles.

Analytical ultracentrifugation is the principal technique used to determine Hsp27 concentration dependent self–association in standard conditions at 20 °C. The wild–type protein and a variant that mimics the behavior of phosphorylation *in vitro* (Rogalla *et al.*,

1999) as well as their counterpart with an histidine–tag at the N–terminus, were analyzed using sedimentation velocity experiments and, in some cases, sedimentation equilibrium analyses. Since temperature and other physical parameters can influence oligomerization, a thorough analysis of the effects of pH, ionic strength and temperature on the two biologically relevant variants without the histidine tag was undertaken. Moreover, site–directed mutagenesis was used to generate a number of deletion and point variants, not previously described, to understand the role in self–association of the two extremities of the protein, as well as the only cysteinyl residue at position 137. A schematic representation of the variants analyzed in this work is summarized in Figure 1.9.

These results provide new insights into the solution properties of Hsp27 that have implications for the interpretation of previous work with this protein and for the design of future experiments.

In the second part of this thesis the subunit exchange properties of the wild–type protein and selected variants (*e.g.*, the phosphorylation mimic variant and the two variants lacking either the first 14 or the last 24 amino acids) were studied by FRET experiments. Moreover, chaperon activity was studied by measuring the inhibition of DTT–induced insulin unfolding. Such investigation provides a means of determining the extent to which each domain influences the chaperon activity and how chaperon activity is influenced by protein size, subunit exchange and temperature. Lastly a model for Hsp27 chaperon activity is proposed.

Some of this work has been published prior to the completion of this dissertation (Lelj-Garolla & Mauk, 2005; Lelj-Garolla & Mauk, 2006)

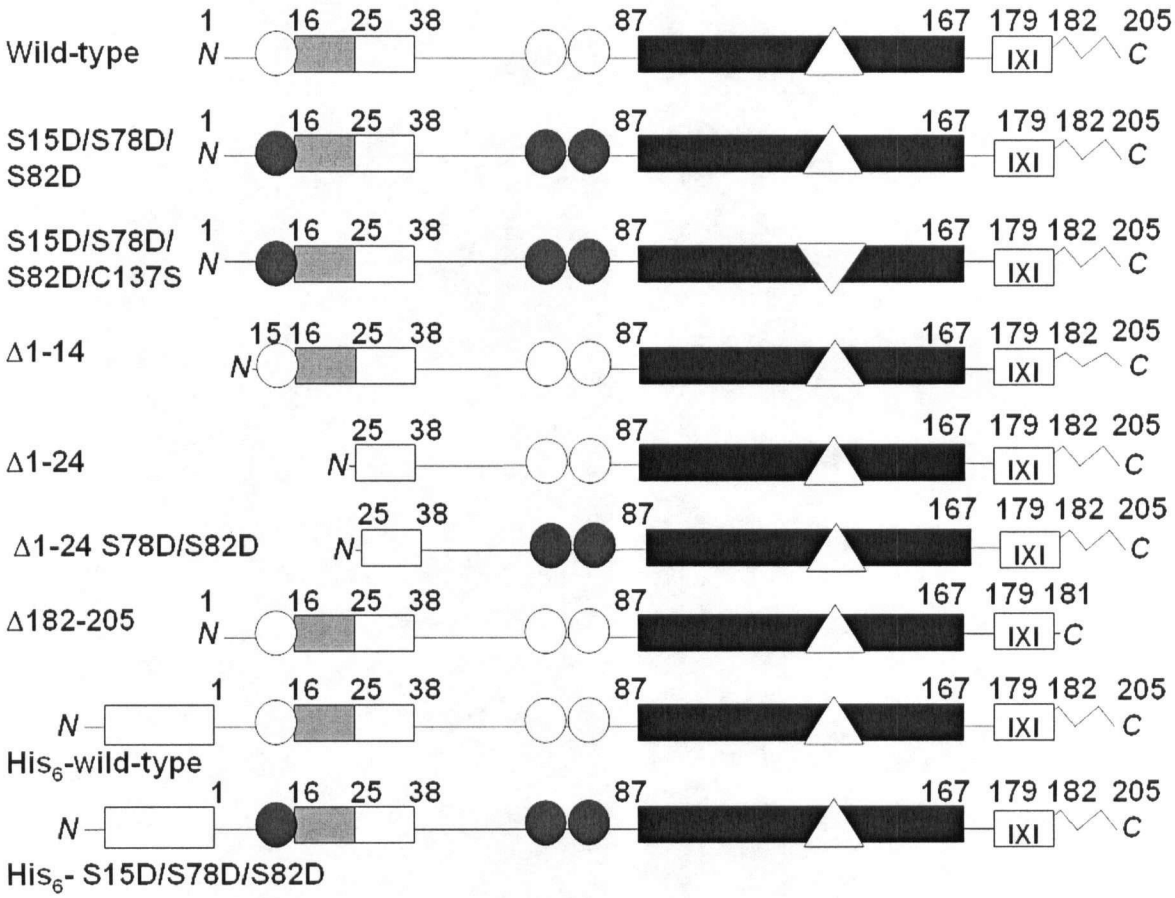

Figure 1.9 Hsp27 variants. The sequence domains of Hsp27 are represented as follows: Black, conserved α–crystallin domain; dark gray, WDPF–domain; white, conserved N–terminal region; IXI box, conserved IXI sequence at the C–terminus; zigzag line, flexible C–terminal tail; circles, phosphorylatable seryl residues; white circles, seryl residues; black circles, Ser to Asp substitutions; triangles pointing up, Cys137; triangle pointing down, Cys to Ser mutation; light gray box, His_6 tag followed by a thrombin cleavage site. Figures above the scheme denote sequence numbers. The names used for the Hsp27 constructs in the text are indicated on the left.

2. MATERIALS AND METHODS

2.1 Molecular biology of Hsp27

2.1.2 Protein expression

The human heat shock protein 27 was produced in *Escherichia coli* with the plasmid pET30. The coding sequence of the gene was amplified from the plasmid pCI–NeoHSP27human generously provided by Prof. J. Landry, Centre de Recherche en Cancérologie de l'Université Laval, Quebec. The original plasmid was modified because it contained two *EcoRI* cleavage sites at both the 3' and 5' end of the gene, and the *EcoRI* site at the 5'end was located 24 bp upstream of the first methionine. The primers that were used to amply the gene (NdeI–H27:5'–GC ATT ACG CAT *ATG* ACC GAG CGC CGC GTC CCC TTC–3' and EcoRI–H27: 5'–ATC GAA TTC TTA CTT GGC GGC AGT CTC ATC–3') added an *NdeI* cleavage site (underlined) at the 5'– end of the coding sequence that included the ATG of the first coding Met (italics) and an *EcoRI* cleavage site right after the stop codon at the 3'–end of the Hsp27 gene (underlined). The PCR product was cloned into a pET30 vector from Novagen. The resulting vector was labeled pET30–HSP27, and it is shown in Figure 2.1. The cDNA sequence is provided in Figure 2.2.

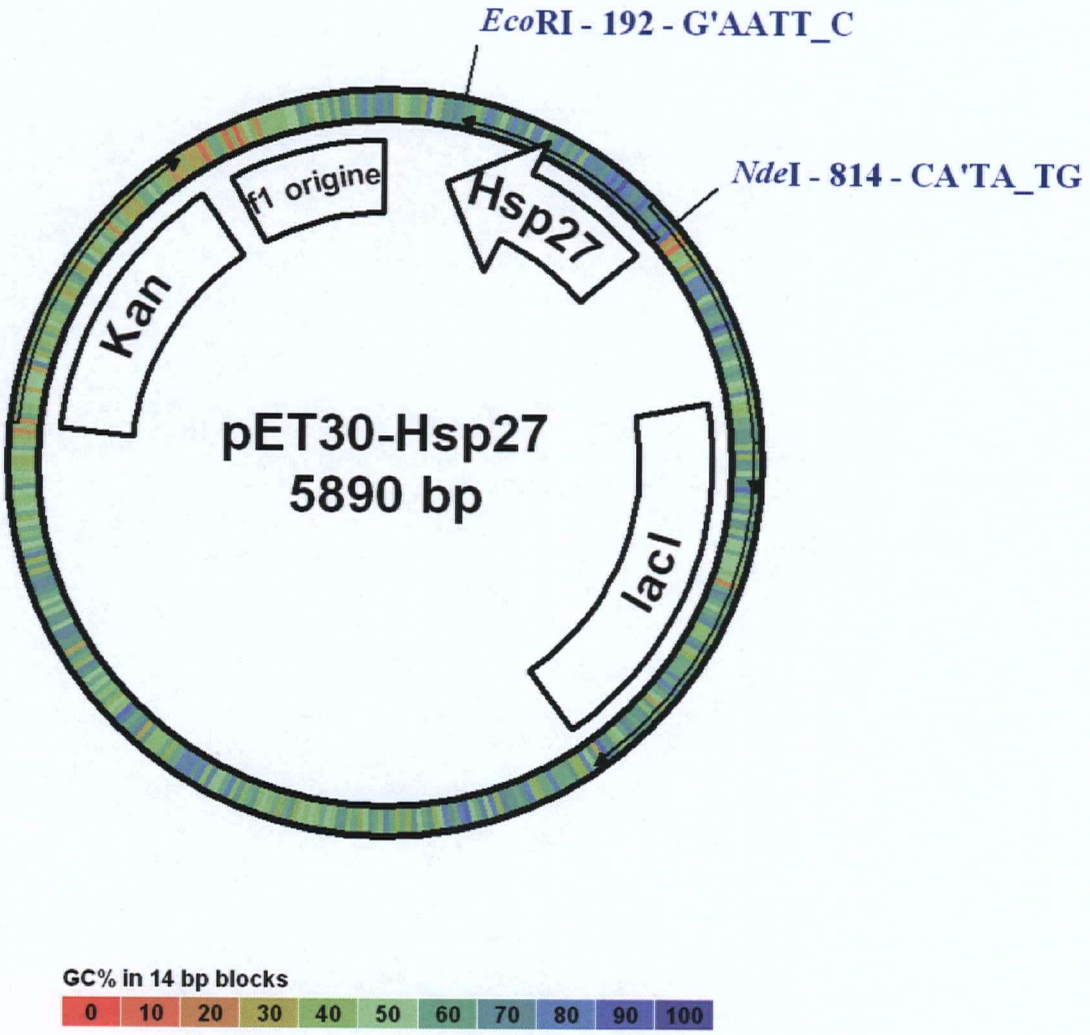

Figure 2.1 Functional map of the 5.89 Kbp plasmid pET30–Hsp27. Selected restriction sites and genes encoded in the plasmid are indicated in the figure.

```
    BspEI                                   BpuEI
  1 ATCCGGATAT AGTTCCTCCT TTCAGCAAAA AACCCCTCAA GACCCGTTTA

 51 GAGGCCCCAA GGGGTTATGC TAGTTATTGC TCAGCGGTGG CAGCAGCCAA

101 CTCAGCTTCC TTTCGGGCTT TGTTAGCAGC CGGATCTCAG TGGTGGTGGT

                  EagI          SalI    SacI   EcoRI
          XhoI    NotI     HindIII       EcoICRI
151 GGTGGTGCTC GAGTGCGGCC GCAAGCTTGT CGACGGAGCT CGAATTCTTA
                                                      *    Frame 6

                                                    PspOMI
                                        PspOMI      ApaI
                                        ApaI       BseYI
201 CTTGGCGGCA GTCTCATCGG ATTTTGCAGC TTCTGGGCCC CCAAGCTGGG
      K   A   A   T   E   D   S   K   A   A   E   P   G   G   L   Q     Frame 6

                                                    NheI
                      BmrI                          BmtI
251 CCCGCGACTC GAAGGTGACT GGGATGGTGA TCTCGTTGGA CTGCGTGGCT
    A   R   S   E   F   T   V   P   I   T   I   E   N   S   Q   T   A    Frame 6

                                                          BseRI
301 AGCTTGGGCA TGGGGGCCTC CACGGTCAGT GTGCCCTCAG GGGACAGGGA
     L   K   P   M   P   A   E   V   T   L   T   G   E   P   S   L   S   Frame 6

               TaqII
351 GGAGGAAACT TGGGTGGGGT CCACACCGGG GGGCAGCGTG TATTTCCGCG
      S   S   V   Q   T   P   D   V   G   P   P   L   T   Y   K   R     Frame 6

                                              BseRI
                                        BsrBI  BssSI
401 TGAAGCACCG GGAGATGTAG CCATGCTCGT CCTGCCGCTC CTCGTGCTTG
    T   F   C   R   S   I   Y   G   H   E   D   Q   R   E   E   H   K    Frame 6

451 CCGGTGATCT CCACCACGCC ATCCTTGGTC TTGACCGTCA GCTCGTCCGG
     G   T   I   E   V   V   G   D   K   T   K   V   T   L   E   D   P   Frame 6

                                                  BtsI
501 GGCGAAGTGG TTGACATCCA GGGACACGCG CCAGCGGTCC GCAGTGTGCC
      A   F   H   N   V   D   L   S   V   R   W   R   D   A   T   H     Frame 6

                                  NgoMIV
          BsaI                    NaeI       BssHII
551 GGATCTCCGA GACCCCGCTG CTGAGTTGCC GGCTGAGCGC GCGGCTGTAG
    R   I   E   S   V   G   S   S   L   Q   R   S   L   A   R   S   Y    Frame 6

               BtsI
601 GCGGGCGCGG CCACTGCGGG GCTCTCGATG GCGGCGGGGG GCAGGGGGCG
     A   P   A   A   V   A   P   S   E   I   A   A   P   P   L   P   R   Frame 6

            MscI PvuII                  BtsI        BseRI
651 CACGTAGCCT GGCCAGCTGC TGCCGCCTAA CCACTGCGAC CACTCCTCCG
      V   Y   G   P   W   S   S   G   G   L   W   Q   S   W   E   E     Frame 6
```

```
                                                        KpnI
                        StuI        EarI                Acc65I
701 GCAGCCGGGG CAGCCCGAAG GCCTGGTCGA AGAGGCGGCT ATGCGGGTAC
    P  L  R  P   L  G  F   A  Q  D   F  L  R  S   H  P  Y    Frame 6

                          BseYI
                        PvuII  PspOMI
                     BseYI     ApaI
751 CAGTCGCGGA AGGGGTCCCA GCTGGGGCCC CGCAGGAGCG AGAAGGGGAC
     W  D  R   F  P  D  W   S  P  G   R  L  L   S  F  P  V   Frame 6

           TaqII NdeI
801 GCGGCGCTCG GTCATATGTA TATCTCCTTC TTAAAGTTAA ACAAAATTAT

      R  R  E   T  M                                       Frame 6

     XbaI                BsrBI
851 TTCTAGAGGG GAATTGTTAT CCGCTCACAA TTCCCCTATA GTGAGTCGTA
```

Figure 2.2 Sequence of the Hsp27 cDNA. All the restriction enzymes that recognize at least 6 bps are reported.

2.1.2 Site–directed mutagenesis

The pET30–HSP27 vector was used as template to obtain all Hsp27 point variants and the following deletion variants: Hsp27 Δ1–14, Hsp27 Δ1–24 and Hsp27 Δ182–205. The polymerase chain reaction (PCR) was performed with the following program: 95 °C/5 min; 30 cycles at 95 °C/45 sec, 55 °C/45 sec, 72 °C/1 min; 72 °C/10 min. The reaction was carried out in the presence of 1 M betaine (note: not betaine–HCl) due to the high GC content of the Hsp27 gene (~ 68%). The PCR conditions for a standard reaction are reported in Table 2.1:

Table 2.1 Conditions for polymerase chain reactions for amplification of the Hsp27 gene.

Reagent	Concentration of stock	Volume (µl)	Final Concentration
Betaine (in H_2O)	1.4 M	71	1 M
Buffer	10×	10	1×
Template	50–150 ng/µL	1.5	0.75–2.25 ng/µL
Forward Primer	100 ng/µL	5	5 ng/µL
Reverse Primer	100 ng/µL	5	5 ng/µL
dNTPs	5–10 mM	5	0.2–0.5 mM
$MgSO_4$	100 mM	1.5	1.5 mM
VENT polymerase	200 U	1	1–3 U

To mimic phosphorylation *in vitro*, a triple variant was constructed with the three seryl residues that are phosphorylated *in vivo* changed to aspartyl residues (Rogalla *et al.*, 1999). The triple mutation construct pET30–HSP27S15D/S78D/S82D was created by a two–step site–directed mutagenesis protocol. First, two primers were used to change Ser^{78} and Ser^{82} to aspartyl residues (5'–CGC GCG CTC GAC CGG CAA CTC GAC AGC

GGG G–3' and 5'–C CCC GCT GTC GAG TTG CCG GTC GAG CGC GCG–3'), and then the resulting gene (Hsp27–S78D/S82D) was used as a template to obtain the fully modified gene Hsp27–S15D/S78D/S82D, (5'–GG GGC CCC GAC TGG GAC CC–3' and 5'–G GAA GGG GTC CCA GTC GGG GCC CGC AGG–3'). This product was then cloned between the *NdeI* and *EcoRI* sites of the pET30 vector. The resulting pET30–HSP27S15D/S78D/S82D vector was used as a template to replace the only cysteine (C^{137}) with a seryl residue (pET30–HSP27–S15D/S78D/S82D/C137S) (5'–GGC TAC ATC TCC CGG AGC TTC ACG CGG–3' and 5'–CCG CGT GAA GCT CCG GGA GAT GTA GCC–3'). The same primers were used to modify the wild–type protein to Hsp27–C137S. In addition to point variants, a number of deletion variants were also synthesized. The primers used to prepare these constructs are indicated in Table 2.2:

Table 2.2 Primers used for amplification and mutagenesis of Hsp27 deletion variants.

Variant	Cloning sites:	Forward Primer	Reverse Primer
Hsp27 Δ1–14	*NdeI* and *EcoRI*	5'-GC ATT ACG CAT *ATG* AGC TGG GAC CCC TTC CGC GAC TGG-3'	EcoRI-H27
Hsp27 Δ1–24	*NdeI* and *EcoRI*	5'-GC ATT ACG CAT *ATG* CAT AGC CGC CTC TTC GAC CAG GCC TTC G-3'	EcoRI-H27
Hsp27 Δ182–205	*NdeI* and *BamHI*	NdeI-H27	5'-CG GGA TCC *TTA* GAT GGT GAT CTC GTT GGA CTG CGT GGC-3'

The Δ1–24 S78/S82 variant was constructed with the same primers as the Δ1–24 Hsp27 variants but with the pET30–S15D/S78D/S82D vector as template. The histidine tagged forms of wild–type Hsp27 and the triple variant were also prepared. The plasmid bearing the genes for these proteins was created by cloning the genes for the wild–type Hsp27 and the S15D/S78D/S82D variant into a pET28 plasmid from Novagen containing a histidine tag followed by a thrombin cleavage site at the N–terminus of the protein.

All the synthetic oligonucleotides were obtained from QIAGEN, and plasmid sequences were verified by DNA sequencing at the NAPS unit (UBC). Plasmids were transformed into DH5α cells (Invitrogen) and plated on LB plates containing kanamycin (KM) (50 μg/mL). Colonies were screened for inclusion of the plasmids with standard T7 phage primers (#69348–3 and #69337–3, Novagen). Selected colonies were grown, and the plasmids were purified (QIAGEN purification kit) and transformed into *E. coli* cells strain BL_{21}(DE3)–RIL (Stratagene) for protein expression.

2.1.3 Protein purification

A single colony was selected from each plate and grown in Luria–Bertani (LB) medium (1 mL, 37 °C/250 rpm) supplemented with kanamycin (KM) (1 μL, 50 mg/mL). An innoculum of 100 μL was added to LB medium (50 mL) supplemented with KM (50 μL, 50 mg/mL) for overnight growth (37 °C/250 rpm). LB media (1 L) with KM (1 mL, 50 mg/mL) was inoculated with the overnight culture (1 mL) and grown at 37 °C/250 rpm. Protein expression was induced with IPTG (Isopropyl β–D–1–thiogalactopyranoside) (1 mL, 50 mg/mL) when the OD_{600} was >1.0. Cell growth was allowed to proceed under the same conditions overnight at which point bacteria were

pelleted at 8,000 rpm and lysed with a French Press in 20 mM Tris–HCl pH 8.4 and 100 mM NaCl. The resulting homogenate was clarified by centrifugation (1 h/13,000 rpm/4 °C).

The wild–type protein and all the variants without the histidine–tag were purified as described elsewhere (Behlke *et al.*, 1991). In brief, the supernatant fluid was saturated to 35% ammonium sulfate and stirred on ice for 2 h. The precipitate was pelleted by centrifugation (1 h/13,000 rpm/4 °C), re–dissolved in 20 mM Tris–HCl (pH 8.4) and filtered (0.2 μm filters, Pall) prior to loading onto a HiPrep desalting column (2.6 × 10 cm, Amersham–Biosciences) equilibrated with 20 mM Tris–HCl pH 8.4, 100 mM NaCl. The desalted protein was loaded onto a column (1.6 × 10 cm) of Sepharose–Q resin (Amersham–Biosciences), eluted with an NaCl gradient (0 to 50% B in 12.5 Column Volume (CV), 1 CV= 20.5 mL, A= 20 mM Tris–HCl pH 8.4, 100 mM NaCl and B= 20 mM Tris–HCl pH 8.4, 1 M NaCl), and the fractions containing the protein were pooled, concentrated by centrifugal ultrafiltration (Centricon 10K, Amicon) and the buffer exchanged to 20 mM Tris–HCl pH 8.4, 100 mM NaCl by dialysis overnight. The protein was then loaded onto a Mono–Q column (1.0 × 10 cm, Amersham–Biosciences) and eluted with the same NaCl gradient. Fractions containing the protein were pooled and concentrated. The resulting protein was eluted (400 mL injections) over a manually packed gel filtration column with Superdex 200 resin (0.5 × 40 cm, Amersham–Biosciences).

The His_6–tag–Hsp27 variants were purified on a HiTrap Ni–NTA column (Amersham–Biosciences) by increasing the imidazole concentration from zero to 500 mM. After elution, the protein was pooled, concentrated and dialyzed extensively against 4 L buffer (20 mM Tris–HCl pH 8.4, 100 mM NaCl). The His_6–tag could not be removed with

thrombin after repeated attempts. Therefore, both the His_6–tag and the thrombin cleavage site were left flanking the N–terminus of the protein. For all the variants, fractions were analyzed by SDS–PAGE followed by Coomassie blue staining, concentrated and stored at –80 °C in multiple samples after flash freezing in small volumes of liquid nitrogen. The purification yield varied with the variants expressed, purification of wild–type Hsp27 produced up to ~ 50 mg of pure protein per liter of culture.

2.2 Analytical Ultracentrifugation (AUC)

2.2.1 Sedimentation Velocity.

Experiments were conducted with a Beckman Optima XLI analytical ultracentrifuge equipped with both absorbance and interference optics. Unless otherwise stated, the experiments were run at 20 °C in 20 mM Tris–HCl (pH 8.4), 100 mM NaCl with 400–450 μL of sample. The samples were diluted to the final concentration and dialyzed overnight against 1.5 L of buffer just prior to analysis. Before starting any run, samples were thermally equilibrated in the centrifuge for at least 1 h after the instrument reached 20 °C under vacuum. Sedimentation velocity experiments were performed with the 4–hole (AnTi60) and 8–hole (AnTi50) rotors and with 12 mm aluminum-filled epon double sector centerpieces. Sapphire windows were used with interference optics while quartz windows were used with absorbance optics. Radial absorbance data were acquired at 280 nm or 230 nm, depending on protein concentration, and radial increments of 0.003 cm with no averaging in continuous scan mode. For both interference and absorbance, no time interval was set between scans. Rotor speed was either 35,000 rpm for the high molecular weight species (wild–type Hsp27, C137S Hsp27, Δ182–205 Hsp27,

His6–tag wild–type and His6–tag S15D/S78D/S82D) or, 60,000 or 50,000 for the low molecular weight species (S15D/S78D/S82D Hsp27, S15D/S78D/S82D/C137S Hsp27, Δ1–14 Hsp27, Δ1–24 Hsp27).

When experiments were performed at temperatures other than 20 °C, care was taken to equilibrate the rotor at the desired temperature outside the centrifuge. Notably, as the experimental temperature approached the upper limit of temperature that is accessible with the Optima XL–I (40 °C), oil vapor from the vacuum pump collected on the optical elements during data collection. For this reason, the optics were cleaned after each experiment performed under such conditions.

2.2.2 Data analysis of sedimentation velocity experiments

Most data were analyzed as a *c(s)* distribution of the Lamm equation solutions calculated with the program SEDFIT (Schuck *et al.*, 2002) and regularization parameters of p=0.95 and 200 sedimentation coefficient increments in the appropriate range for each sample, both the meniscus and the frictional ratios were floated. The density of the solution and the partial specific volume were calculated with the program SEDNTERP (Laue *et al.*, 1992). The monomer molecular weights and the extinction coefficients were calculated from the amino acid sequence with the program ProtParam that is available at the Expasy web site. All the values used together with the protein concentrations are reported in Table 2.3. The isotherm fits were performed with the appropriate fitting function in the SEDPHAT program (Schuck, 2003).

All the average sedimentation coefficients (S_{av}) reported in this work are corrected to the viscosity and density of water at 20 °C. When values of S_{av} are reported, the program SEDFIT was used to obtain a plot of *c(s) vs.* sedimentation coefficient, and the peaks in the

c(s) plots were integrated to obtain the S_{av} values and the total signal. The curves were then normalized by dividing the curves by the total signal obtained in the *c(s)* distribution. The program SEDNTERP was then used to obtain the values corrected to the density and

Table 2.3 Physical parameters for all Hsp27 derivatives studied.

Variants of Hsp27	M.W. (Da)	ε_{280} (L/g×cm)	$\bar{\nu}$ (mL/g)
Wild–type	22651.3	1.790	0.7275
S15D/S78D/S82D	22866.5	1.773	0.7267
S15D/S78D/S82D/C137S	22719.3	1.784	0.7268
Δ1–14	21141.5	1.918	0.7264
Δ1–24	19791.1	1.409	0.7279
Δ182–205	20107.5	2.01	0.7285
His_6–wild–type	24814.6	1.634	0.7242
His_6–S15D/S78D/S82D	24898.6	1.628	0.7234

Molecular weight and molar absorptivities were derived with the program ProtParam provided by the ExPasy web site (Gill & von Hippel, 1989). Partial specific volume was calculated with the program SEDNTERP (Laue *et al.*, 1992).

viscosity at 20 °C. This analysis permits the direct comparison of S_{av} values obtained at various temperatures with each other. For wild–type Hsp27, the ranges used at each temperature were as follows: 10 °C (1–30 S), 20 °C (1–30 S), 30 °C (1–50 S), and 40 °C (1–50 S). The S_{av} for samples with low concentration of the triple variant were obtained by integrating the *c(s)* curves up to 5.5 S. Further analysis was performed with the program SEDPHAT which corrects for standard conditions. The *c(s)* curves where obtained with the hybrid local continuous distribution model with Tikhonov regularization $p = 0.95$ and allowing the frictional coefficient to float. At least 300 points were used for each curve in the appropriate range of sedimentation coefficients. In the case of all the other variants, appropriate ranges were used depending on the positions of the peaks. Additional details are reported in the Results section.

2.2.3 Sedimentation Equilibrium.

Sedimentation equilibrium experiments were performed on wild–type Hsp27 and Hsp27 S15S/S78D/82D at several concentrations specified in the results section. All the experiments were performed with Beckman Optima XL–I analytical ultracentrifuge at 20 °C with samples prepared in 20 mM Tris–HCl (pH 8.4), 100 mM NaCl. Samples were loaded into a 6–channel carbon–filled epon centerpiece and spun in the 4–hole (AnTi60) rotor. Data were collected at 280 nm or with interference optics depending on protein concentrations. Wild–type Hsp27 was run at 9,000 rpm for 42 h, and scans were collected every hour. Experiments with S15S/S78D/S82D Hsp27 were run at 8,000 rpm, 12,000 and 20,000 rpm. When the absorbance optics were used, radial scans were set at 0.001 cm increments and each data set is an average of 10 scans. Achievement of equilibrium was

verified with the program WinMatch (Jeffrey & Yphantis), and analysis was performed with the program WinNonlin (Johnson *et al.*, 1981).

2.3 Circular Dichroism (CD)

2.3.1 Wild–type Hsp27

Circular dichroism spectra of wild–type Hsp27 (10 μM, 10 mM phosphate buffer, pH 7.4) were collected with a quartz cuvette (0.1 cm path length) and a Jasco–810 spectropolarimeter equipped with a Peltier device for temperature control. Temperature was maintained at 20 °C and each spectrum is an average of 3 scans.

2.3.2 Thermal denaturation of wild–type and variants

Thermal denaturation was measured at 222 nm and a protein concentration of 10 μM (10 mM phosphate buffer, pH 6.7 or 7.7) with a Jasco 810 spectropolarimeter by increasing the temperature of the sample from 25 to 90 °C with a gradient of 1°C/min. CD spectra were recorded at 25 °C before and after unfolding. Temperature was regulated with a Peltier device under computer control.

2.4 Activity assay

2.4.1 Insulin unfolding

Unfolding of insulin was measured at various temperatures, protein concentrations and pH to identify conditions under which unfolding was detectable within 20 to 30 minutes. Insulin solutions (90 μM) were prepared at various values of pH and incubated at the final temperature at least 10 minutes before addition of DTT (1 M, 60 μL).

Aggregation was monitored by measuring light scattering at right angles to the incident light with a Varian Cary Eclipse spectrofluorometer equipped with a Peltier device for temperature control. Both the emission and excitation wavelengths were set at 465 nm (the band pass 2.5 nm). Kinetics traces are reported as the average of two measurements.

2.4.2 Unfolding in the presence of Hsp27 variants

Chaperon activity was measured by monitoring the DTT–induced aggregation of insulin in the absence and presence of Hsp27 and variants. For the experiments performed in the absence of Hsp27, aggregation was initiated by unfolding insulin with the addition of DTT solution (1 M, 60 μL) to a solution of insulin (90 μM, 590 μl). The same experiments were repeated in a solution containing varying concentrations of wild–type or variant Hsp27 in sodium phosphate buffer (20 mM, pH 6.7) that had been incubated for 10 min at the desired temperature. The final pH was adjusted just before incubation at the desired temperature. Hsp27 chaperon activity was measured at two ratios of insulin:Hsp27 (0.05 and 0.2 (mol/mol)) and at least two temperatures (20 and 40 °C). When appropriate, the percentage activity was calculated as $100[(I_{Ins} - I_{Ins+Hsp})/I_{Ins}]$ where I is the intensity of light scattering observed after 20 min.

2.5 Förster resonance energy transfer (FRET)

2.5.1 Protein labeling

Wild–type Hsp27 and selected variants were labeled at the unique cysteinyl residue present in the monomeric protein at position 137 with either 4-aceto-4'-((iodoacetyl)amino) stilbene-2,2'-disulfonic acid (AIAS, λ_{ex}= 329 nm, λ_{em}= 408 nm) or

lucifer yellow iodoacetamide (LYI, λ_{ex}= 426 nm, λ_{em}= 531 nm) (Figure 2.3). Labeling was performed with a protocol previously described (Bova *et al.*, 1997; Bova *et al.*, 2000). In brief, recombinant protein was diluted to 1 mg/mL with buffer (100 mM NaCl, 20 mM MOPS, pH 7.9). Solid AIAS was added to a final concentration of 3.2 mM in a final volume of 1 mL, and the reaction was allowed to proceed overnight at room temperature in the dark. Unreacted AIAS was separated chromatographically from the fluorescently-labeled Hsp27 with a Hi–Trap desalting column (5 mL, equilibrated with 100 mM NaCl, 2 mM DTT, 50 mM sodium phosphate (pH 7.5), Amersham–Biosciences) developed with an AKTA chromatography system. Hsp27 was also covalently labeled with LYI at a final concentration of 8.4 mM under the same conditions. AIAS and LYI were both from Invitrogen. The extinction coefficients used to determine the labeling efficiency were 39,000 $M^{-1}cm^{-1}$ for AIAS and 11,000 $M^{-1}cm^{-1}$ for LYI.

2.5.2 FRET experiments

Fluorescence resonance energy transfer was used to determine the rate of subunit exchange of wild–type Hsp27 and variants as a function of temperature. The exchange reaction was initiated by mixing equimolar (5 μM final) AIAS–labeled and LYI–labeled protein in a quartz cuvette (1 cm path length) in a total volume of 160 μL (50 mM sodium phosphate (pH 7.5), 100 mM NaCl, 2 mM DTT). The excitation wavelength was 335 nm, and quenching was followed by measuring fluorescence emission (412 nm) with a Cary Eclipse spectrofluorometer. Protein was incubated in a water bath at the desired temperature for at least 15 min prior to each experiment, and the cuvette was maintained at constant temperature with a Peltier device during data collection. The rate of subunit

exchange was calculated from the equation $F(t) = y_0 + Ae^{-x/t_{mrd}}$, where $F(t)$ is the fluorescence intensity at 412 nm and t_{mrt} is mean reaction time (Espenson, 1981). The rate constant k, which is equal to $1/t_{mrt}$, was determined by nonlinear regression analysis of the data using the first order exponential decay fit from the software Origin (ver. 7.0). The activation energy (E_a) for subunit exchange was determined from Arrhenius plots (1/T (K^{-1}) *vs.* ln(k)). The data points where fitted by a linear least squares fit to $y = A + B \cdot x$ where $A = \Delta S/R$ and $B = -\Delta H/R$ (R = gas constant), and the activation energy was calculated from the relationship $E_a = \Delta H + RT$.

A

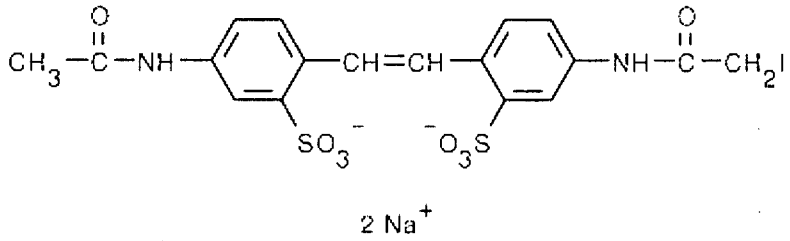

B

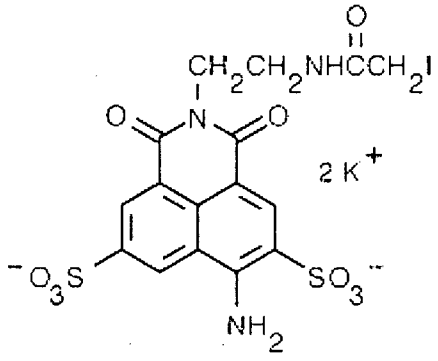

Figure 2.3 Structures of AIAS and LYI. A, Sodium 4-aceto-4'-((iodoacetyl)amino) stilbene-2,2'-disulfonate (AIAS); B, potassium salt of lucifer yellow iodoacetamide.

3. RESULTS

3.1 Self–association

To define the mechanism by which Hsp27 functions, it is essential to understand first the most fundamental aspects of the behavior of the protein in solution, the manner in which this behavior is dictated by solution conditions (pH, temperature, ionic strength) and the contributions of key structural elements of the protein to this behavior. For a self–associating protein, such as Hsp27, the most fundamental issue is the distribution of oligomers that occurs in solution, the manner in which this distribution is influenced by the factors defined above, and the structural determinants of this distribution.

The results presented below provide this information for human Hsp27 through the use of analytical ultracentrifugation and then consider the relationship between the oligomerization of the protein and its structural modifications on the chaperon activity of the protein.

3.1.1 Oligomerization of wild–type Hsp27 in standard conditions

The first step towards the characterization of Hsp27 oligomerization was to determine the self–association of the protein in standard conditions, defined here as 20 mM Tris–HCl pH 8.4, 100 mM NaCl at 20 °C. Sedimentation velocity analysis of the behavior of Hsp27 is followed by the analysis of sedimentation equilibrium experiments to establish that oligomerization in standard condition is highly dynamic and that most of the protein is present in a 12/16–mer state in equilibrium with smaller oligomers.

Velocity data obtained with wild–type Hsp27 protein samples of 0.03 to 1.96 mg/mL were analyzed by modeling the sedimentation boundaries as a superposition of finite elements of the Lamm equation for non–interacting species with the program SEDFIT (Schuck & Rossmanith, 2000). The resulting distribution functions of sedimentation coefficients *c(s)* are shown in Figure 3.1A. The *c(s)* distribution of the wild–type protein exhibits several peaks, consistent with polydisperse speciation.

For all protein concentrations, 70–95% of the sample exhibits a sedimentation coefficient in the range 4.6–30 S, 2–30% sediments with S of 2–4.6, and just 2–3% has S >30 S, indicating that under these conditions, wild–type Hsp27 has a discrete upper limit in size.

The breadth of the peaks observed in the *c(s)* distribution is greater than expected for discrete, non–interacting components, and the apparent sedimentation coefficients for each peak vary directly with protein concentration. This result indicates that the boundaries observed are "reaction boundaries" in which the sedimenting species interconvert on a timescale that is at least as great as that of sedimentation. As a consequence, the observed peaks do not correspond to a particular oligomeric assembly but instead reflect some weight–average of the sedimenting species. However, by increasing the protein concentration sufficiently, the peak of the *c(s)* distribution approaches the peak of the largest oligomer. In the current case, the major peak shifted toward an upper value of ~13 S without increasing to higher S values as protein concentration was increased from 0.5 to 1.96 mg/mL. This behavior indicates that at these concentrations, true sedimenting species are observed and that a reaction boundary is seen only at the lowest concentration.

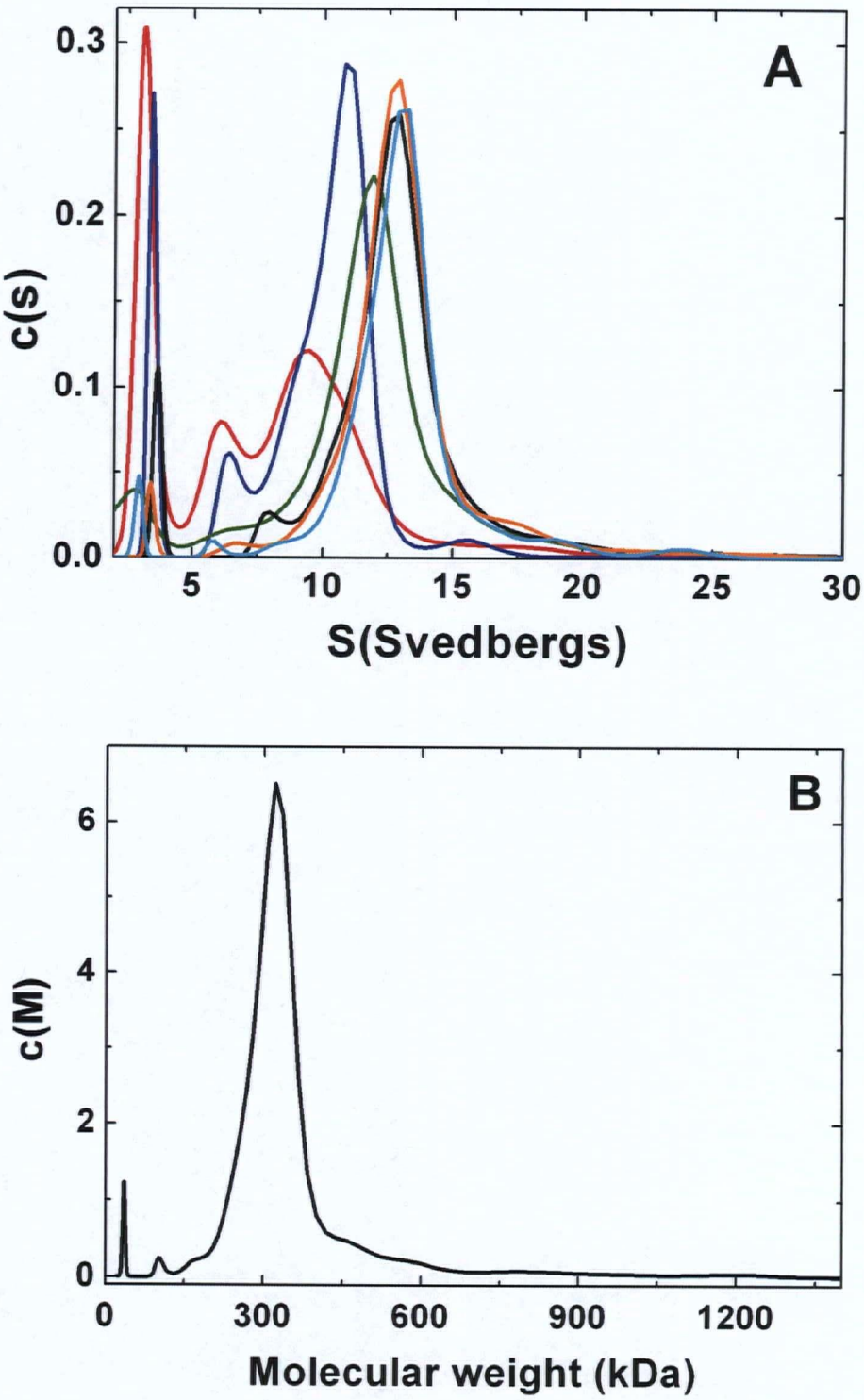

Figure 3.1. Sedimentation velocity analysis of wild–type Hsp27 (Tris–HCl buffer (20 mM (pH 8.4), 100 mM NaCl, 20 °C)). A, *c*(*s*) distribution: red line, 0.03 mg/mL; blue line, 0.09 mg/mL; olive green line, 0.2 mg/mL; orange line, 0.5 mg/mL; black line, 0.89 mg/mL; cyan line, 1.96 mg/mL. B, *c*(*M*) distribution for [Hsp27] of 1.96 mg/mL assuming f/f_0=1.29.

The sedimentation coefficients calculated for spherical species with the molecular weights of a 12–mer (15.10 S), 14–mer (16.73 S) and for 16–mer (18.29 S) are as indicated. As the sedimentation coefficient of a protein must be smaller than that of a sphere of equal molecular weight, all models considered here could be correct. S_{max}/S is equal to f_0/f, so $S = S_{max}/(f/f_0)$ where S_{max} is the sedimentation coefficient of a sphere with molecular weight equal to the species being analyzed. The frictional coefficient obtained with SEDFIT is $f/f_0 = 1.29$, so the expected sedimentation coefficient would be 11.7 S (or 15.1/1.29) for a 12–mer, 13.0 S (or 16.73/1.29) for a 14–mer and 14.3 S (18.29/1.29) for a 16–mer. The last two values are very close to both the experimental value obtained from the *c(s)* distribution at high concentrations (S=13.2), and the value derived from the SEDPHAT fits for the largest species in the assembly (S=13.9) (read below for further analysis).

As a result, the *c(s)* distribution of the 1.96 mg/mL sample can be transformed into a *c(M)* distribution with confidence. The frictional ratio used for this transformation (f/f_0=1.29) was obtained from the fit to the data provided by SEDFIT. The value of this parameter is allowed to float during data analysis with SEDFIT because independent information concerning the average degree of boundary spreading and sedimentation can be extracted from the experimental data (Schuck *et al.*, 2002). The f/f_0 value provides an estimate of the extent to which the shape of a protein differs from a compact, unhydrated sphere of the same mass and density (Cantor & Schimmel, 1980). A globular, hydrated protein would have a frictional coefficient of 1.2–1.4, a moderately elongated protein (*e.g.*, fibronectin coiled up in low salt) would have a frictional coefficient of 1.6–1.9 while very elongated proteins (*e.g.*, fibrinogen) would have a frictional coefficient of 2–3. Together

with the S–value, the f/f_0 allows estimation of the molecular weight of the sedimenting species (Lebowitz *et al.*, 2002).

As previously mentioned, the presence of multiple species in solution complicates the interpretation of the frictional ratio obtained with SEDFIT for a *c(s)* distribution. However, the use of a single average frictional coefficient in the interpretation of the sedimentation data of an oligomerization process has been quite successful, for example, in the study of ligand–linked association of tubulin (Frigon & Timasheff, 1975). For proteins that interact on the time–scale of sedimentation, an additional contribution to boundary spread is the interconversion of species by dissociation and re–association of the oligomers (a chemical process). With the exception of repulsive interactions at protein concentrations exceeding those used in the present study, such a chemical process leads to excess boundary spreading, which can result in artificially high apparent diffusion and consequently low frictional ratios at concentrations in the range of K_d of the interaction (Schuck, 2003). It was shown recently in the "constant bath" theory for heterogeneous interactions that the sedimentation/diffusion process of reacting systems may be described to a good approximation as that of sedimentation and diffusion of non–reacting systems with the apparent sedimentation and diffusion coefficients following a binding isotherm (Dam & Schuck, 2005; Dam *et al.*, 2005). This result suggests that at conditions close to saturation of the largest oligomer, the apparent weight–average f/f_0 value from *c(s)* should be close to the true f/f_0 value of the largest oligomers. Any error in this approximation would lead to an underestimation of the molecular weight and underestimation of the shape asymmetry.

Therefore, if multiple species are present, the frictional ratio derived with SEDFIT for a *c(s)* distribution is an approximation of the true f/f_0 because it is calculated as an average of the frictional ratios of all the species present. In the sample at 1.96 mg/mL, >90% of the total protein sediments as the 13 S peak; therefore, the fitted f/f_0 is a good approximation of the true frictional ratio of the 13 S sedimenting species. The resulting *c(M)* distribution is shown in Figure 3.1B and indicates that the larger oligomers have an average molecular weight of ~320–330 kDa, which is consistent with a ~14–mer.

As mentioned above, the *c(s)* distribution of wild–type Hsp27 also exhibits peaks with other S values. Between 2 S to 4 S there is a peak that does not shift with increasing protein concentration but that decreases in relative amount with increasing protein concentration. Thus, wild–type Hsp27 forms large oligomers, but a small fraction of the protein always takes the form of smaller oligomers that are probably monomers or an equilibrium mixture of monomers and dimers, which are in equilibrium with the larger oligomers. The final peak observed in the *c(s)* distribution (4 S–6 S) is presumably an intermediate in the association reaction.

The data obtained from this analysis are not sufficiently detailed to define a model for association of wild–type Hsp27, but the weight average sedimentation coefficients S_{av} can nonetheless be fitted to various models with the isotherm fitting routine of the SEDPHAT program which provides a rigorous means of deriving association constants for systems of this type (Schuck, 2003). The present data for wild–type Hsp27 fit well as a monomer ↔ tetramer ↔ n–mer with n = 12, 14 or 16. Discrimination between these three models is not possible, but the smallest square root of variance was obtained for n = 16. Notably, inclusion of the tetrameric intermediate in the model was required for

convergence. The fits of the data to these models with and without the tetrameric intermediate are shown in Figure 3.2A–D.

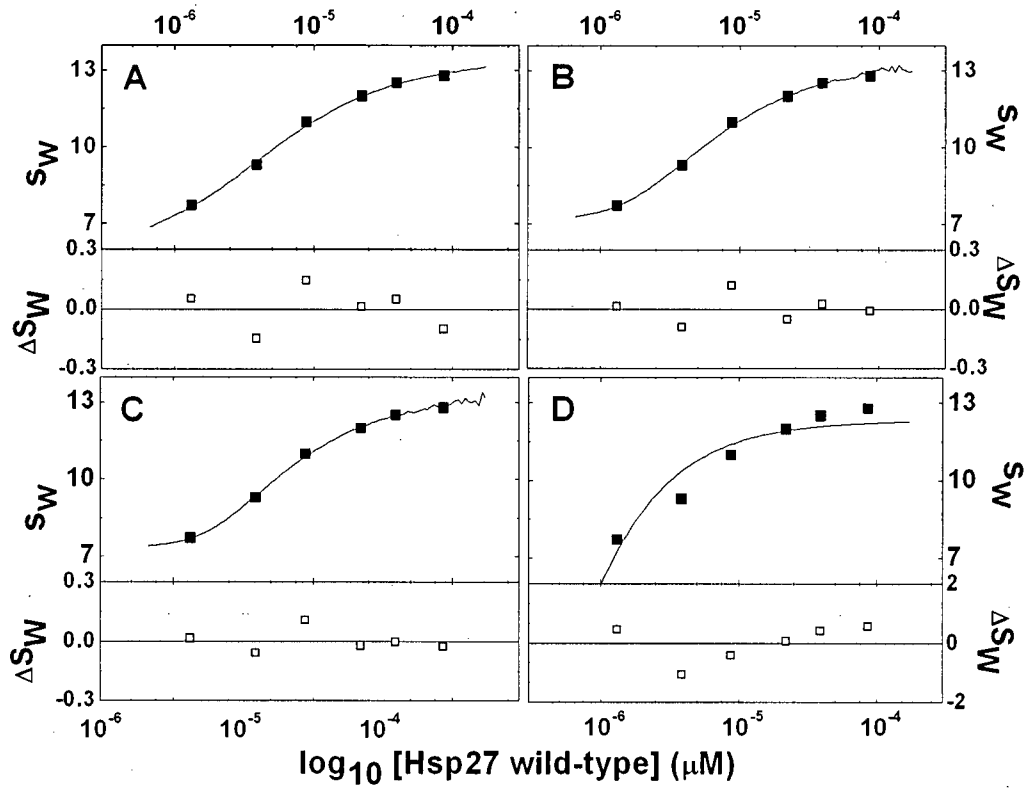

Figure 3.2. Isotherm fitting of the S_{av} of wild–type Hsp27. The isotherm fitting option in the program SEDPHAT was used to fit the S_{av} of the Hsp27 wild–type. Fitting as A, 1 ↔ 4 ↔ 12; B, 1 ↔ 4 ↔ 14; or C, fitting as 1 ↔ 4 ↔ 16. D, Fitting as 1 ↔ 12 without including an intermediate species.

Although the simplest model that fits the data is monomer ↔ tetramer ↔ 12–mer, the other two models are equally in agreement with the experimental data. The association constants obtained from the Sedphat fits are $0.2 \times 10^8\,M^{-3}$ for the monomer ↔ tetramer equilibrium from all the fits and $0.7 \times 10^6\,M^{-2}$ and $0.7 \times 10^6\,M^{-3}$ for the tetramer ↔ 12–mer and tetramer ↔ 16–mer equilibrium respectively. This result can be seen in the *c(s)* distributions in that most of the protein occurs in the 13 S species at the highest concentration used (86.5 μM) while at the lowest concentration (1.3 μM) the S_{av} is 8.02, indicating that most of the protein is present in the tetramer ↔ 12/16–mer equilibrium. The association constants are large, but the kinetics of self–association are fast on this time scale, and some smaller oligomers are present under all circumstances.

Sedimentation equilibrium experiments were run to confirm the velocity experiment results. In equilibrium, the sedimentation profile is directly proportional to the protein size and does not depend on hydrodynamic factors such as protein shape; hence, the results are complementary to velocity experiments and can be more precise for the determination of association constants. On the other hand, data analysis of equilibrium runs is highly dependent on the model to which the data are fit.

Sedimentation equilibrium experiments (9,000 rpm) were performed with wild–type Hsp27 at six protein concentrations (0.3–1.5 mg/mL). The apparent molecular weight obtained by a global fit is 390 kDa, and the data are fit well in terms of a monomer ↔ 18–mer equilibrium (floating N gave N = 17.7) with square root of variance of 1.6×10^{-2} (Figure 3.3A–C). The best fit (square root of variance = 9.9×10^{-3}) for the three lowest concentrations (0.3, 0.45, 0.6 mg/mL) was obtained with the model for the monomer ↔ 14–mer equilibrium (allowing N to vary produces N= 14.3) (Figure 3.4A–C).

The apparent molecular weight obtained from the global fit at all protein concentrations is slightly greater than that derived from the sedimentation velocity experiments. This result might reflect the presence of some aggregates with sedimentation coefficient >13 S and the inability of this technique to discriminate between species in a complex mixture. Interestingly, at the lowest Hsp27 concentration, the sedimentation equilibrium results agree exactly with the results obtained from the sedimentation velocity experiments.

3.1.2 Ionic strength, pH and ion–specific dependence of self–association

The self–association of wild–type Hsp27 (~1 mg/mL) was studied as a function of ionic strength at pH 8.4, and the data were analyzed with the program SEDFIT. The variation of the weight average sedimentation coefficients (S_{av}) as a function of [NaCl] obtained from this analysis (Figure 3.5A) demonstrates that the state of oligomerization does not change significantly upon increasing the ionic strength from 0.05 to 1 M sodium chloride.

To evaluate the possible role of titratable functional groups in Hsp27 oligomerization, sedimentation velocity experiments were performed from pH 6.5 to 8.4. The results obtained with the wild–type protein (0.6 mg/mL) (Figure 3.5B) establish that the self–association of this protein (as reflected by S_{av}) is independent of pH between pH 7 and 8.4. On further lowering the pH to 6.5, the wild–type protein exhibited an increase in S_{av}.

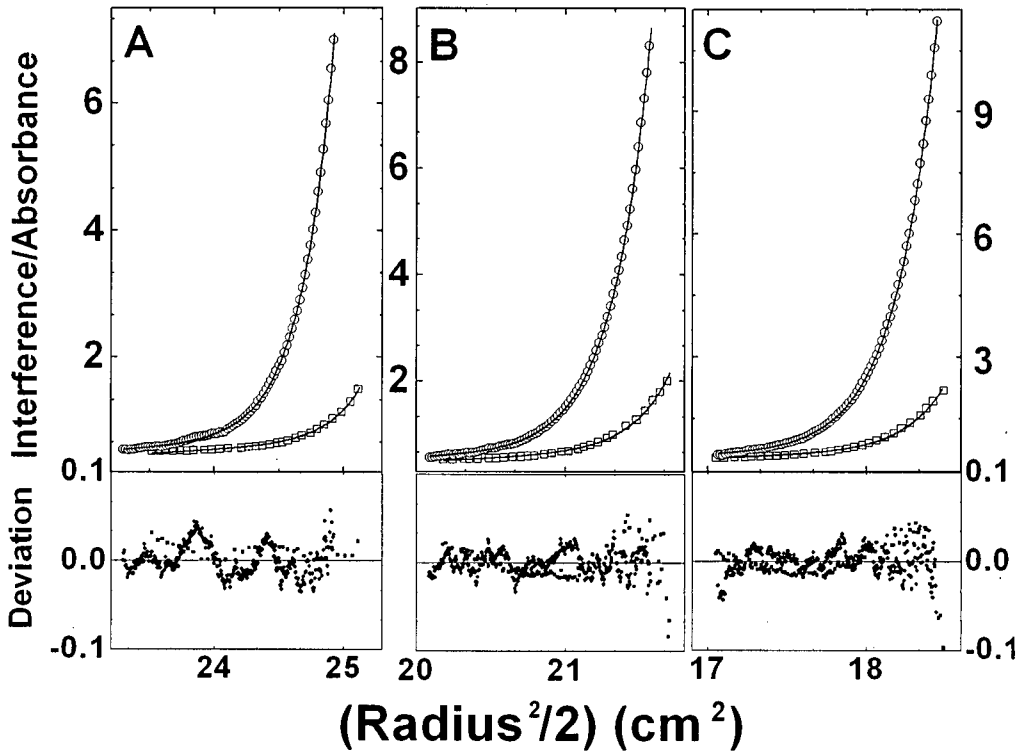

Figure 3.3. Sedimentation equilibrium analysis of wild-type Hsp27 (Tris–HCl buffer (20 mM (pH 8.4), 100 mM NaCl, 20 °C)). Global fitting analysis assuming a monomer ↔ 18mer model for [Hsp27] of A, 0.3 mg/mL (open square) and 0.75 mg/mL (open circle); B, 0.45 mg/mL (open square) and 1.0 mg/mL (open circle) and C, 0.6 mg/mL (open square) and 1.5 mg/mL (open circle). For clarity, only every third point is shown. Closed circles and squares represent deviation. The square root of variance is 1.6×10^{-2}

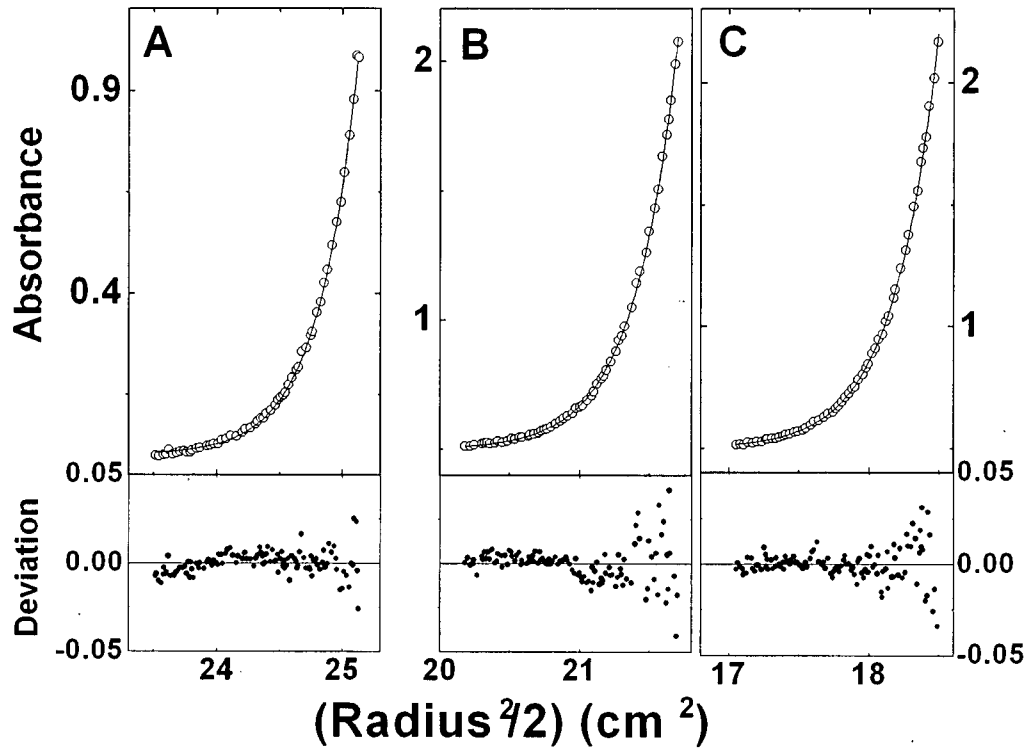

Figure 3.4. Sedimentation equilibrium analysis of wild-type Hsp27 at low concentration (Tris–HCl buffer (20 mM (pH 8.4), 100 mM NaCl, 20 °C)). Global fitting analysis assuming a monomer ↔ 14mer model for [Hsp27] of A, 0.3 mg/mL; B, 0.45 mg/mL and C, 0.6 mg/mL. For clarity, only every second point is plotted. Closed circles indicate the deviation; the square root of variance is 9.9×10^{-3}.

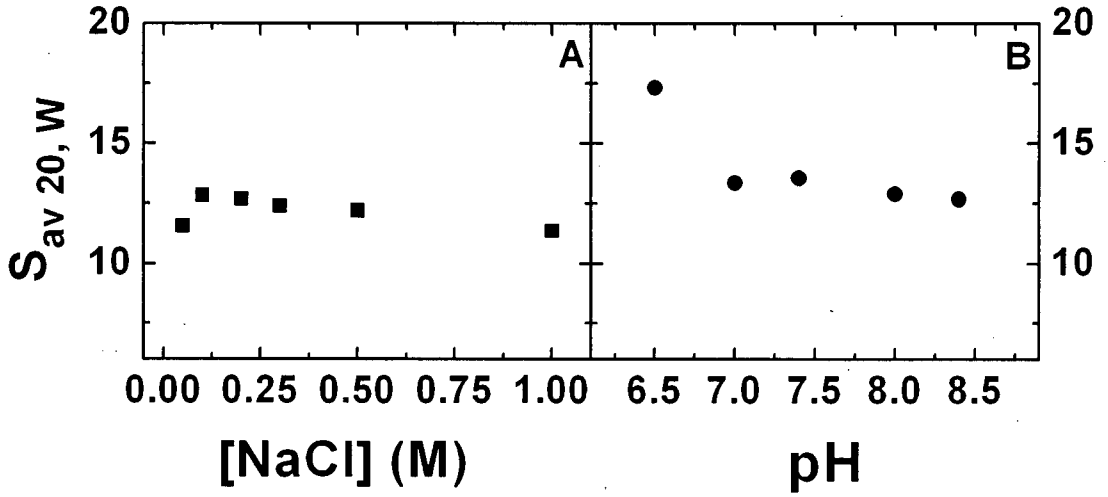

Figure 3.5. Sedimentation velocity analysis of wild–type Hsp27 as a function of pH and ionic strength. A, dependence of S_{av} on [NaCl] for wild–type Hsp27 (0.6 mg/mL); B, dependence of S_{av} on pH for wild–type Hsp27 (1 mg/mL).

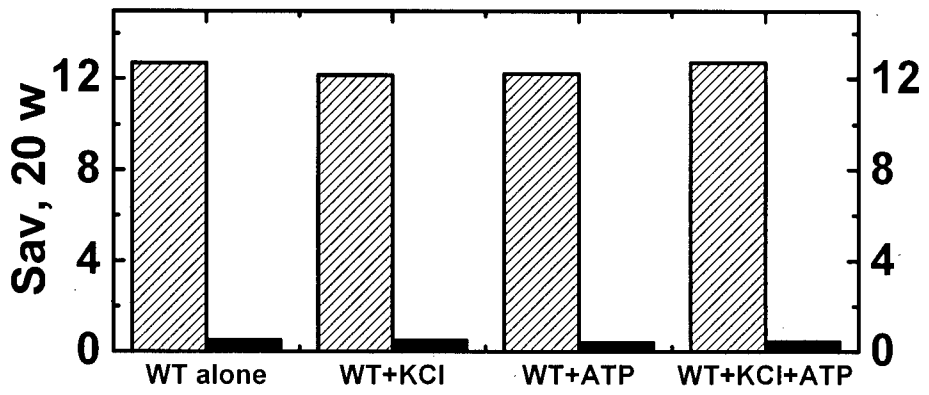

Figure 3.6. Sedimentation velocity analysis of wild–type Hsp27 in the presence of KCl and/or ATP. Grey columns, S_{av} for wild–type Hsp27 KCl 10 mM and/or ATP 10 mM, black columns, protein concentration in mg/mL.

This behavior is presumably related to the fact that Hsp27 is not soluble at its p*I* (predicted to be ~ 6.0 (Gasteiger *et al.*, 2005)). α–Crystallin has been shown to bind unfolding polypeptide to form stable complexes. In the presence of ATP, K^+ and Mg^{2+}, the complexes become unstable and release of the unfolded polypeptide is observed (Wang & Spector, 2001). In this study, the presence of potassium (10 mM) and ATP (10 mM) do not alter the self–association of wild–type Hsp27 (27 μM) (Figure 3.6). Similar results were obtained in the presence of 2.2 mM Mg^{2+} (data not shown).

3.1.3 Thermally induced self–association of wild–type Hsp27

Sedimentation velocity analyses of wild–type Hsp27 at 10, 30 and 40 °C and protein concentrations ranging from 0.04 to 1.79 mg/mL were compared with the corresponding results previously described and obtained at 20 °C. The *c(s)* data obtained as a function of temperature (10, 20, 30 and 40 °C) are shown in Figure 3.7. As well, the weight average sedimentation coefficients as a function of protein concentration and the S_{av} *vs.* temperature for a given concentration (~0.9 mg/mL) are shown in Figure 3.8A–B).

As observed previously at 20 °C, the width of the peaks observed in the *c(s)* distribution at the various temperatures studied in this work are greater than expected for discrete, non–interacting components. However, as previously mentioned, by increasing the protein concentration sufficiently, the peak of the *c(s)* distribution approaches the peak of the largest oligomer. Therefore, the increase in S_{av} with increased protein concentration at all temperatures studied (10 to 40 °C) is consistent with our previous observations at 20 °C and indicates that at all temperatures, Hsp27 behaves as a self–associating system.

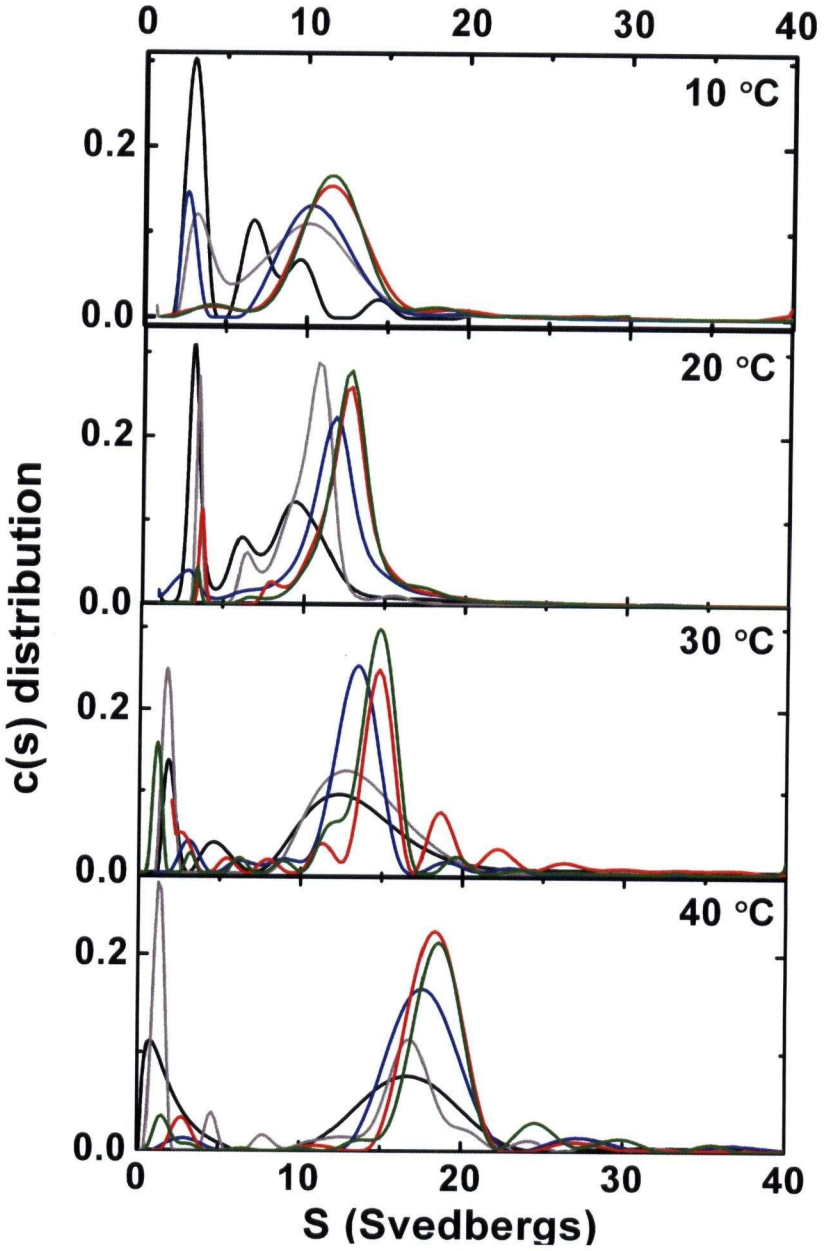

Figure 3.7. Sedimentation velocity analysis of wild–type Hsp27 as function of temperature and concentration (20 mM Tris–HCl, pH 8.4, 100 mM NaCl). From to panel: *c*(*s*) distribution at 10 °C: black line, 0.06 mg/mL; gray line, 0.1 mg/mL; blue line, 0.18 mg/mL; red line, 0.69 mg/mL; olive line, 1.09 mg/mL. *c*(*s*) distribution at 20 °C: black line, 0.03 mg/mL; light gray line, 0.09 mg/mL; blue line, 0.2 mg/mL; red line, 0.5 mg/mL; olive line, 0.89 mg/mL; *c*(*s*) distribution at 30 °C: black line, 0.04 mg/mL; light gray line, 0.1 mg/mL; blue line, 0.16 mg/mL; red line, 0.86 mg/mL; olive line, 1.79 mg/mL. *c*(*s*) distribution at 40 °C: black line, 0.05 mg/mL; gray line, 0.08 mg/mL; blue line, 0.17 mg/mL; red line, 0.56 mg/mL; olive line, 0.95 mg/mL.

Moreover, the fact that the S_{av} seems to reach a plateau indicates that the largest oligomers formed at each temperature were approached. Surprisingly, however, self–association of Hsp27 exhibits an unusual dependence on temperature such that on increasing the temperature from 10 to 40 °C, even larger oligomers form (Figure 3.8A). The *c(s)* plots (Figure 3.7) show that at all temperatures some small oligomers are present in solution especially at the lowest concentration analyzed.

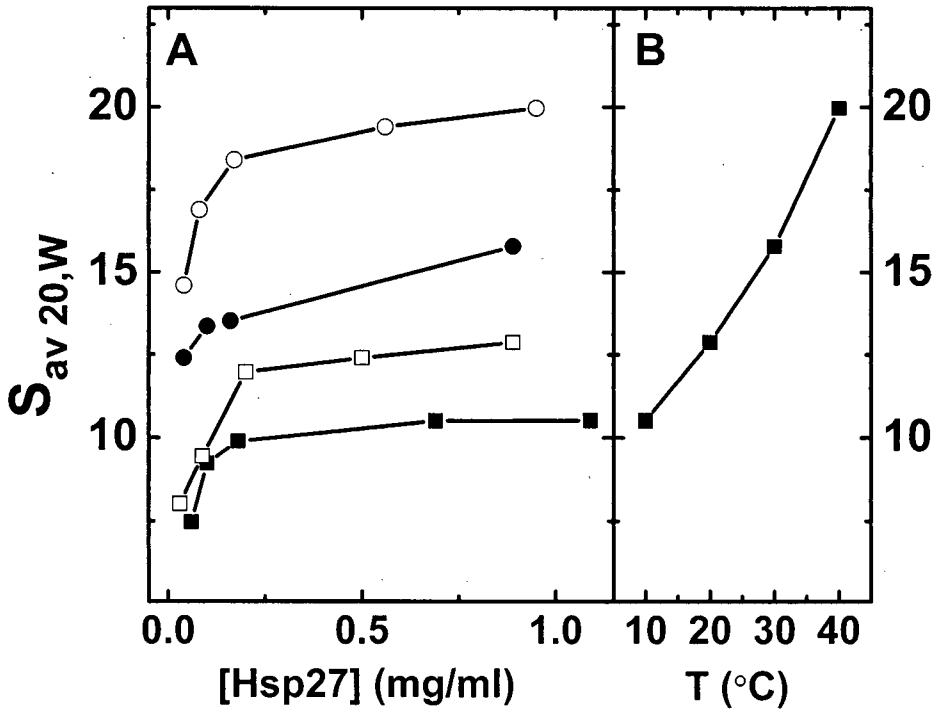

Figure 3.8. Average sedimentation coefficient of wild–type Hsp27 as a function of concentration and temperature. A, concentration dependent S_{av} distribution; closed squares, 10 °C; open squares, 20 °C; closed circles, 30 °C; open circles, 40 °C. B, dependence of S_{av} on temperature of the samples at 10 °C (1.09 mg/mL or 0.69 mg/mL), 20 °C (0.95 mg/mL) 30 °C (0.95 mg/mL), and 40 °C (0.89 mg/mL).

Consequently, the conclusion that Hsp27 dissociates into monomers and dimers independent of the temperature at which the experiments are run while the upper limit of oligomer size varies directly with temperature was drawn.

While the three–dimensional structure of Hsp27 is not known, the few available crystal structures of small heat shock proteins and all results derived from electron microscopy indicate that sHsps are nearly spherical proteins. This characteristic is reflected by the frictional coefficient (1.2 to 1.4) obtained from analysis of the current data with SEDFIT and molecular weights consistent with the known masses of sHsps. At the highest protein concentrations used in this study, the obtained frictional coefficients ratios (f/f_0) of 1.30 (10 °C), 1.37 (30 °C) and 1.22 (40 °C). Assuming these values as the frictional coefficient for the largest Hsp27 oligomers observed at each temperature, we can deduce that self–association results in fairly compact quaternary structures and can estimate the size of the oligomers formed at each temperature. At 10 °C, a broad peak spans from small S values up to 10 S, indicating that the largest sedimenting species is probably no larger than an 8–10–mer. At 30 °C, the main peak has an S value that spans 13–15 S, indicating that the main sedimenting species has the size of a 16–mer to 20–mer. At 40 °C, the main component sediments with S of 18–22 S, indicating that the main sedimenting species is in the range of a 22–mer to a 30–mer.

Repetition of velocity experiments with wild–type Hsp27 in phosphate buffer (20 mM pH 7.4, 100 mM NaCl, 40 °C) resulted in identical behavior, so this result does not arise from the thermodynamic properties of the buffer (data not shown). The reversibility of this temperature dependent self–association was demonstrated by the observation that *c(s)* plots obtained from samples that were heated for 2 h at 42 °C prior to

sedimentation velocity analysis at 20 °C exhibited the same degree of self–association as observed for protein maintained at 20 °C (Figure 3.9). This latter result indicates that oligomerization of Hsp27 at elevated temperature is attributable to the formation of well–defined, higher order oligomers rather than to non–specific aggregation.

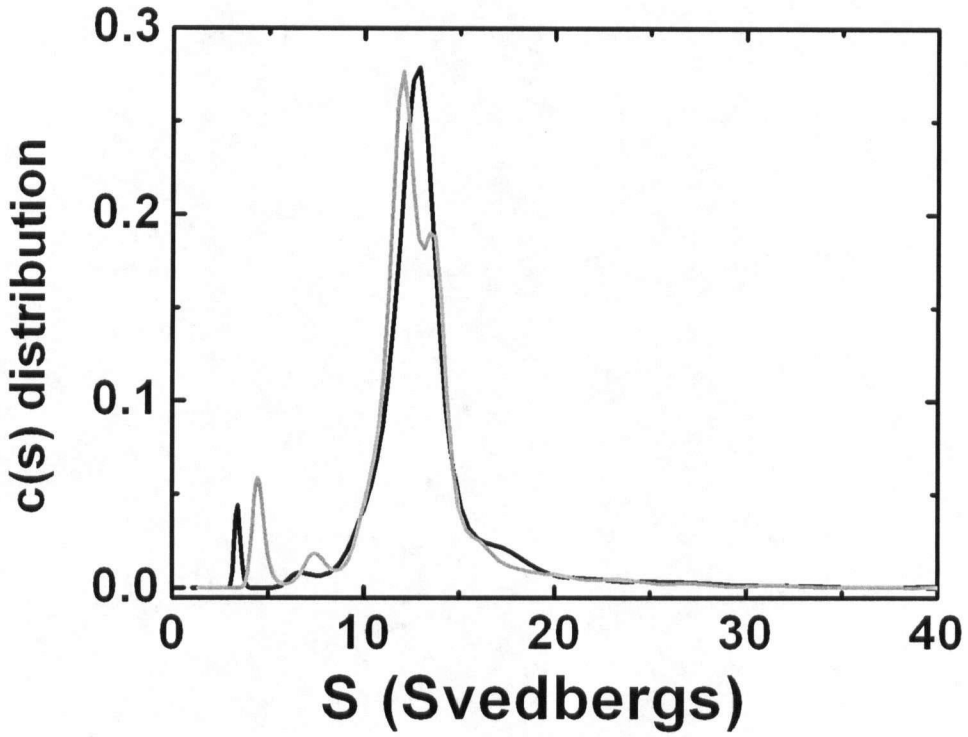

Figure 3.9. Reversibility of the temperature dependent self–association of wild–type Hsp27. Sedimentation velocity analysis of wild–type Hsp27 (Tris–HCl buffer (20 mM (pH 8.4), 100 mM NaCl, 20 °C)). *c*(*s*) distribution: black line, 0.9 mg/mL sample kept at 20 °C; grey line, 0.9 mg/mL sample incubated at 42 °C and run in the centrifuge at 20 °C.

Moreover, incubation at 40 °C for longer periods of time (up to 8 h prior to start the sedimentation velocity experiments) did not change the upper limit of size of oligomers formed (data not shown). As indicated above, limitations in instrument design prevented use of higher temperatures in these experiments.

3.1.4 Effect of phosphorylation on Hsp27 oligomerization

Replacement of three key serine residues (position 15, 78, 82) with aspartic acid mimics the effect of Hsp27 phosphorylation *in vitro* (Rogalla *et al.*, 1999). The corresponding Hsp27 S15D/S78D/S82D variant (Figure 1.9), was purified to determine what effect the introduction of these charged residues has on protein oligomerization.

Velocity experiments with the S15D/S78D/S82D Hsp27 variant were carried out at concentrations ranging from 0.03 to 2 mg/mL. The resulting *c(s)* distributions obtained for these samples establish that the principal form of this variant sediments at ~ 2.7 S, but smaller forms sedimenting at greater S values are also evident (Figure 3.10). At the lowest concentration (0.03 mg/mL), 95% of the protein sediments at 2.6 S (monomer or monomer ↔ dimer), and only 5% of the protein sediments with $S_{av} = 8.7$ (total $S_{av} = 2.83$). Increasing the concentration of the variant to 2.0 mg/mL increases S_{av} to 3.94 as expected for a self–associating protein. A similar pattern was observed for the S15D/S78D/S82D/C137S Hsp27 variant, indicating that the sole cysteinyl residue of Hsp27, Cys^{137}, does not influence the self–association of Hsp27 significantly through disulfide bond formation (Figure 3.11).

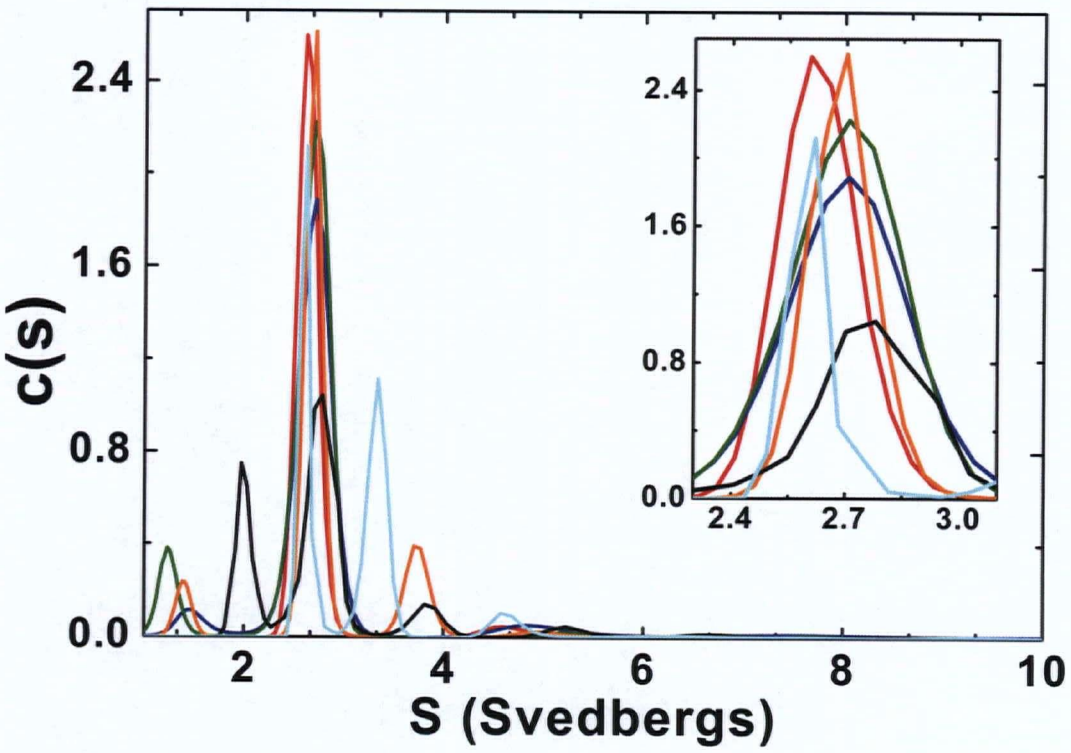

Figure 3.10. Sedimentation velocity analysis of S15D/S78D/S82D Hsp27 (Tris–HCl buffer (20 mM (pH 8.4), 100 mM NaCl, 20 °C)). *c(s)* distribution of S15D/S78D/S82D Hsp27: red line, 0.03 mg/mL; blue line, 0.14 mg/mL; olive green line, 0.31 mg/mL; orange line, 0.6 mg/mL; black line, 1.0 mg/mL; cyan line, 2.0 mg/mL. The inset expands the region of 2.3 to 3.1 S for clarity

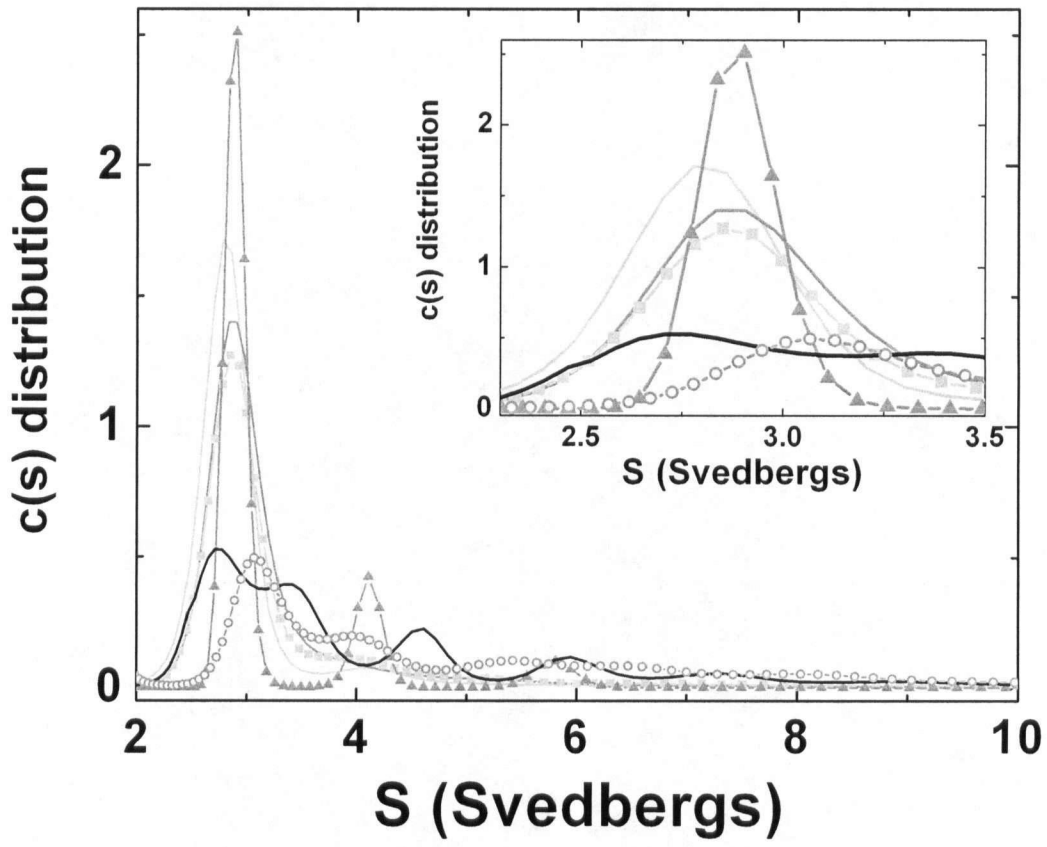

Figure 3.11. Sedimentation velocity analysis of S15D/S78D/S82D/C137S Hsp27 (Tris–HCl buffer (20 mM (pH 8.4), 100 mM NaCl, 20 °C)). *c(s)* distribution: light grey, 0.28 mg/mL; grey line, 0.34 mg/mL; light grey squares, 0.37 mg/mL; grey triangles, 0.6 mg/mL; black line, 1.2 mg/mL; grey open circles, 2.4 mg/mL. The inset expands the region of 2.3 to 3.5 S for clarity

As for the wild–type protein, sedimentation equilibrium experiments were performed with the triple variant to corroborate the results of the velocity experiments. Indeed, sedimentation equilibrium analyses of the S15D/S78D/S82D variant confirmed that this protein is a self–associating system. The apparent molecular weight of this variant varies directly with protein concentration (Table 3.1), reflecting both the reversibility of the association and its polydispersity. The best fit to these data was obtained for a monomer $\leftrightarrow$ 12–mer model (square root of variance = 1.46×10^{-2}). Nevertheless, acceptable uncertainties were also obtained for monomer $\leftrightarrow$ octamer and monomer $\leftrightarrow$ 16–mer models. As for the wild–type protein, this variant is capable of forming large oligomers, but the equilibrium is shifted toward smaller species, primarily monomers and/or dimers.

Sedimentation velocity experiments were performed with the triple variant as a function of ionic strength, pH and at temperature to determine if any of these factors can influence the oligomerization of this protein.

Table 3.1. Apparent molecular weight of the S15D/S78D/S82D Hsp27 variant as a function of protein concentration and rotor speed.

[Hsp27 S15D/S78D/S82D]	8,000 rpm	12,000 rpm	20,000 rpm
0.12 mg/mL	85.0 kDa	32.2 kDa	24.4 kDa
0.3 mg/mL	94.6 kDa	57.9 kDa	30.2 kDa
0.6 mg/mL	97.7 kDa	81.5 kDa	40.5 kDa

Values are calculated from the fit of each species separately in the program. Experiments were performed in Tris–HCl buffer (20 mM (pH 8.4), 100 mM NaCl, 20 °C), and data were analyzed with the program WinNonlin.(Johnson *et al.*, 1981)

The S15D/S78D/S82D Hsp27 variant (0.3 mg/mL) exhibited unchanging self–association from pH 6.0 to 8.0. Moreover, the largest oligomers are observed in the presence of 0.2 M NaCl (Figure 3.12A–B), and, as for the wild–type protein, S_{av} was essentially independent of ionic strength.

The S15D/S78D/S82D Hsp27 variant was also studied at 40 °C to determine if an increase in temperature shifts the equilibrium towards the formation of larger oligomers as observed for the wild–type protein. As indicated in the *c(s)* plots (Figure 3.13A) and by the corresponding S_{av} values (Figure 3.13B), the self–association behavior of this variant at low concentration does not change when the temperature is raised from 20 to 40 °C

To identify the oligomeric species of the triple variant present in solution at 40 °C, the discrete species model in SEDPHAT (Schuck, 2003) was used to provide a global analysis of the data at all three concentrations. The best fit was obtained by fixing the molecular weight and fitting the sedimentation coefficients for a mixture of monomers and dimers. The sedimentation coefficients obtained were 2.14 S for the monomer and 3.01 S for the dimer (Figure 3.13A, inset). The square roots of variance for the three concentrations were 13, 12 and 11 millifringes for high, medium and low concentrations, and the deviations were scattered randomly.

Interestingly, at much greater protein concentration (3.3 mg/mL), the *c(s)* plot indicated the presence of small amounts of larger oligomers that sediment with S similar to that observed for the wild–type protein, indicating that self–association of the triple variant

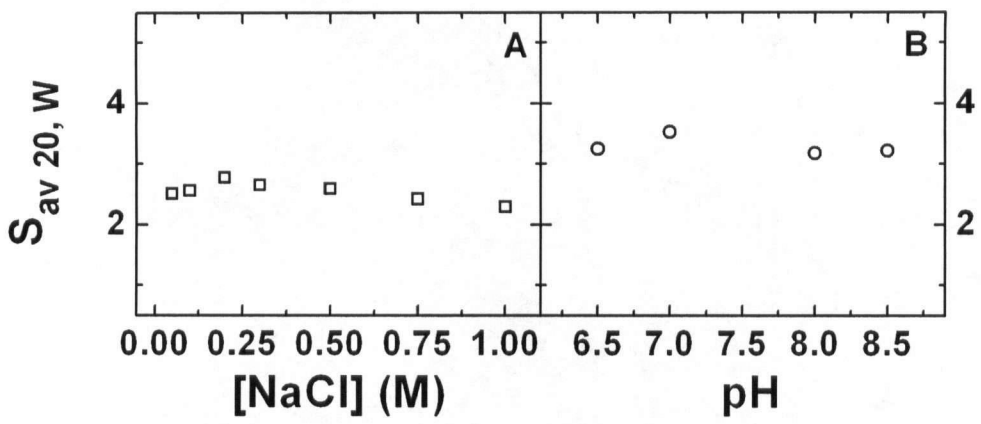

Figure 3.12 Sedimentation velocity analysis of the S15D/S78D/S82D Hsp27 variant as a function of pH and ionic strength. (a) Dependence of S_{av} on [NaCl] (0.6 mg/mL), and (b) Dependence of S_{av} on pH (0.3 mg/mL).

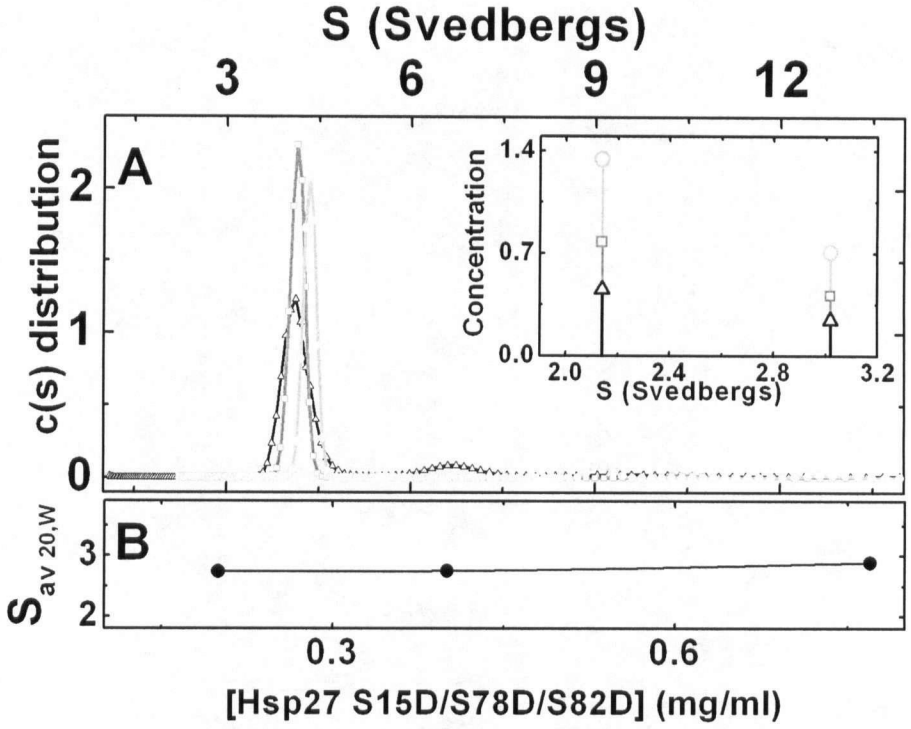

Figure 3.13. Sedimentation velocity analysis of the S15D/S78D/S82D Hsp27 variant at 40 °C in Tris–HCl buffer (20 mM, pH 8.4, 100 mM NaCl, 40 °C). A. *c(s)* distribution of S15D/S78D/S82D Hsp27: black triangles, 0.20 mg/mL; dark grey squares, 0.40 mg/mL; light grey circles, 0.77 mg/mL. Inset: SEDPHAT analysis for a monomer/dimer mixture. B. Dependence of $S_{av\ 20,W}$ on concentration of the triple variant protein.

is also dependent on temperature. In fact, at this protein concentration, 55% of the variant sediments with 2–10 S (S_{av}= 3), 5% with 10–20 S (S_{av}= 9.6) and 40% with 20–40 S (S_{av}= 20). From this analysis, it is clear that the size of the larger oligomers formed by the triple variant at elevated temperature is similar to that observed for the wild–type protein under the same conditions, but the variant forms little of these large species.

3.1.5 Role of the N– and C– termini in Hsp27 oligomerization.

To evaluate the role of the highly conserved N–terminal WDPF domain in Hsp27 oligomerization, the Δ1–14 Hsp27 variant (which lacks the first 14 residues but retains the WDPF domain) and the Δ1–24 Hsp27 variant (which lacks the first 24 amino acids including the WPDF domain) (Figure 1.9) were studied by sedimentation velocity analysis. Both the Δ1–14 Hsp27 variant (0.02 to 1.5 mg/mL) and the Δ1–24 Hsp27 variant (0.02 to 1.2 mg/mL) exhibit diminished oligomeric size and more discrete speciation in the *c(s)* distribution (Figure 3.14A–B) than observed for the wild–type protein (Figure 3.8)

Notably, the S_{av} for the Δ1–14 Hsp27 variant is greater than that for the Δ1–24 Hsp27 variant, and both are less than S_{av} for the wild–type protein (Figure 3.15). This observation establishes that while the WDPF domain contributes to formation of larger oligomeric species, the entire N–terminal sequence is required to form oligomers of the size exhibited by wild–type Hsp27. The position of each of the peaks in the *c(s)* distribution of the variants changes slightly, but none of the peaks is eliminated at higher protein concentration, and S_{av} of the Δ1–24 Hsp27 variant does not change significantly with increasing protein concentration.

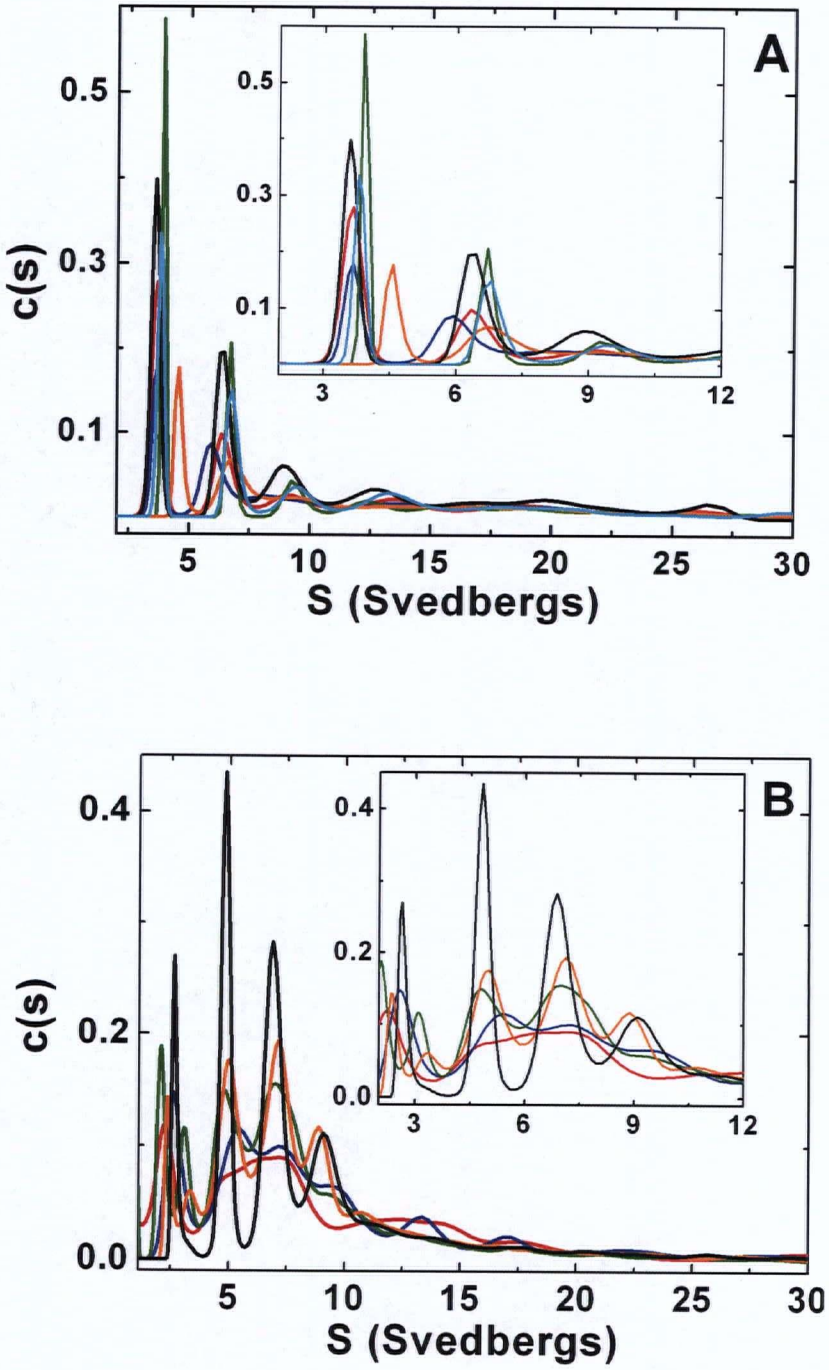

Figure 3.14. Sedimentation velocity analysis of Hsp27 N–terminal deletion variants (Tris–HCl buffer (20 mM (pH 8.4), 100 mM NaCl, 20 °C)). (A) *c(s)* distribution of the Δ1–14 Hsp27 variant: red line, 0.02 mg/mL; blue line, 0.07 mg/mL; olive green line, 0.14 mg/mL; orange line, 0.55 mg/mL; black, 1.08 mg/mL; cyan line, 1.5 mg/mL. (B) *c(s)* distribution of Δ1–24 Hsp27: red line, 0.02 mg/mL; blue line, 0.14 mg/mL; olive green line, 0.42 mg/mL; orange line, 0.77 mg/mL; black line, 1.23 mg/mL. The insets expand the region of 4–12 S for clarity.

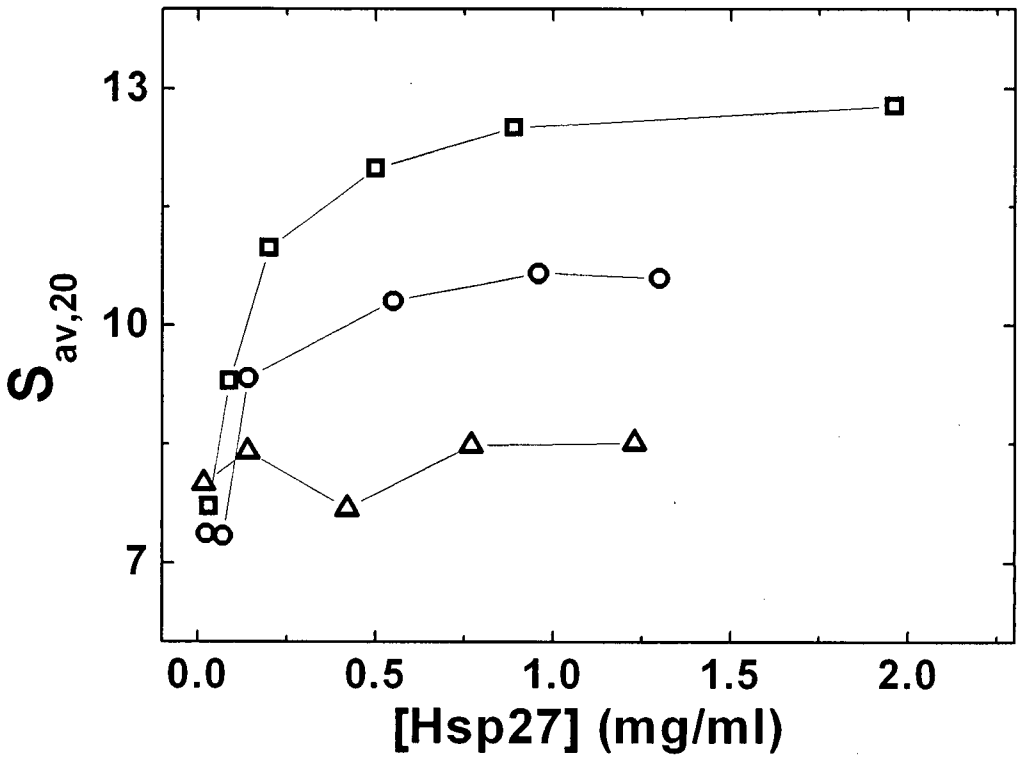

Figure 3.15 S_{av} *vs.* Hsp27 concentration for wild–type Hsp27 vs. ΔN–deletion variants. Wild–type Hsp27 (square), Δ1–14 Hsp27 (circle), and Δ1–24 Hsp27 (triangle).

Interestingly, the variant Δ1–24 S78D/S82D Hsp27, which not only lacks the first 24 residues but also contains two of the three Ser→Asp substitutions behaves more like the Δ1–24 Hsp27 variant than the S15D/S78D/S82D Hsp27 variant. A concentration dependent shift in oligomerization is observed (Figure 3.16) for this variant in which the largest species sediments with an S value only slightly smaller than that observed for the Δ1–24 Hsp27 variant.

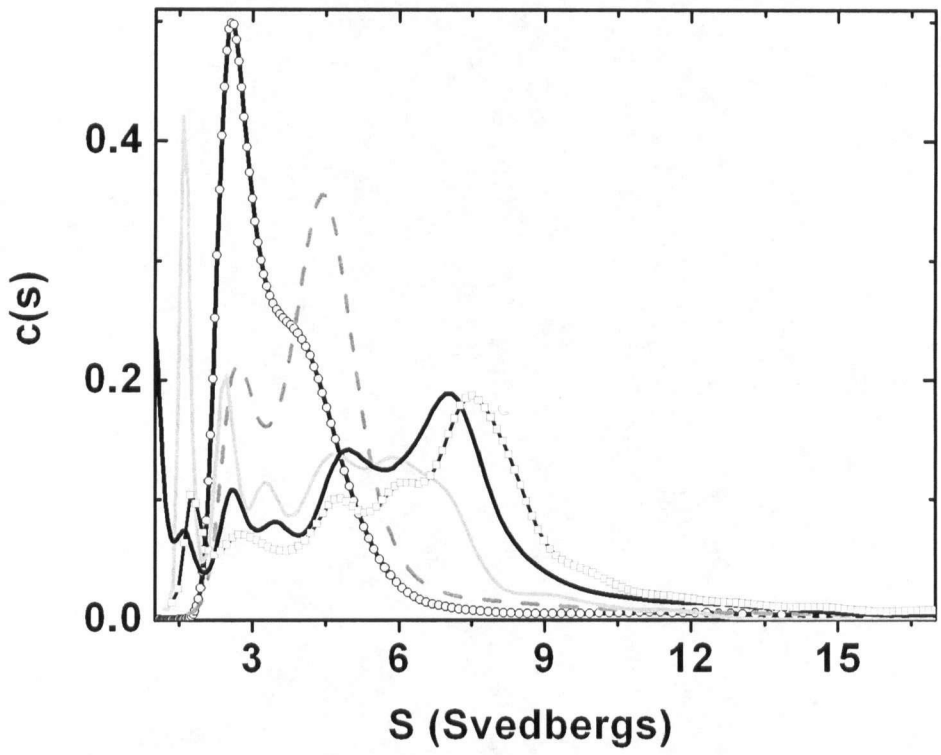

Figure 3.16. Sedimentation velocity analysis of Δ1–24 S78D/S82D Hsp27 in Tris–HCl buffer (20 mM, pH 8.4, 100 mM NaCl, 20 °C). *c(s)* distribution: open circles, 0.05 mg/mL; broken grey line, 0.20 mg/mL; light grey line, 0.4 mg/mL; black line, 0.83 mg/mL; open squares, 1.6 mg/mL.

Although, small heat shock proteins have a conserved α–crystallin domain near the C–terminus, the actual C–terminal tail is highly variable in length and amino acid sequence; it is very flexible, and its role in self–association it is not well understood. A variant of Hsp27 that lacks the last 24 amino acids (Δ182–205 Hsp27) (Figure 1.9) was prepared to evaluate the role of this region on protein self–association.

Under standard conditions (20 mM Tris–HCl pH 8.4, 100 mM NaCl at 20 °C), the Δ182–205 Hsp27 variant exhibits the *c(s)* concentration–dependent (0.02 to 0.75 mg/mL) distributions shown in Figure 3.17. The sedimentation behavior of this variant differs from that of the wild–type protein in that the species sedimenting at 13 S is not present, and a new, highly asymmetrical component sediments at higher S–values. In addition, the relative amount of protein sedimenting as the component with low S is greater than that observed for wild–type Hsp27. The Δ182–205 Hsp27 variant retains the highly conserved IXI sequence, which has been shown to form important hydrophobic intermolecular interactions in Hsp16.9 (van Montfort *et al.*, 2001), so this variant does retain some residues in this region that are believed to be important in self–association. Nevertheless, deletion of the 24 C–terminal residues of Hsp27 compromises oligomerization. On one hand, the total percentage of larger oligomers formed is reduced. On the other hand, the larger oligomers that do form are larger than those formed by the wild–type protein, indicating that the ability of this variant to control the upper limit of the larger oligomers has been compromised.

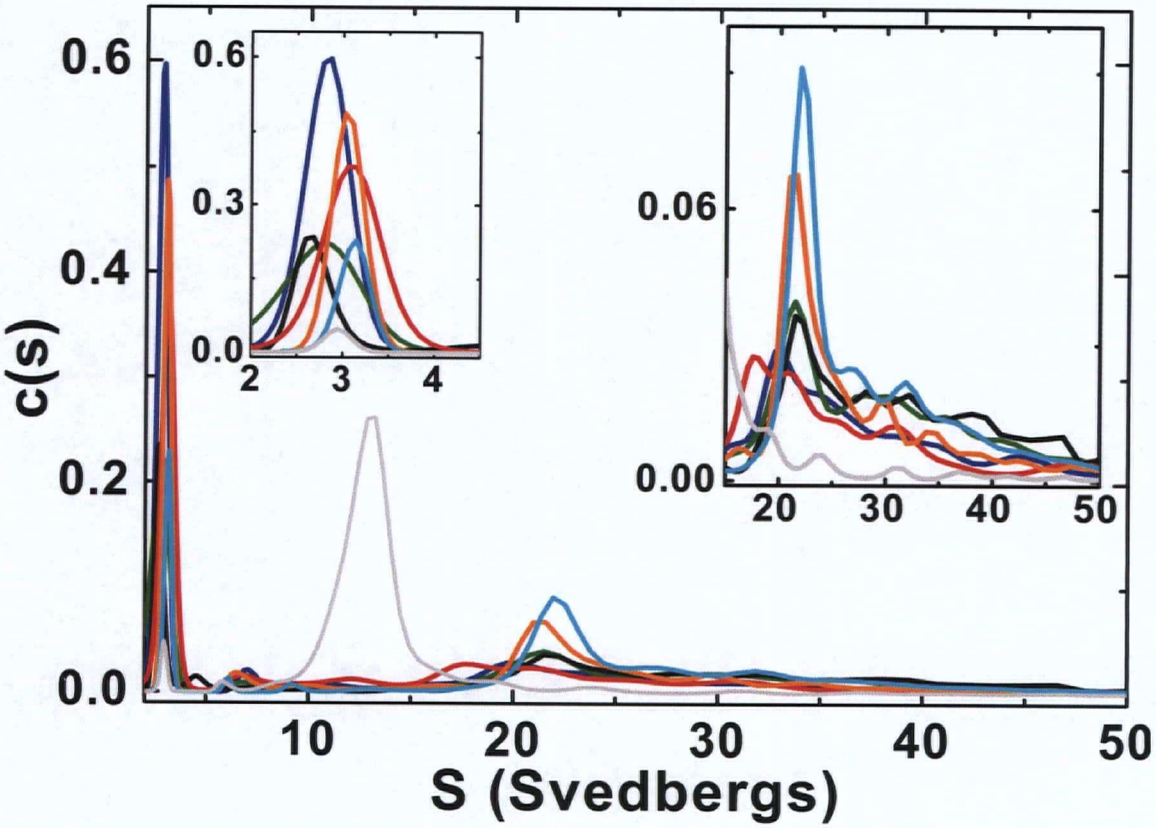

Figure 3.17 Sedimentation velocity analysis of Hsp27 C–terminal deletion variant (20 mM Tris–HCl buffer (pH 8.4), 100 mM NaCl, 20 °C). *c*(*s*) distribution analysis of the Δ182–205 Hsp27 variant: red line, 0.02 mg/mL; blue line, 0.09 mg/mL; olive green, 0.2 mg/mL; orange line 0.38 mg/mL; black line, 0.49 mg/mL; cyan line, 0.75 mg/mL. The grey line is the *c*(*s*) for wild–type Hsp27 at 1.96 mg/mL. The inset expands the regions of 2–5 S and 15–50 S for clarity.

3.1.6 Role of the N– and C– termini in temperature dependent self–association

The self–association behavior of the N–terminal deletion variant as observed by *c(s)* plots for sedimentation velocity data collected at 40 °C (Figure 3.18), is virtually unchanged from the behavior observed at 20 °C. The only difference observed is that a larger fraction (~ 40%) of the protein forms large aggregates with sedimentation coefficient between 30 and 150 S at elevated temperature.

Similar analysis of the C–terminal deletion variant Δ182–205 Hsp27 at 40 °C (Figure 19, gray line) reveals a major component around 30–32 S that corresponds to a 20–22 S species at 20 °C, and a less abundant smaller species (3.5 S). The *c(s)* plot of the Δ182–205 variant at 40 °C also differs slightly from the corresponding plot obtained at 20 °C in that the major peak is more symmetric, but the sedimentation coefficient of the primary sedimenting species at 20 and 40 °C is the same. Thus, self–association of the C–terminal deletion variant is independent of temperature as observed for the N–terminal deletion variant. However, while the N–terminal deletion variant exhibits small oligomers at 20 and 40 °C, the C–terminal deletion variant exhibits large oligomers at both temperatures. These results indicate that the C–terminus has a significant role in the thermally induced self–association of wild–type Hsp27. As discussed later, this result provides compelling evidence for a significant role for this C–terminal domain in the increased size of oligomers observed for the wild–type protein at elevated temperature.

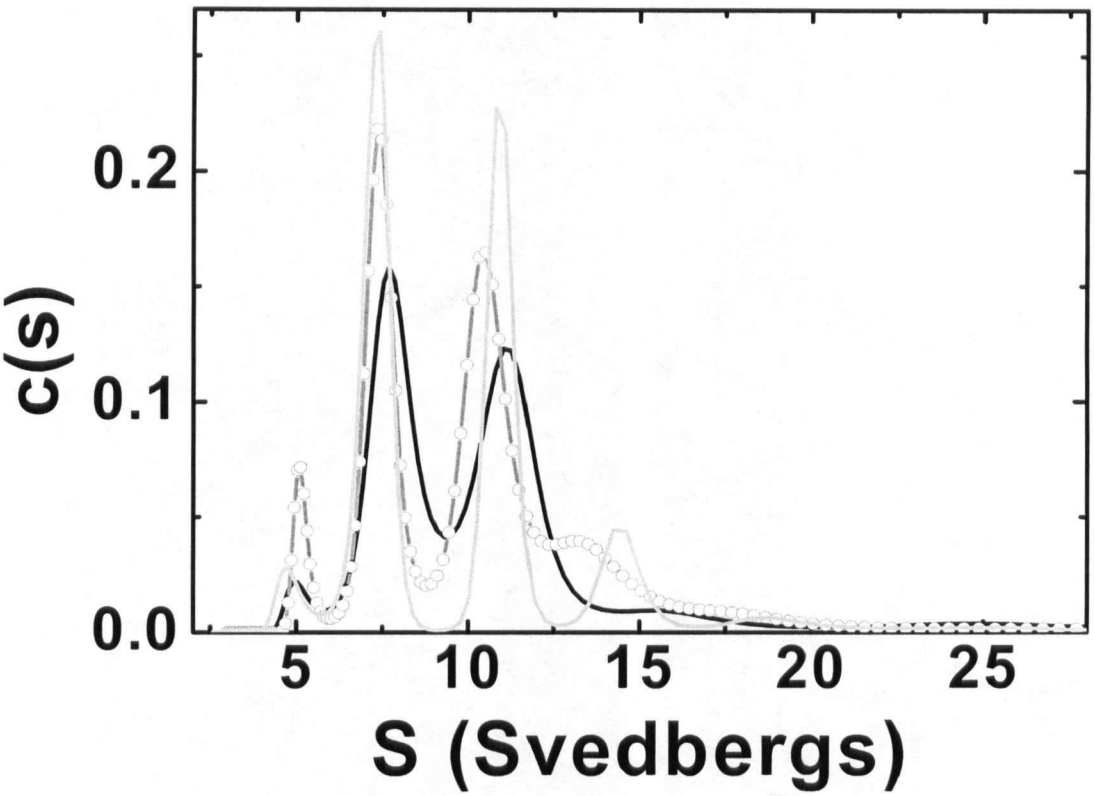

Figure 3.18 Sedimentation velocity analysis of the Hsp27 Δ1–24 N–terminal deletion variant at 40 °C (Tris–HCl buffer (20 mM (pH 8.4), 100 mM NaCl, 40 °C)). *c(s)* distribution: black line, 0.4 mg/mL; dark grey circles, 0.65 mg/mL; light grey line, 1.58 mg/mL.

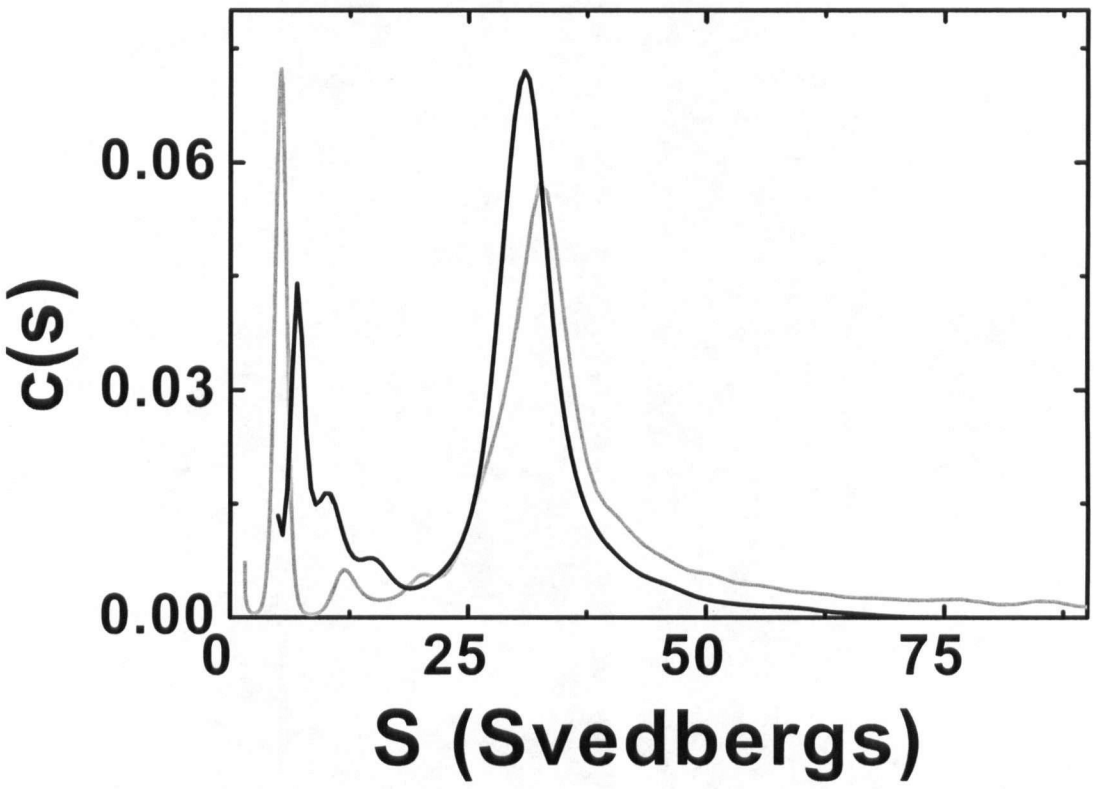

Figure 3.19 Sedimentation velocity analysis of Δ182–205 Hsp27 *vs.* wild-type Hsp27 at 40 °C. Gray line, *c*(*s*) distribution of Δ182–24 Hsp27 (0.20 mg/mL); black line, *c*(*s*) distribution of Δ182–24 Hsp27 (0.23 mg/mL). Analysis done with the program SEDFIT.

3.1.7 Oligomerization of His_6–tag Hsp27 variants

In view of the ease with which His–tagged proteins can be expressed and purified, and the fact that His_6–sHsp have been used in various experiments to represent the behavior of the wild–type protein (Guo & Cooper, 2000), two His_6–tagged proteins were characterized by sedimentation velocity analysis to determine if this longer Hsp27 behaves like the wild–type protein. The two variants of Hsp27 possessing N–terminal His_6–tag sequences (His_6–Hsp27 and His_6–S15D/S78D/S82D Hsp27) were purified, and, as indicated above (p 39), were found to resist efforts to use thrombin for removal of the His_6–tag. The *c(s)* distribution curves obtained at various concentrations of His_6–Hsp27 demonstrate that the N–terminal His_6–tag promotes much larger oligomeric forms than exhibited by the wild–type protein (Figure 3.20). Notably, a large component sedimenting between 25 and 75 S that is observed at protein concentrations as low as 0.08 mg/mL corresponds to a molecular weight of 0.5–5 MDa. A similar result is obtained for the His_6–S15D/S78D/S82D Hsp27 variant. In this case, a component sediments between 20 and 60 S at a protein concentration of 0.02 mg/mL (Figure 3.20). These results argue strongly against the use of any His–tagged form of Hsp27 as a substitute for the wild–type or any variant form of the protein in studies for which the state of oligomerization is a concern.

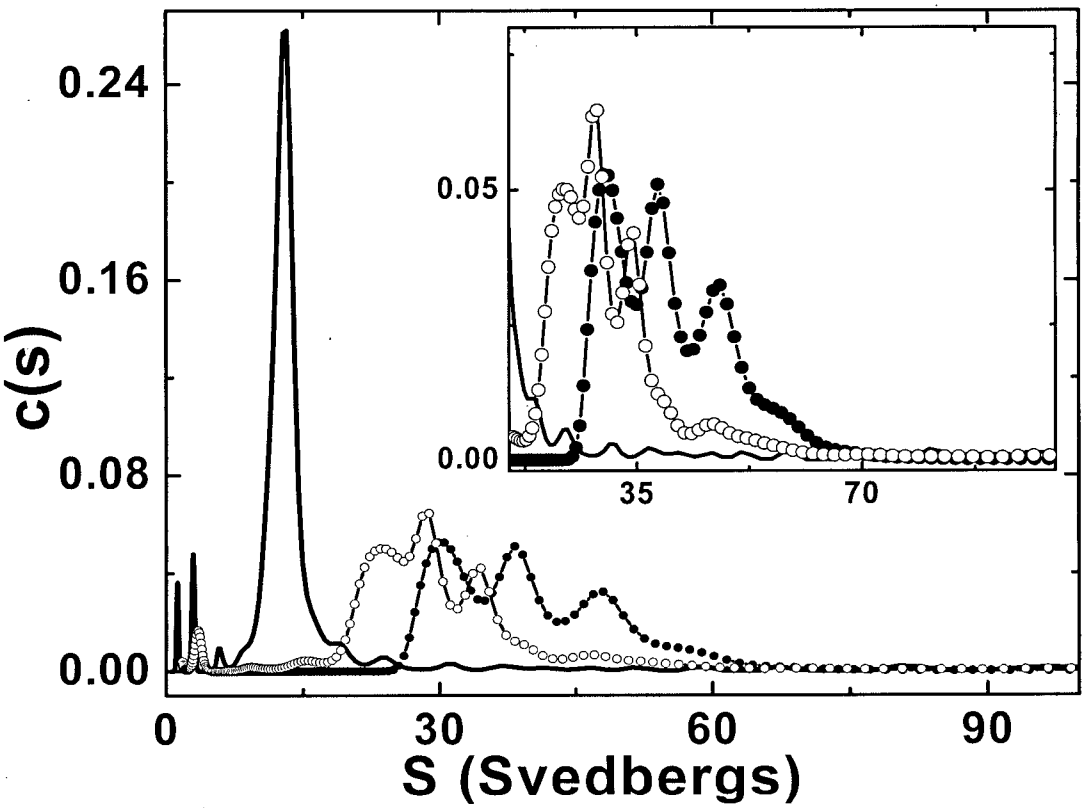

Figure 3.20 Sedimentation velocity analysis of His_6–tag Hsp27. *c(s)* distribution of His_6–wild–type Hsp27 (closed circles, 0.08 mg/mL; black line, 1.96 mg/mL) and His_6–tag S15D/S78D/S82D Hsp27 variant (open circles, 0.02 mg/mL). The inset expands the region of 25 to 90 S for clarity.

3.2 Thermal stability

3.2.1 Wild–type Hsp27

Thermostability of the wild–type protein was measured between 20 and 95 °C at pH 6.7 and 7.7 (Figure 3.21) by monitoring the changes in ellipticity at 219 nm as temperature was increased at a constant rate (1 °C/min). The resulting trace exhibits an unusual shape indicating that ellipticity decreases linearly with increasing temperature until a sharper decrease in ellipticity is observed between 63 and 70 °C. Presumably this behavior is related to the tendency of the protein to form larger oligomers as the temperature increases prior to unfolding. Assuming that the unfolding transition is responsible for the abrupt decrease in ellipticity between 60 and 75 °C, the T_m for the wild–type Hsp is ~67 °C at both values of pH. The circular dichroism spectra of wild–type Hsp27 (pH 6.7, 20 mM NaP buffer) at 25 °C before and after unfolding and at 95 °C is also reported in Figure 3.23

3.2.2 Other variants

Thermostability was evaluated in a similar manner for several other Hsp27 variants as shown in Figure 3.23A–D. The traces obtained for the S15D/S78D/S82D triple variant show a pattern similar to that obtained for wild–type Hsp27 but less pronounced. Moreover, there seems to be no effect caused by one unit pH increase. This result is in agreement with the fact that the triple variant forms large oligomers, but the amount of oligomers is reduced compared to the wild–type protein. The variant lacking the 24

C–terminal residues is extremely stable at high temperature as shown in panel B of Figure 3.23 where no transition was observed. At higher pH (7.7) this variant could not be unfolded completely, and no precipitate was observed even at 99 °C.

The unfolding profiles of the species lacking the N–terminus differ from those observed for all the other variants. At low pH, both Δ1–14 Hsp27 and the Δ1–24 Hsp27 show a classic unfolding profile with ellipticity increasing up to complete unfolding, and both proteins precipitated at high temperatures (Figure 3.23C–D). This is in agreement with the fact that the N–terminal domain is involved in protein self–association and that the formation of larger oligomers increases the overall solubility and stability of the protein.

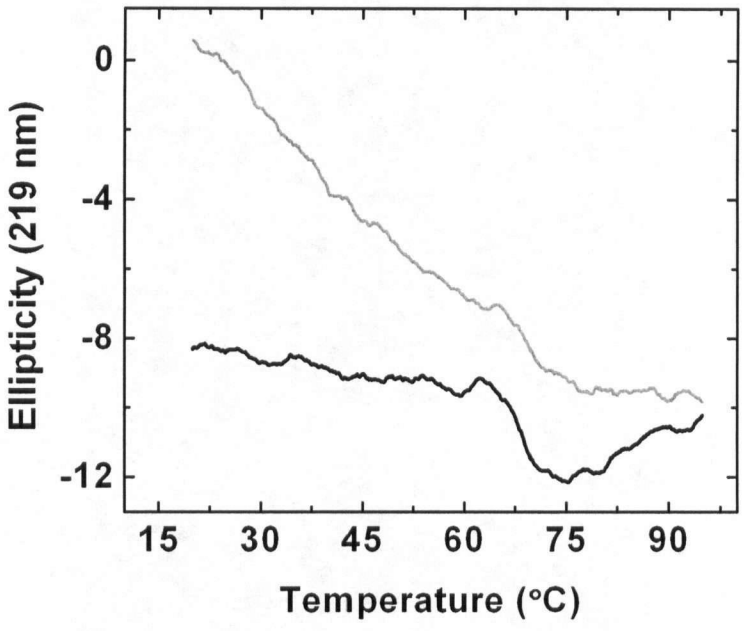

Figure 3.21 Thermal denaturation of wild–type Hsp27 monitored by far UV CD. Hsp27 10 μM; black line, 20 mM Na Phosphate buffer pH 6.7. Grey line, 20 mM Na Phosphate pH 7.7

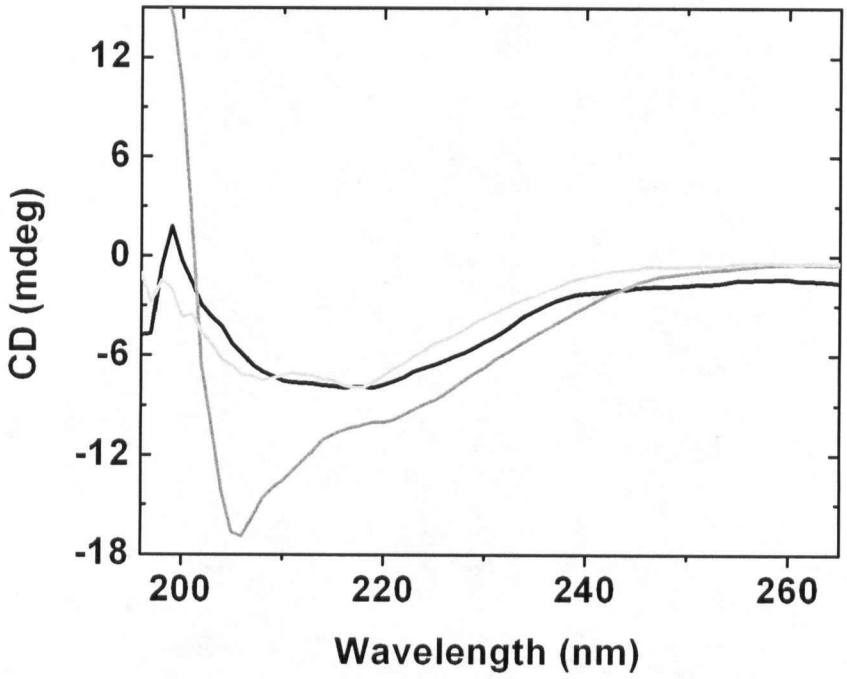

Figure 3.22 Circular dichroism spectra of wild–type Hsp27. Hsp27 10 μM, 20 mM Na Phosphate buffer pH 6.7. Black line, 25 °C; dark grey line, 95 °C; light grey line, 25 °C after unfolding to 95 °C.

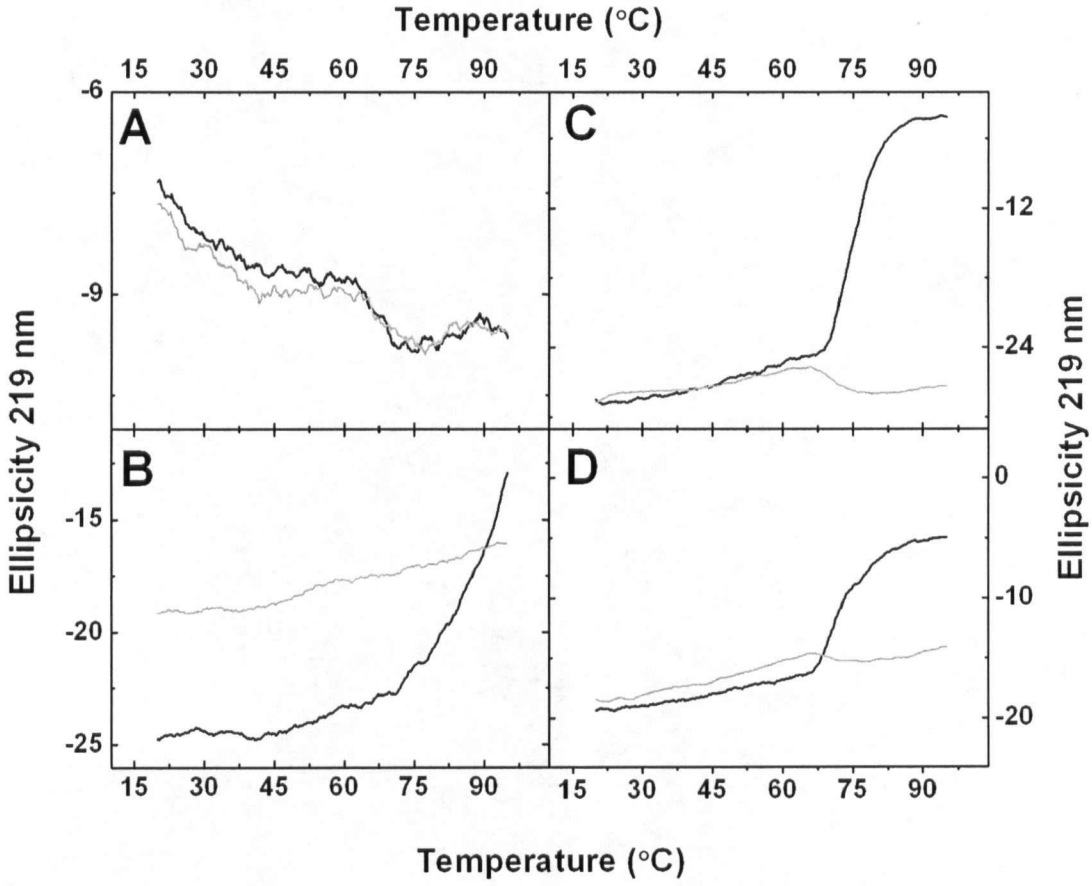

Figure 3.23 Thermal denaturation of Hsp27 variants. Black line, Hsp27 10 µM in 20 mM NaP buffer pH 6.7. Grey line, Na phosphate pH 7.7. A, S15D/S78D/S82D Hsp27; B, Δ182–205Hsp27; C, Δ1–14 Hsp27; D, Δ1–24 Hsp27

3.3 Chaperon activity

3.3.1 Insulin unfolding and effect of pH

To evaluate the chaperon activity of Hsp27, the ability of the wild–type and variant proteins to decrease DTT–induced aggregation of insulin was evaluated. Native insulin denatures irreversibly upon addition of a thiol reagent as the result of disulfide scrambling. Eventually the protein breaks down to form oxidized A– and B–chains (Jiang & Chang, 2005), and it precipitates. Precipitation of the denatured protein can be followed by measuring light scattering at 90° in a fluorometer as described in the Materials and Methods section (p. 45).

The DTT–induced unfolding profile for insulin alone as a function of pH was studied initially (Figure 3.24). As seen from these results denaturation is minimal at pH 7.3, but the rate of denaturation increases dramatically as the pH is lowered to 6.3

3.3.2 Inhibition of insulin unfolding by wild–type Hsp27

To evaluate the chaperon activity of Hsp27, the influence of varying concentrations of Hsp on the kinetics of DTT–induced denaturation of insulin was monitored at 20 °C. As expected, Hsp27 exhibited activity that is dependent on protein concentration (Figure 3.25). At ratios (mol/mol) of 1:0.048 and 1:0.24 (Ins:Hsp27), insulin unfolding was completely inhibited by wild–type Hsp27.

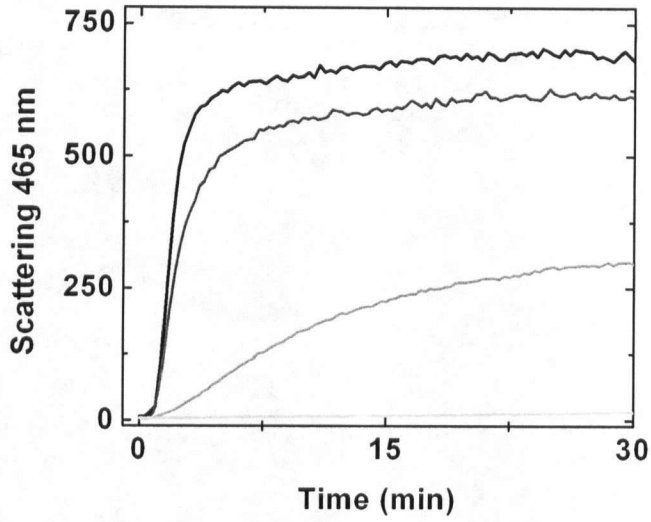

Figure 3.24 pH–dependent insulin unfolding at 40 °C. DTT–induced aggregation profile of insulin (0.24 mg/mL) in 20 mM phosphate buffer, 100 mM NaCl, 40 °C. Black line, pH 6.3; dark grey line, pH 6.7; grey line, pH 6.9; light grey line pH 7.3.

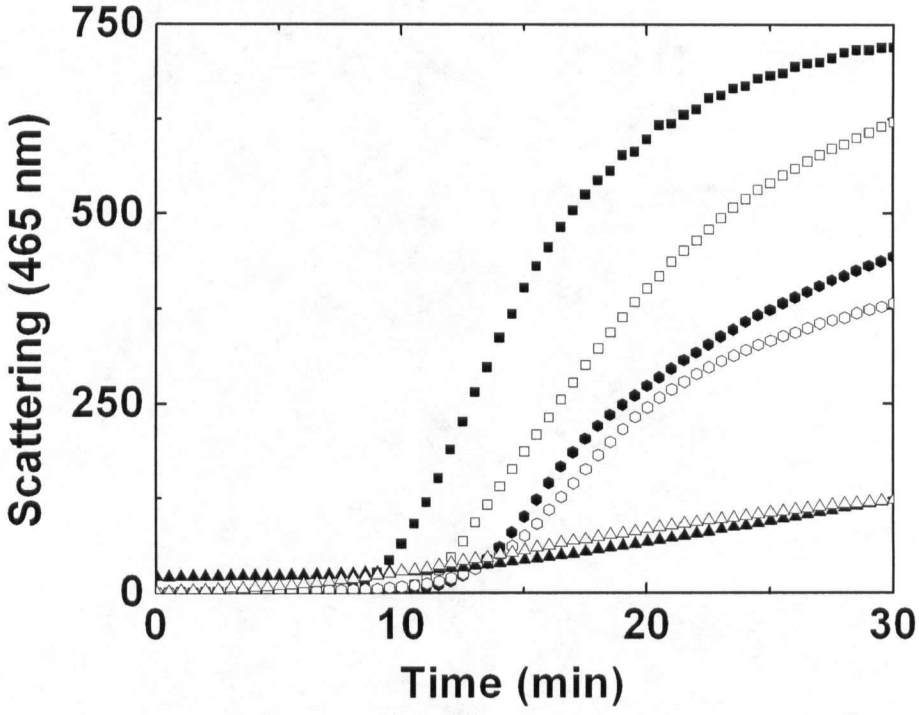

Figure 3.25 Chaperon activity of wild–type Hsp27 at 20 °C. DTT–induced aggregation profile of insulin (0.24 mg/mL) in 20 mM Phosphate buffer pH 6.3, 100 mM NaCl, 20 °C. Solid squares, insulin alone; open squares, wild–type Hsp27/insulin (mol/mol) of 0.012:1; solid circles, 0.024:1; open circles, 0.036:1; solid triangles, 0.048:1; open triangles,0.24:1.

3.3.3 Temperature dependent chaperon activity

To evaluate the influence of temperature and oligomer size on the chaperon activity of Hsp27, the ability of the wild–type protein to decrease DTT–induced aggregation of insulin was evaluated as a function of temperature. Experiments similar to the one performed at 20 °C were carried out at an insulin:Hsp27 ratio of 1:0.012 (mol/mol) from 20 to 48 °C. The results are reported in Figure 3.26 as percentage of inhibition versus temperature. Notably, the most acute sensitivity to increasing temperature was observed at temperatures that are relevant to the physiological heat–shock response (34–43 °C).

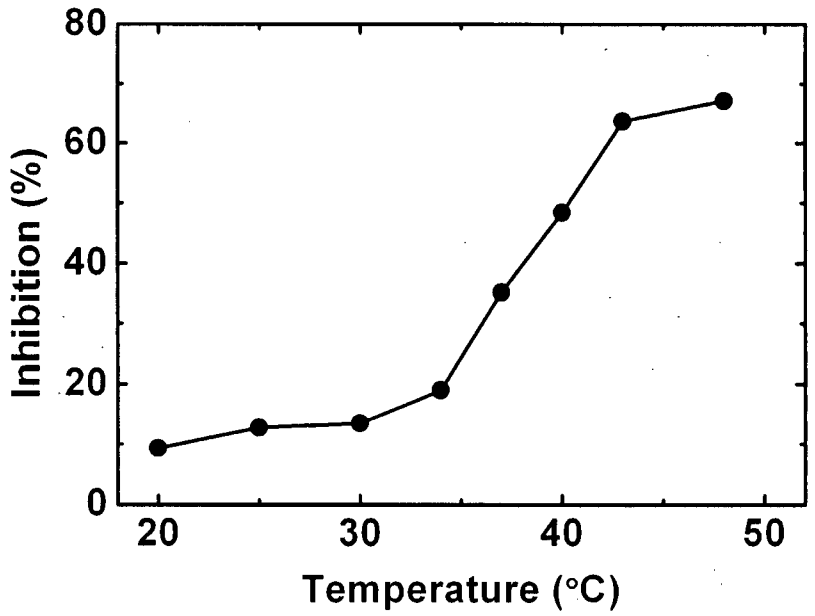

Figure 3.26 Temperature dependent chaperon activity of wild–type Hsp27. Hsp27 activity was calculated as $\frac{(I_{Ins} - I_{Ins+Hsp})}{I_{Ins}} \times 100$. Where I is the intensity of light scattering observed after 20 min with ($I_{ins+Hsp}$) or without Hsp (I_{ins}). 20 mM Phosphate buffer, 100 mM NaCl, insulin:Hsp27 ratio of 1:0.012 (mol/mol).

3.3.4 The effect of Hsp27 variants on insulin unfolding

The S15D/S78D/S82D Hsp27 triple variant was also able to inhibit insulin aggregation in a temperature dependent manner, but the extent of inhibition (Figure 3.27A–B) was much less than that observed with the wild–type protein. At 40 °C and an insulin:Hsp27 ratio of 1:0.012 (mol/mol), the wild–type protein inhibits aggregation by 64% while the triple variant exhibited just 15% inhibition. At the same insulin:Hsp27 ratio but at 20 °C, the triple variant did not inhibit aggregation. These findings are in accord with the observation that larger oligomers have chaperon activity, that the triple variant forms only small amounts of larger oligomers even at high temperature and that the size of this larger oligomer is temperature dependent for both proteins.

The lack of the first 14 residues of the N–terminus almost completely abolishes chaperon activity (Figure 3.28A–B). Any effect observed was essentially independent of the concentration of this variant. Moreover, no increase of activity of the Δ1–14 Hsp27 variant was observed on increasing temperature from 20 to 40 °C. Similarly, no chaperon activity was detected for the Δ1–24 variant (data not shown).

The variant that lacks the 24 C–terminal residues (Δ182–205 Hsp27) failed to inhibit DTT–induced insulin precipitation at 20 °C (Figure 3.29A). In fact, the rate of turbidity formation increased with addition of this variant, presumably owing to aggregation of and scattering of light by complexes of Hsp27–insulin that are larger than the wild–type Hsp27–insulin complexes. On the other hand, evidence of chaperon activity was observed for this variant at 40 °C (Figure 3.29B)

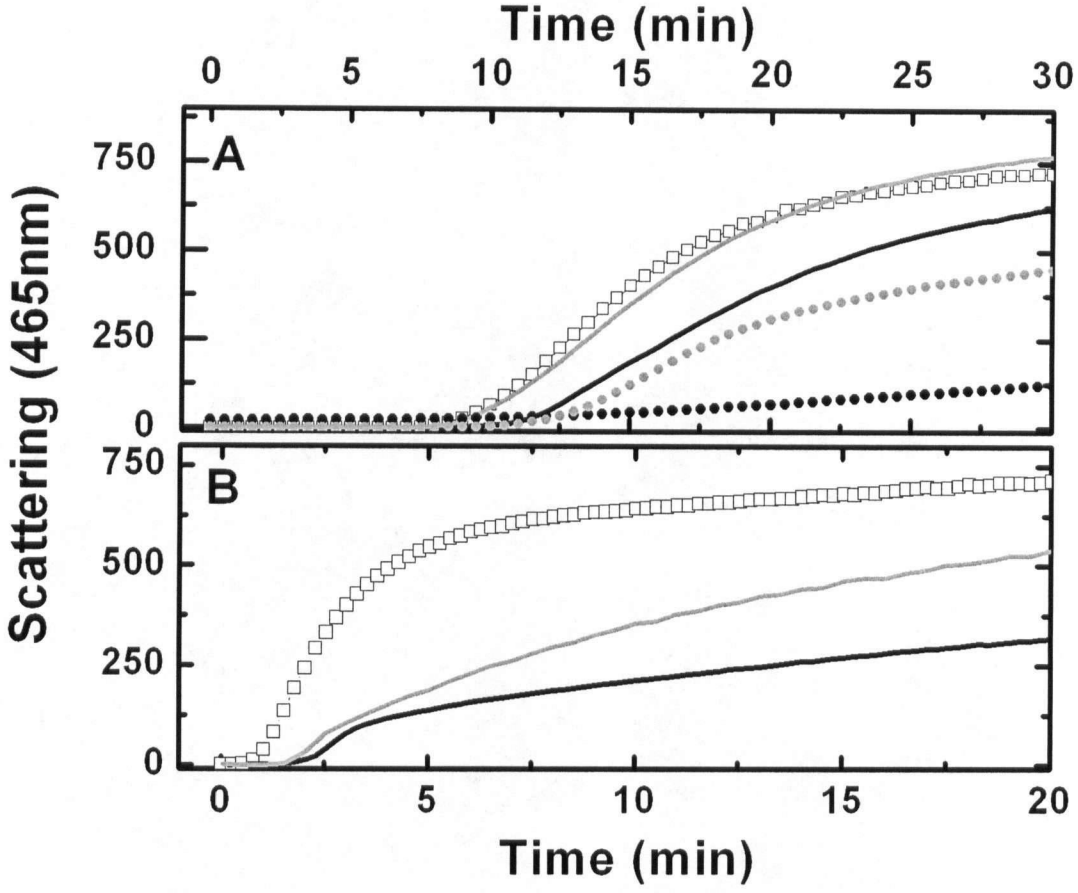

Figure 3.27 Chaperon activity of the S15/S78D/S82D triple variant and wild–type Hsp27. A, 20 °C; B, 40 °C. Open squares, insulin alone; black line, Hsp27 wild–type/insulin (mol/mol) of 0.012:1; grey line, Hsp27 S15D/S78D/S82D/insulin (mol/mol) of 0.012:1; black circles, Hsp27 wild–type/insulin (mol/mol) of 0.048:1; grey circles, Hsp27 S15D/S78D/S82D/insulin (mol/mol) of 0.048:1.

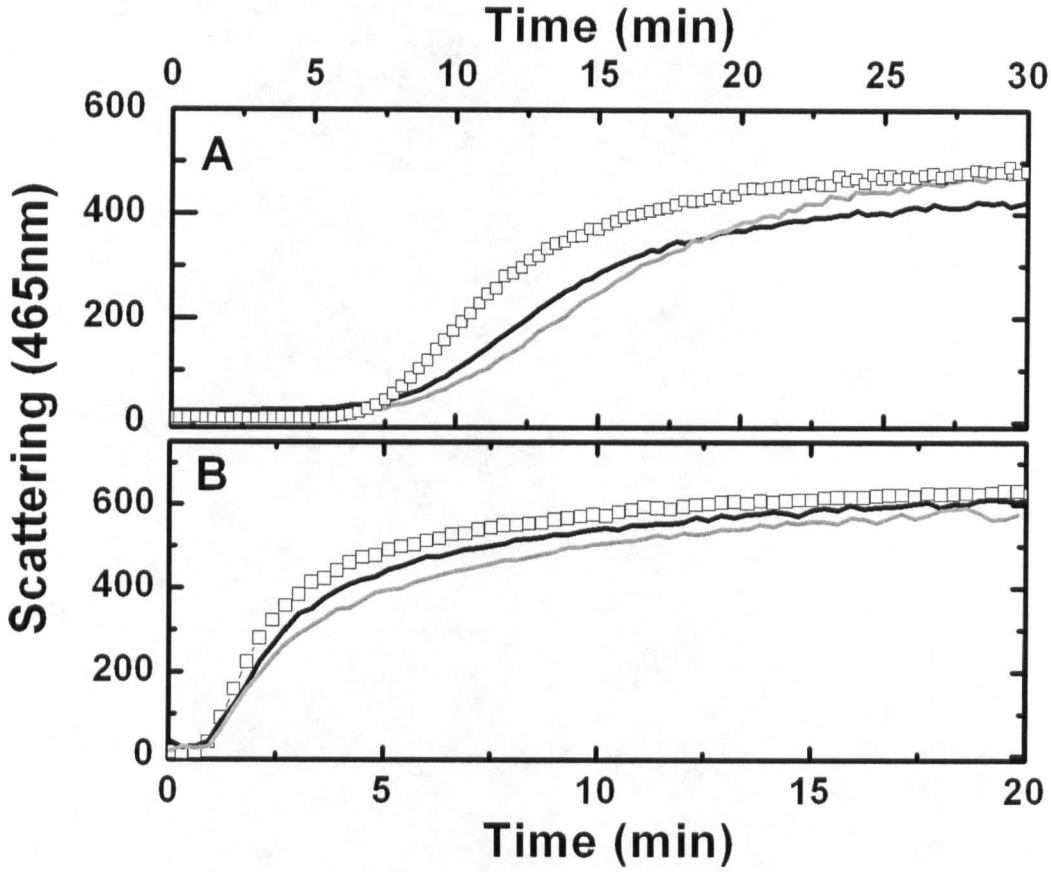

Figure 3.28 Chaperon activity of Δ1–14 Hsp27. DTT–induced aggregation profile of insulin (40 μM) in 20 mM phosphate buffer, 100 mM NaCl pH 6.7. Open squares, insulin alone; black line, Hsp27/insulin (mol/mol) of 0.02:1; grey line, 0.1:1. A, 20 °C; B, 40 °C.

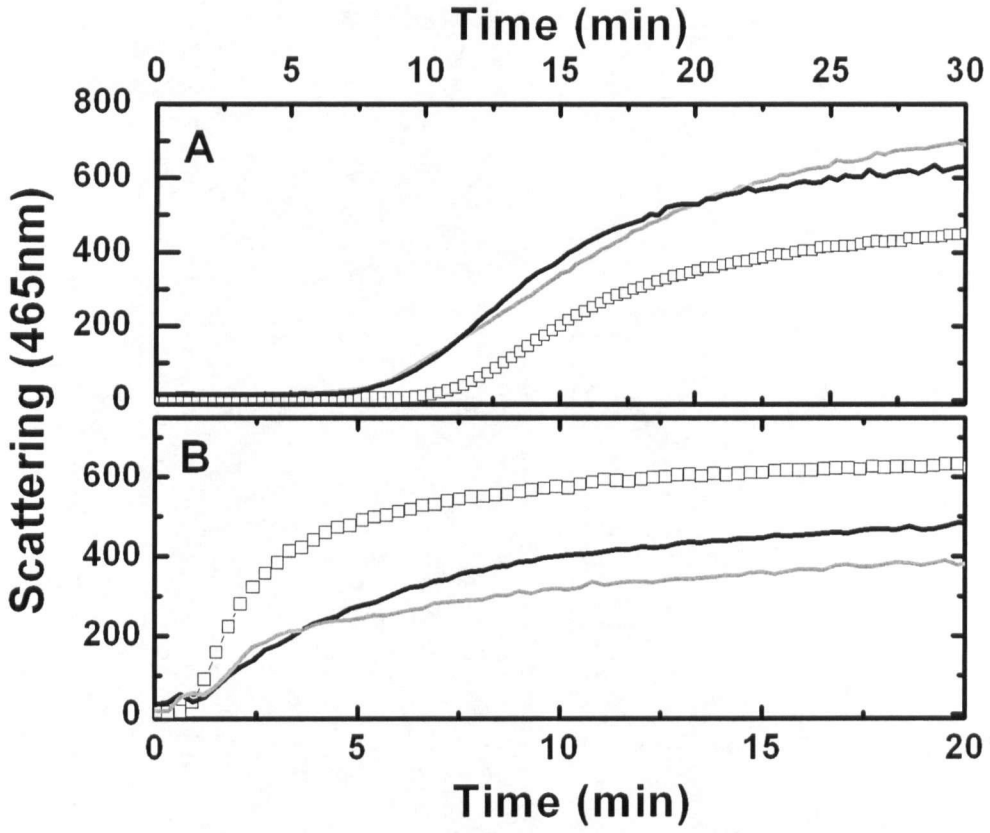

Figure 3.29 Chaperon activity of Δ182–205 Hsp27. DTT–induced aggregation profile of insulin (40 μM) in 20 mM phosphate buffer, 100 mM NaCl pH 6.73. Open squares, insulin alone; black line, Hsp27/insulin (mol/mol) of 0.02:1; grey line, 0.1:1. A, 20 °C; B, 40 °C.

3.4 Subunit exchange

At physiological temperature, mammalian sHsps have a dynamic structure best characterized by a rapid exchange of subunits between oligomers (Bova *et al.*, 1997; Bova *et al.*, 2000). Although little is known about the mechanism or kinetics of this process, increasing evidence suggests that it is essential for chaperon activity (Fu *et al.*, 2003; Jiao *et al.*, 2005; Usui *et al.*, 2004a). To determine if the ability to dissociate and re–associate in solution is linked to chaperon activity, the subunit exchange kinetics of wild–type Hsp27 were compared to those of the triple variant S15D/S78D/S82D and the two deletion variants Δ1–14 Hsp27 and Δ182–205 Hsp27.

Fluorescence resonance energy transfer (FRET) experiments were used for measurements of these rates.

3.4.1 Protein labeling

Hsp27 and the variants previously described were labeled with 4-acetamido-4'-((iodoacetyl)amino) stilbene-2,2'-disulfonic acid, disodium salt (AIAS) to serve as a FRET donor. Other samples of these same proteins were modified with lucifer yellow iodoacetamide, dipotassium salt (LYI) to serve as FRET acceptor. The maximum absorbance of LYI occurs at a wavelength (426 nm) close to the wavelength of maximum emission of AIAS (408 nm). These two probes have been characterized previously and used to monitor the subunit exchange of α–crystalline and other small heat shock proteins including Hsp27 (Bova *et al.*, 1997; Bova *et al.*, 2002; Bova *et al.*, 2000). Hsp27 contains a single cysteine residue (Cys^{137}), and this residue is used to attach these sulfhydryl–specific

fluorophores. The spectroscopic properties of the modified proteins are shown in Figure 3.30. In both preparations the molar ratio of Hsp27 and the fluorophore is 1:1.

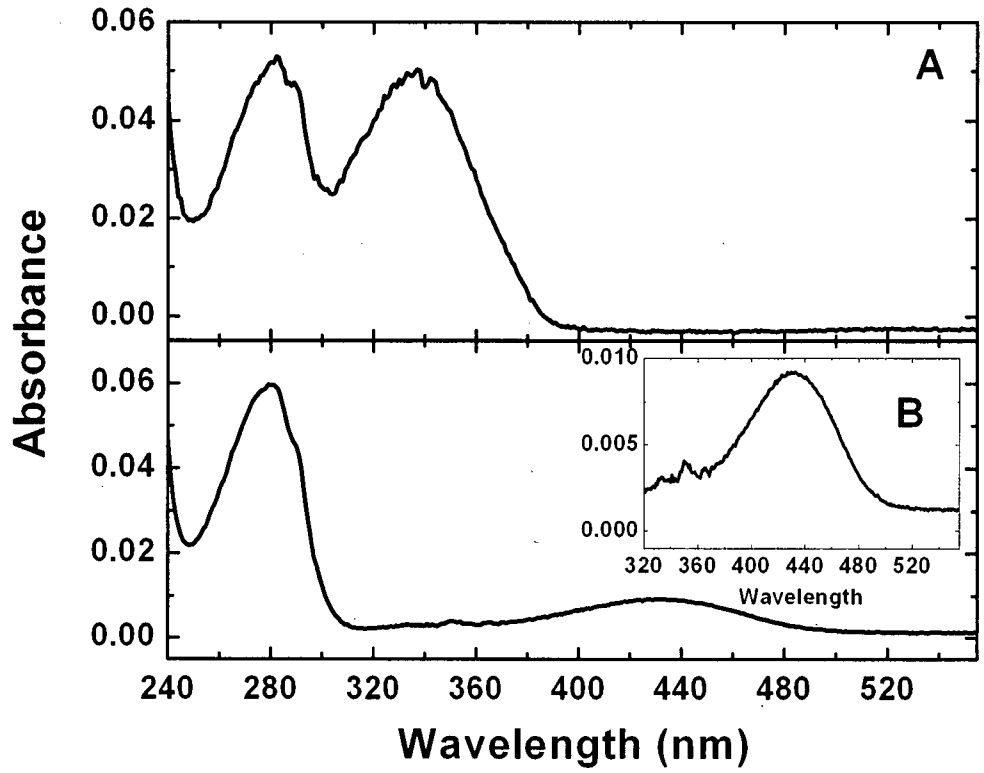

Figure 3.30 Electronic absorption spectra of AIAS–labeled and LYI–labeled wild–type Hsp27. A, Wild–type Hsp27 labeled with AIAS; B, wild–type Hsp27 labeled with LYI. Inset expands the region between 320 and 555 nm for clarity.

3.4.2 Wild–type Hsp27

The AIAS–modified Hsp27 has a characteristic fluorescence emission spectrum with a maximum at 412 nm. The modified protein is stable, and the emission intensity does not change in solution over a two hour period (Figure 3.31).

When samples of the two differently modified forms of wild–type Hsp27 are combined, subunit exchange occurs, and the two fluorophores achieve sufficient proximity to each other that energy transfer from AIAS to LYI is observed. In fact, the emission spectrum of an equimolar mixture of AIAS–Hsp27 and LYI–Hsp27 decreases in intensity at 412 nm (λ_{em}= AIAS) as a function of time, and a corresponding increase is observed at 520 nm (λ_{em}= LYI) (Figure 3.32). This rate of change in emission intensity (412 nm) was used to monitor the rate of subunit exchange, and the resulting kinetics traces were fitted (Origin 7.0) with the simplest model that fit the data well. Results obtained for the wild–type protein Hsp27 (30 °C) are shown in Figure 3.33. The mean reaction time (t_{mrt}) and the first order rate constant for subunit exchange k which is defined as $1/t_{mrt}$, were measured to be 6.1 ± 0.5 min and $k = 2.7\times10^{-6}$ sec^{-1}. Results obtained for wild–type Hsp27 at other temperatures are summarized in Figure 3.34.

Wild–type Hsp27 exhibits an increased rate of subunit exchange k with increasing temperature as observed previously for other small Hsps and α–crystalline (Bova *et al.*, 1997; Bova *et al.*, 2002). Analysis of the temperature–dependence of the rate constant for subunit exchange by means of an Arrhenius plot (Figure 3.35) provided a reaction activation energy of 22.5 kcal/mol at 40 °C and a ΔH° of 21 ± 2 kcal · mol^{-1}.

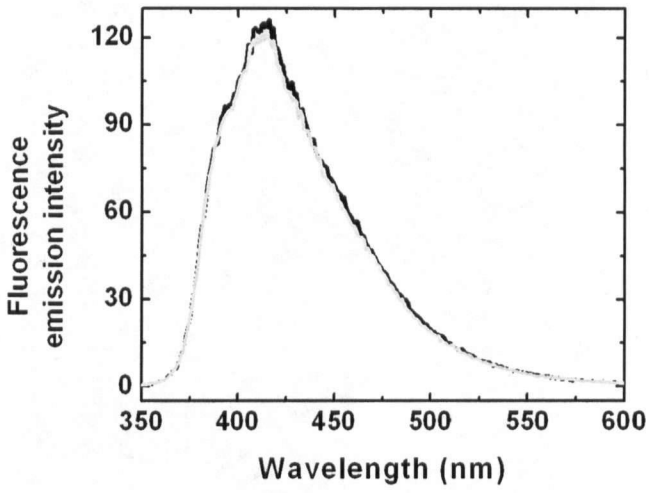

Figure 3.31 Fluorescence emission spectra of AIAS modified wild–type Hsp27 (MOPS buffer 20 mM (pH 7.9), 100 mM NaCl). The sample was incubated at 40 °C for at least 20 min prior to measuring the fluorescence spectrum. The sample was excited at λ_{ex} 335 nm, while fluorescence emission was detected between 350 and 600 nm. Black line, time zero; light grey line, time 120 min.

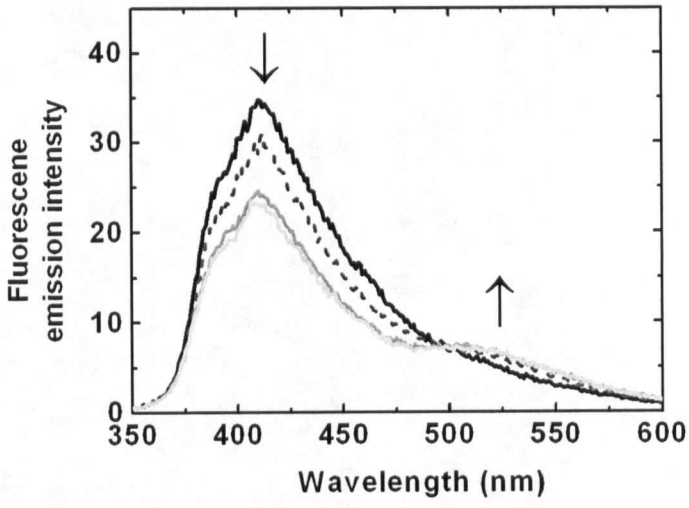

Figure 3.32 Emission spectra of an equimolar mixture of AIAS and LYI modified wild–type Hsp27 (MOPS buffer 20 mM (pH 7.9), 100 mM NaCl, 40 °C). Black line, 15 sec; dark grey dashed line, time 135 sec; grey line 315 sec; light grey line, time 615 sec.

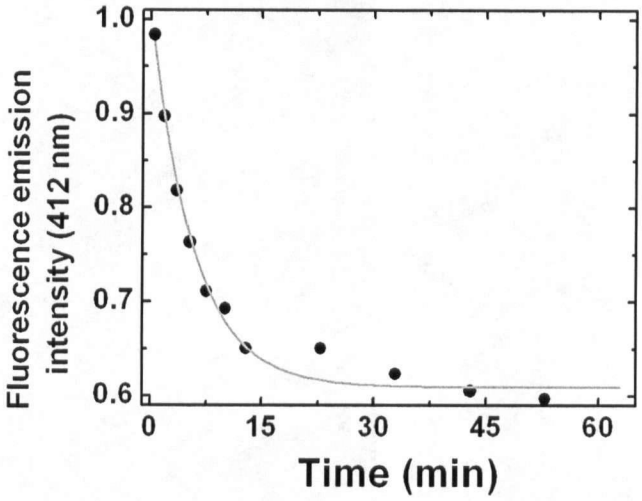

Figure 3.33 Kinetics of subunit exchange of human Hsp27 as measured by fluorescence quenching at 30 °C (412 nm). Equimolar amounts of AIAS modified wild–type Hsp27 and LYI modified wild–type Hsp27 where mixed, and fluorescence was detected at regular intervals at 30 °C (50 mM sodium phosphate (pH 7.5),100 mM NaCl, 2 mM DTT). The nonlinear regression fit of the data to a first order exponential decay is shown (grey line).

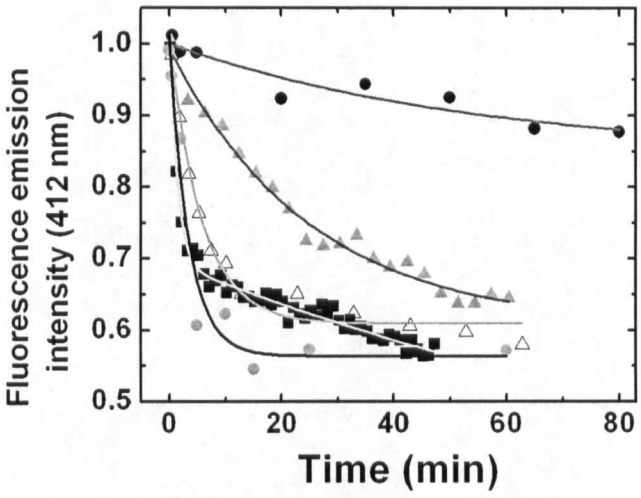

Figure 3.34 Kinetics of subunit exchange of human Hsp27 at various temperatures. Experimental conditions are the same as for Figure 3.32. 10 °C (black circles), 20 °C (light grey triangles), 30 °C (open triangles), 37 °C (grey circles) or 40 °C (black squares). Nonlinear regression fit of the data to a first (10, 20, 30, 37 °C) or bi–exponential (40 °C) decay are shown.

3.4.3 Subunit exchange of Hsp27 variants

Subunit exchange was evalutated for the triple variant that mimics phosphorylation *in vitro* (Figure 1.9). This variant exhibits a very slow exchange rate compared to the wild–type protein. Moreover, the exchange rate seems to be independent of temperature with virtually no subunit exchange observed at either 20 or 40 °C (Figure 3.36).

The rate of subunit exchange for the N–terminal deletion variant 1–14 Hsp27 exhibited more complex behavior than did the wild–type protein in that a first order exponential decay did not always give the best fit to the data. For this reason, first order and bi–exponential nonlinear regression fits are shown in Figure 3.37A–B, and the resulting parameters are summarized in Table 3.2. At low temperature (20 and 30 °C), a first order exponential fits the data reasonably well, but at elevated temperature (37 and 40 °C), a fast exchange occurs in the first few minutes after mixing, and the data are best described as a bi–exponential decay. Generally, this variant exhibits slower subunit exchange rate than the wild–type protein, and the exchange rate increases with increased temperature (Figure 3.37). This truncated variant was unable to inhibit insulin unfolding, but as shown in these results, it does manifest temperature induced subunit exchange. Therefore, the lack of chaperon activity does not result from the inability to exchange subunits but presumably results from the absence of critical residues at the N–terminus of the protein.

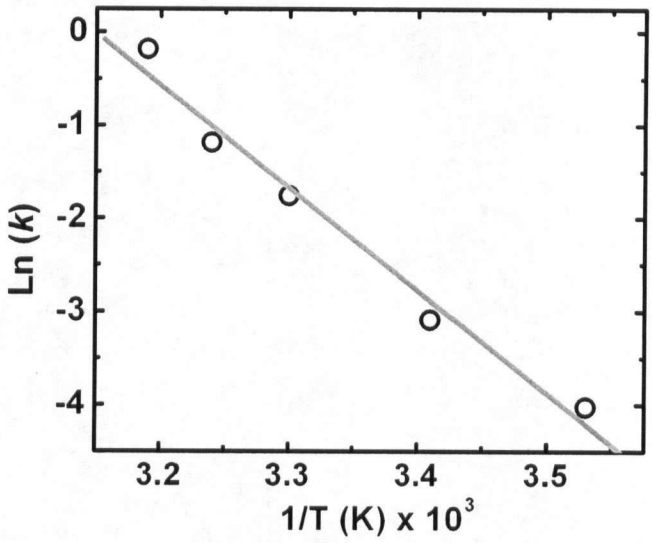

Figure 3.35 Arrhenius plot for wild–type Hsp27. Values of k $(=1/t_{mrt})$ where obtained by fitting the quenching data shown in Figure 3.34. When a double exponential was the best fit for the data, the value of t_{mrt1} was used to generate k. Linear fit to the Arrhenius plot (grey line)

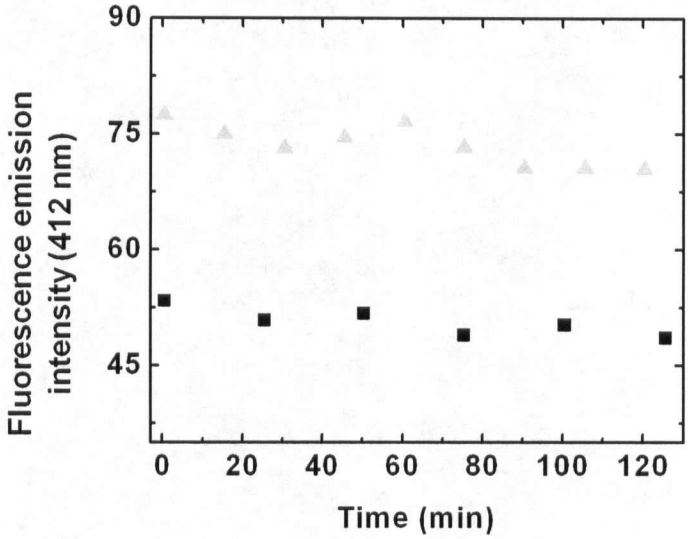

Figure 3.36 Kinetics of subunit exchange of S15D/S78D/S82D Hsp27 as measured by fluorescence quenching at 20 and 40 °C (412 nm). Equimolar amounts of AIAS modified and LYI modified S15D/S78D/S82D Hsp27 where mixed and fluorescence was detected at regular intervals at 20 °C (Light grey triangles) or 40 °C (black squares) (50 mM sodium phosphate (pH 7.5), 100 mM NaCl, 2 mM DTT).

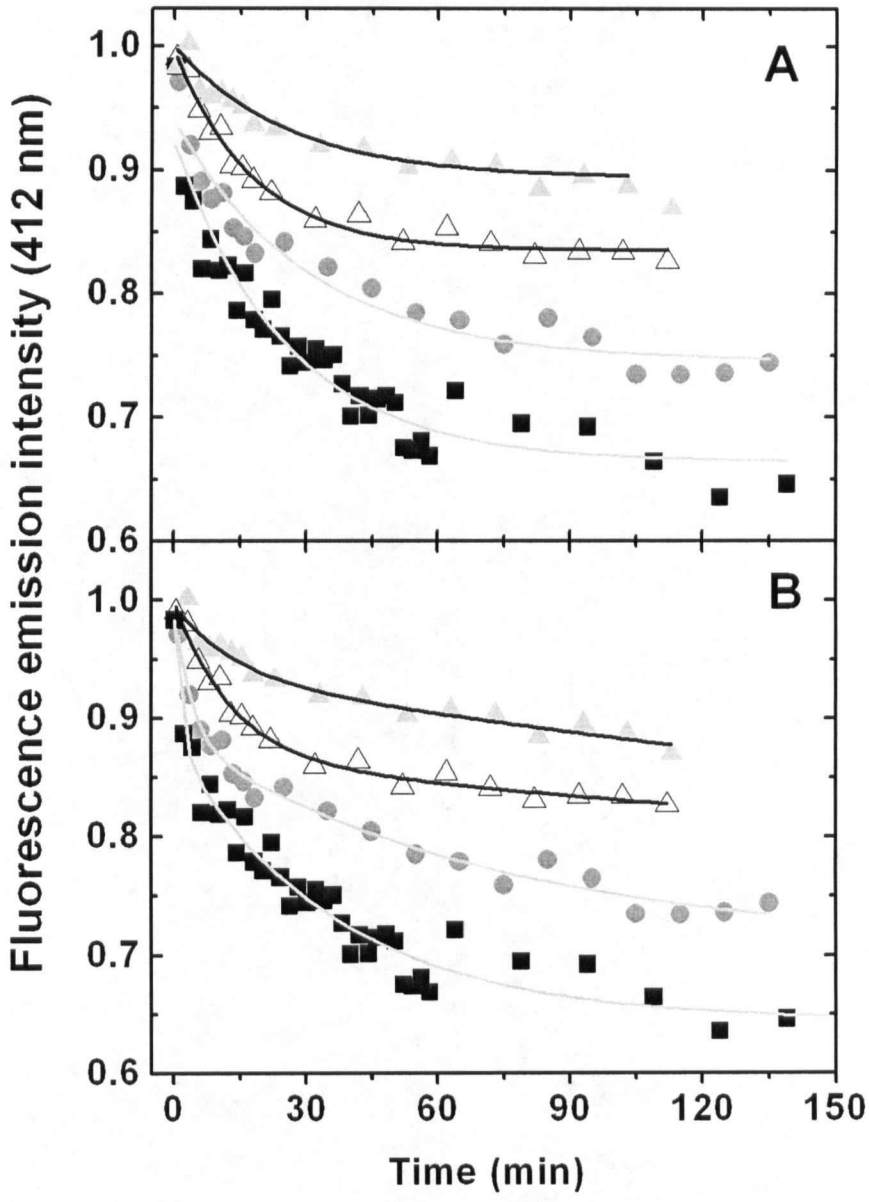

Figure 3.37 Kinetics of subunit exchange of Δ1–14 Hsp27 as measured by fluorescence quenching at various temperature (412 nm). Equimolar amounts of AIAS modified and LYI modified Δ1–14 Hsp27 were mixed, and fluorescence was detected at regular intervals at 20 °C (light grey triangles), 30 °C (open triangles), 37 °C (grey circles) or 40 °C (black squares) (50 mM sodium phosphate (pH 7.5), 100 mM NaCl, 2 mM DTT). Nonlinear regression fit of the data to a first (A) or bi–exponential (B) decay.

Table 3.2 Summary of values for first and bi–exponential decay fit for FRET experiments of wild–type and Δ1–14 Hsp27.

Wild–type

T (°C)	$y = y_0 + Ae^{-x/t_{mrt}}$	
	t_{mrt} *(min)*	$R^{\wedge 2}$
20	22 ± 3	0.983
30	5.8 ± 0.9	0.985
37	3.3 ± 0.5	0.964
40	1.2 ± 0.1	0.984

Δ1–14

T (°C)	$y = y_0 + Ae^{-x/t_{mrt}}$		$y = y_0 + A_1e^{(-x/t_{mrt1})} + A_2e^{(-x/t_{mrt2})}$		
	t_{mrt} *(min)*	$R^{\wedge 2}$	t_{mrt1} *(min)*	t_{mrt2} *(min)*	$R^{\wedge 2}$
20	26 ± 5	0.941	15 ± 7	N/A	0.957
30	18 ± 2	0.981	13 ± 5	N/A	0.986
37	31 ± 6	0.945	3.7 ± 1.4	72 ± 25	0.982
40	26 ± 3	0.919	1.4 ± 0.8	37 ± 4	0.958

Analysis of the temperature–dependence of the rate constant for subunit exchange was obtained with the values of t_{mrt} (20 °C) or t_{mrtl} (30, 37 and 40 °C) (Figure 3.37) and provided a reaction activation energy of 26 kcal/mol at 40 °C and a ΔH° of 25 ± 6 kcal · mol^{-1} (Figure 3.38). Because data obtained at 20 °C could be fit with only a first order exponential decay, the activation energy and ΔH° were also calculated from the data obtained at 30, 37 and 40 °C by fitting only the values of k obtained from t_{mrtl} (Figure 3.39). In this case a reaction activation energy of 41 kcal/mol at 40 °C and a ΔH° of 40 ± 7 kcal · mol^{-1} were obtained.

The Δ182–205 Hsp27 variant lacking the C–terminal tail (Figure 1.9) also undergoes subunit exchange, but over the range 20 to 40 °C the subunit exchange rate for this protein is not influenced by temperature (Figure 3.40). The fit obtained at 20 °C and 37 °C for single exponential decay is also shown in this figure, and the t_{mrtl} obtained from the data is 5.4 ± 0.9 min ($k = 3.1 \times 10^{-6}$ sec^{-1}) and 6.0 ± 0.6 min ($k = 2.8 \times 10^{-6}$ sec^{-1}) respectively. Moreover, the total quenching was not as extensive as observed for the wild–type protein. While the explanation of this is not apparent, it is possible that some of the protein undergoes subunit exchange or that the geometry of subunit exchange of the wild–type protein and the Δ182–205 variant differs.

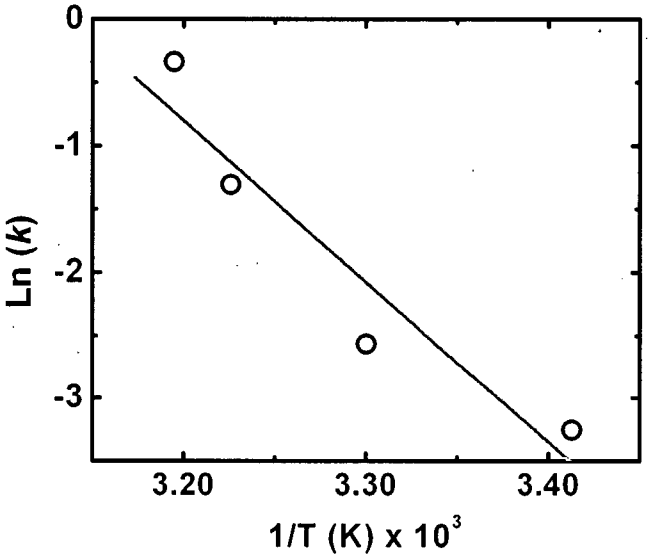

Figure 3.38 Arrhenius plot for Δ1–14 Hsp27 from data obtained between 20–40 °C. Values of k ($=1/t_{mrt}$) where obtained by fitting the quenching data shown in Figure 3.34. When a double exponential was the best fit for the data, the value of t_{mrt1} was used to obtain the values of k. Linear fit to the Arrhenius equation (grey line)

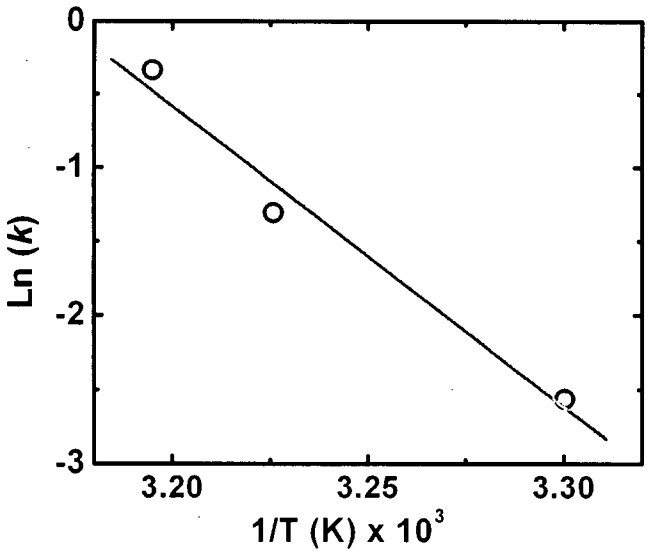

Figure 3.39 Arrhenius plot for Δ1–14 Hsp27 from data obtained between 30–40 °C. Values of k where obtained by fitting the quenching data shown in Figure 3.37. The values of t_{mrt1}, obtained by fitting the data to a double exponential decay, were used to determine k and construct the plot. Linear fit to the Arrhenius equation (grey line)

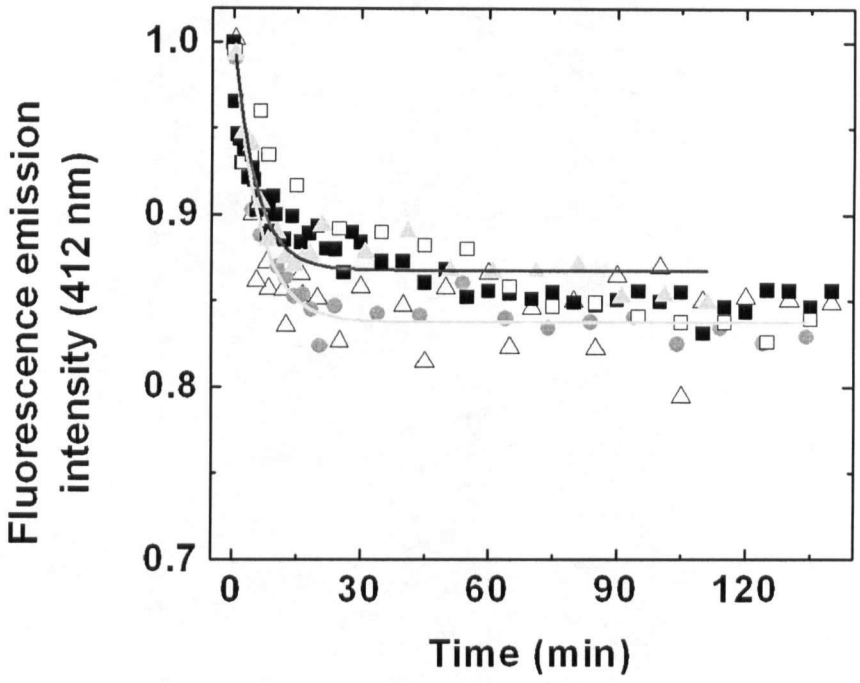

Figure 3.40 Fluorescence quenching for Δ182–205 Hsp27 at various temperatures (412 nm). Equimolar amounts of AIAS modified Δ182–205 Hsp27 and LYI modified Δ182–205 Hsp27 were mixed and fluorescence was detected at regular intervals at 20 °C (light grey triangle), 25 °C (open squares) 30 °C (open triangle), 37 °C (grey circles) or 40 °C (black squares). Single exponential decay fits are shown for the data obtained at 20 °C (black line) and at 37 °C (light grey line).

4. DISCUSSION

4.1 Overview

The work reported in this dissertation describes the behavior of the small human Hsp27 in solution with particular focus on self–association and chaperon activity. The study began with the use of analytical ultracentrifugation to define Hsp27 oligomerization in solution as a function of concentration, temperature, pH and ionic strength. Sedimentation velocity experiments, activity and subunit exchange assays were then used in combination with site–directed mutagenesis to characterize the self–association and chaperon activity of variants of Hsp27 as a mean of identifying the involvement of several regions of the protein in these processes.

Hsp27 is an attractive representative of the small heat shock proteins in general insofar as it has been shown to be involved in a number of cellular processes (Garrido & Solary, 2003; Gusev *et al.*, 2002) and to possess chaperon activity (Jakob *et al.*, 1993). Moreover, the functional properties of Hsp27 appear to be related to the self–association of the protein (Garrido, 2002). As a result, understanding the manner in which Hsp27 assembles to form multimeric forms is essential to understanding how this protein functions.

The use of analytical ultracentrifugation affords greater sensitivity and resolving capability than is possible with gel permeation chromatography that has been the primary means by which Hsp27 oligomerization has been studied previously. To study chaperon activity, inhibition of DTT–induced unfolding of insulin rather than thermal unfolding was employed because it allows measurement of activity as a function of temperature. To complement these results, the rate of subunit exchange was measured by fluorescence

resonance energy transfer experiments to evaluate the role of conserved and variable domains in self–association and activity.

In combination, these results permit development of a model for Hsp27 assembly and function that is proposed here.

4.2 Wild–type Hsp27

4.2.1 Self–association in standard conditions

Initially the self–association of the wild–type small Hsp27 was defined under standard conditions: 20 °C, 20 mM Tris (pH 8.4), 100 mM NaCl. Under these conditions, wild–type Hsp27 self–associates to form oligomers as large as 12–16–mers (~ 320 kDa) with preferential formation of what is probably a tetrameric intermediate. Nevertheless, some monomeric and/or dimeric Hsp27 is present in solution at all times. This behavior could explain the ability of Hsp27 to be translocated from the cytoplasm to the nucleus through a membrane with a much smaller porosity than 300 kDa (Beaulieu *et al.*, 1989). At all concentrations studied, only a small percentage of wild–type Hsp27 was aggregated (>> 320 kDa). The association constants derived from this work are on the order of nM for formation of the tetrameric intermediate (monomer ↔ tetramer) and μM for formation of the larger oligomers (tetramer ↔ 12/16–mer). The current findings differ from previous reports. For example, Behlke *et al.* reported that Hsp27 exhibits a mean molecular weight of 730 kDa (Behlke *et al.*, 1991) while gel filtration experiments reported by Rogalla *et al.* indicated preferential formation of a 24–mer (MW 550 kDa) (Rogalla *et al.*, 1999). Interestingly, electron microscopy showed that Hsp27 is highly asymmetrical (Haley *et al.*,

2000). At least in part, these discrepancies could be attributed to differences in the experimental conditions used in each case (*e.g.*, temperature, pH). However, insofar as gel filtration requires the use of a calibration curve, and self–associating systems may not behave similarly to the standard, monomeric proteins used for calibration of the column, analytical ultracentrifugation is a more rigorous means of obtaining quantitative information concerning self–association.

The frictional coefficient (f/f_0), which provides an indication of the shape of the protein in solution, is 1.29 for the large oligomers of wild–type Hsp27 at 1.96 mg/mL at 20 °C. This value suggests an overall shape of the Hsp27 oligomer that is only slightly elongated. The two crystal structures of sHsps that have been published both describe a spherical protein assembly (Kim *et al.*, 1998; van Montfort *et al.*, 2001). The hydrodynamic data provided in the current study are consistent with such an assembly for Hsp27 as well.

4.2.2 Effect of pH, ionic strength and temperature on self–association

Variation of ionic strength from 0.05 to 1 M and variation of pH between 7.0 and 8.4 had no detectable effect on self–association of wild–type Hsp27. Only when the pH was lowered to 6.5 was an appreciable increase in the sedimentation coefficient observed, a behavior that can be attributed to the insolubility of Hsp27 at its p*I*. These observations argue that oligomerization of wild–type Hsp27 involves neither titratable groups that titrate in this range nor significant general electrostatic stabilization.

The finding that, at 20 °C, wild–type Hsp27 self–associates to form assemblies of no more than 12 to 16 monomers indicates that oligomeric Hsp27 is smaller than

previously believed. The inability of the current data to define a precise upper limit to the size of oligomer formed by the wild–type protein was interpreted as evidence that this protein does, in fact, form oligomers of varying upper limit within the range of 12 to 16–mers under the conditions used. On the other hand, the self–association of wild–type Hsp27 exhibits a significant dependence on temperature between 10 and 40 °C that results in formation of larger oligomers with increasing temperature. At 40 °C, the main component of Hsp27 sediments at 18–20 S while at 10 °C the largest species sediments at 10–11 S. The observation that incubation of Hsp27 at 42 °C prior to sedimentation analysis at 20 °C produced results identical to those obtained for a sample never exposed to elevated temperature demonstrates that thermally–induced oligomerization of this protein is fully reversible.

Thermal stabilization of protein–protein interaction is a relatively rare phenomenon. Previous studies of other small heat shock proteins have reported dissociation of larger oligomers to form smaller assemblies at elevated temperature (Haslbeck *et al.*, 1999; Lentze *et al.*, 2004; Stromer *et al.*, 2004a; Usui *et al.*, 2004a). On the other hand, a few examples of large heat shock proteins that form larger oligomers with increased temperature have been reported. For example, chicken Hsp90 has been reported to be dimeric below 50 °C and to form larger oligomers at higher temperatures (Chadli *et al.*, 1999; Thorne & McQuade, 2004). The endoplasmic glycoprotein chaperon gp96, which is homologous to Hsp90 from yeast (Mazzarella & Green, 1987), also forms larger oligomers and exhibits greater peptide binding affinity at temperatures greater than 50 °C (Thorne & McQuade, 2004). To our knowledge, Hsp27 is the only true small heat shock protein and the only ATP–independent heat shock protein currently known to form

oligomers of increased size as temperature is increased. Other protein–protein complexes that have been reported to exhibit increased stability at elevated temperature include the self–association of RecA (Brenner *et al.*, 1990), an anti–cytochrome *c*–cytochrome *c* complex (Raman *et al.*, 1995b) and cytochrome *c*–cytochrome *c* peroxidase complex formation (Wang & Pielak, 1999).

This ability of the protein to form assemblies of widely varying size may be advantageous in optimizing the various functionalities of Hsp27. For example, the variable extent of Hsp27 oligomerization is presumably an important factor in the ability of Hsp27 to prevent precipitation of unfolding proteins of widely varying size (Stromer *et al.*, 2003). In any case, the improved understanding of the effects of specific modifications to Hsp27 on the ability of the protein to self–associate provided in this thesis should facilitate the design of experiments to test this and other mechanistic hypotheses concerning the role of oligomerization in defining the functional properties of Hsp27.

4.2.3 Activity studies and subunit exchange of wild–type Hsp27

Notably, the thermal dependence of Hsp27 oligomerization is reflected in a pronounced thermal dependence of Hsp27 chaperon activity (Figure 4.1). Specifically, the chaperon activity of Hsp27 increases slightly between 20 °C (9% inhibition of insulin aggregation) and 30 °C (13.5% inhibition) with much greater increases observed between 34 °C (19% inhibition) and 43 °C (64% inhibition). At higher temperature, little further increase in activity results (67% inhibition at 48 °C) (Insulin:Hsp27 1:0.012 (mol/mol)) (Figure 3.26). While increased chaperon activity of α–crystallin and Hsp22 have previously been reported to increase upon increasing temperature from 20 to 50 °C

(Chowdary *et al.*, 2004; Raman *et al.*, 1995a; Raman & Rao, 1994), the direct correlation of thermally activated chaperon activity with increased oligomer size has not been reported

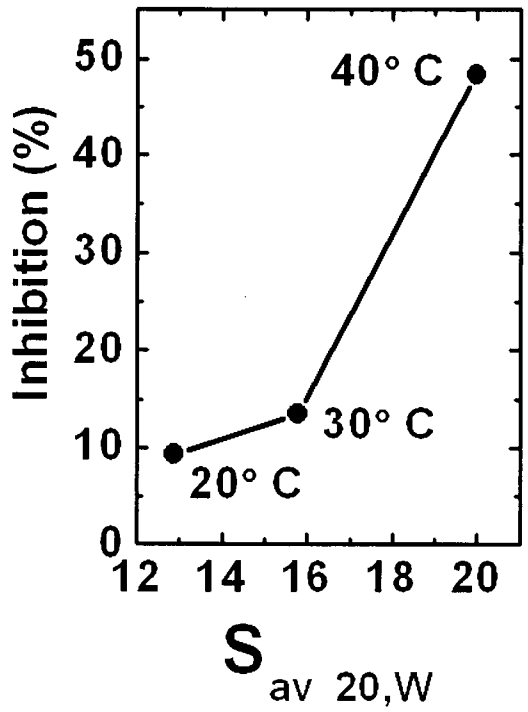

Figure 4.1 Average sedimentation coefficient *vs.* percentage inhibition activity. The S_{av} reported in the *x*–axis is the value obtained at high protein concentration in the sedimentation velocity experiments at 20, 30 and 40 °C. The activity reported in the *y*–axis was obtained at the same temperatures by using 1:0.012 ratio (mol/mol) of insulin to Hsp27 wild–type.

previously. In view of the fact that Hsp27 expression is thermally–induced *in vivo* in the temperature range in which the greatest effects on both oligomerization and chaperon activity were observed, we conclude that these temperature–dependent properties of Hsp27 constitute a previously unrecognized physiological characteristic of this protein.

As previously observed, the rate of subunit exchange increases with increased temperature (Bova *et al.*, 1997; Bova *et al.*, 2000). It is therefore plausible to speculate that subunit exchange is also important for chaperon activity. For the sake of completeness, note that the Arrehnius plot derived from the temperature–dependent FRET data (Figure 3.34) produces an activation energy for subunit exchange of 22 kcal/mol.

4.3 Mimicking phosphorylation

The S15D/S78D/S82D triple variant of Hsp27 has been reported to be capable of forming only tetramers and to exhibit less chaperon activity than the wild–type protein (Rogalla *et al.*, 1999), yet this variant has also been reported to inhibit apoptosis *in vivo*, a characteristic that is believed to require assembly of the protein into large oligomers (Bruey *et al.*, 2000b). Consequently, the behavior of the S15D/S78D/S82D and S15D/S78D/S82D/C137S variants was evaluated to assess the influence of these residues on the self–association of the protein. For both variants, 80% or more of each protein is monomeric and/or dimeric over the concentrations studied here. Nevertheless, larger oligomers were also detected in each case. For the triple variant, sedimentation equilibrium experiments established that oligomers as large as 12–mers could form. The formation of larger oligomers, albeit in lower abundance, presumably explains the ability of this variant to inhibit apoptosis *in vivo*.

The influence of pH and ionic strength on self–association of the S15D/S78D/S82D triple variant was evaluated as well. The results establish that oligomerization of this protein is also independent of pH and ionic strength over the concentration range examined. Thus, while no general electrostatic contribution to self–association seems to be involved in oligomerization of Hsp27, specific electrostatic

effects at the residues substituted in the triple variant can effectively impede self–association.

As observed for wild–type Hsp27, the behavior of this variant at 40 °C provides mechanistic insight into the role of phosphorylation in regulating Hsp27 behavior under simulated heat shock conditions. At 40 °C and low protein concentration, this variant forms a mixture of monomers and dimers. At higher protein concentration, a small fraction of the protein forms oligomers that are comparable in size to the largest oligomers observed for the wild–type protein at 40 °C. This behavior is identical to that reported at 20 °C, so it appears that the inhibition of Hsp27 self–association that results from these electrostatic modifications and from the related electrostatic effects of Hsp27 phosphorylation can inhibit the thermally–induced self–association of the protein. Nevertheless, if the phosphorylated variant is present at high local concentration, it is still capable of forming larger oligomers that retain chaperon activity. This observation is consistent with the previous report by Garrido and colleagues that this variant exhibits some of the features of the wild–type protein in protecting against cell death *in vivo* (Bruey *et al.*, 2000b).

Interestingly, subunit exchange by this variant was not observed at the concentration studied at either 20 or 40 °C, while chaperon activity was only reduced compared to the wild–type protein. These observations suggest behavior a combined effect for chaperon activity such that neither subunit exchange nor oligomer size is sufficient to produce chaperon activity comparable to the wild–type protein.

4.4 The N–terminal domain

The N–terminal domain of Hsp27 and its WDPF domains have been implicated previously in Hsp27 self–association although details of this involvement are somewhat controversial. For example, in the crystal structure of the thermophilic Hsp16.9, the N–terminal region of the protein is buried in the center of the dodecameric oligomer that is stabilized by pairwise intertwining of the six ordered N–terminal arms (van Montfort *et al.*, 2001). Similarly, the Tsp36 chaperon from flatworm forms dimers that are held together by interactions of N–terminal helices (Stamler *et al.*, 2005). N–terminal deletion variants lacking either the first 20 residues (Bova *et al.*, 2000) or the first 33 residues (Guo & Cooper, 2000) retain the ability to oligomerize. On the other hand, deletion of residues 5–23 from Chinese hamster Hsp27 was reported to limit self–association to dimerization (Lambert *et al.*, 1999). N–terminal deletion variants of Hsp16.2 were found to be capable of forming only dimers or tetramers (Leroux *et al.*, 1997), but this protein possesses no WDPF domain. The present results resolve at least some of these discrepancies. At 20 °C, the Δ1–14 Hsp27 variant exhibits diminished ability to oligomerize relative to the wild–type protein, and the Δ1–24 Hsp27 variant exhibits even less extensive oligomerization. However, the extent of self–association exhibited by these variants is greater than that observed for the S15D/S78D/S82D triple variant. Evidently, more of the N–terminal region is involved in self–association of Hsp27 than the WDPF domain alone. In fact, the variant Δ1–24 S78D/S82D exhibits oligomerization intermediate between that observed for the triple variant and that observed for Δ1–24 Hsp27, indicating that the loss of oligomers observed in the triple variant can be partially reversed by eliminating the first

24 residues. Although the loss of these residues influences oligomerization, it does so to a lesser extent than does a negatively charged residue at position 15.

Analyses of the two variants Δ1–14 Hsp27 and Δ1–24 Hsp27 at 40 °C establish that lack of this region of the protein also abolishes the temperature dependence of self–association. Thus, the 24 N–terminal residues of Hsp27 are required for assembly of larger oligomers and for thermally induced self–association.

Further analysis of the Δ1–14 Hsp27 variants provided greater insight into the role of this region in chaperon activity. Removing the first 14 residues completely abolished both chaperon activity and thermally induced oligomerization. On the other hand, the rate of subunit exchange increased with increasing temperature. Thus, although lack of the N–terminus reduces the size of the oligomers formed, these smaller oligomers retain the ability to dissociate and re–associate through the α–crystallin domain, the C–terminal tail, and whatever remains of the N–terminal regions. The lack of these key N–terminal residues abolishes chaperon activity to a level even lower than that observed for the triple variant, indicating that the ability to dissociate into smaller oligomers and exchange subunits is necessary but not sufficient for chaperon activity. This observation is evidence that this region of the protein is necessary to inhibit unfolding of protein substrates, either by directly binding to unfolding polypeptides or by forming stable and soluble oligomers after binding to the unfolding insulin.

The region following the first 24 amino acids of Hsp27 is highly conserved in several small Hsps, and it is predicted to form a helix with amphipathic character with residues Leu^{28}, Phe^{29}, Ala^{32} and Phe^{33} on the hydrophobic face (Pasta *et al.*, 2003). This conserved region is also present in Tsp36, in which residues Val^{31}, Leu^{32}, Asp^{33}, Asn^{34},

Val^{35}, Phe^{36} are part of an N–terminal helix that interacts with a neighboring subunit. It is interesting to compare the results obtained with the variants of Hsp27 previously described with those reported for an α–crystallin deletion mutant that lacks residues 21–28 comprising the conserved sequence S/GRLFDQF/AFG (corresponding to residues 27–35 of Hsp27). The Δ21–28 αA–crystallin variant forms oligomers of diminished size, with increased bis–AIAS binding activity, and with lower stability to urea–induced denaturation, indicating that this sequence is an important determinant of quaternary structure. Moreover, this shortened α–crystallin exhibits a faster exchange rate and enhanced chaperon activity relative to wild–type α–crystallin (Pasta *et al.*, 2003). These results argue for a direct correlation between protein destabilization and chaperon activity.

In general, all variants lacking part of the N–terminus, Δ21–28 α–crystallin as well as Δ1–14 and Δ1–24 Hsp27, exhibit diminished oligomeric assembly, indicating that any alteration to the N–terminal tail reduces the size of the oligomers formed. On the other hand, Hsp27 lacking the first 14 residues but with the intact GRLFDQAFG sequence, lacks chaperon activity, indicating that the size of the oligomers formed or the exchange rate in itself it is not sufficient to determine the ability of these proteins to function as chaperons (Table 4.1).

The deleted portion of the Δ21–28 α–crystallin is analogous to the Hsp16.9 7–SRLF–11 sequence, which contacts the Arg^{109} and Phe^{110} in the α–crystallin domain and contributes to inter– and intra–molecular contacts (van Montfort *et al.*, 2001). The current results support the idea that although oligomer dissociation is important for chaperon activity, the conserved SRLFDQFFG sequence lacks a direct role such as substrate binding as proposed

for the WDPF sequence (Theriault *et al.*, 2004) because a lack of this sequence increases rather than decreases chaperon activity. On the other hand, this role can be attributed to the first 24 residues of Hsp27. Moreover, the current results indicate that both the WDPF domain and the region at the N–terminus of the conserved WDPF domain are involved in chaperon activity and that deletion of the first 24 amino acids reduces oligomerization less than does simply introducing negative charges at position 15 by mutating Ser^{15} to aspartic acid.

Table 4.1 Physical properties of Hsp27 and α–crystallin N–terminal deletion variants compared to the wild–type proteins. Δ1–14 and Δ1–24 Hsp27 and Δ21–28 from α–crystallin (1) (Pasta *et al.*, 2003).

Hsp27 or α–crystallin variant	Oligomer size *vs.* wild–type	Chaperon Activity *vs.* wild–type	Subunit exchange vs. wild–type
Wild-type 			
Δ1-14 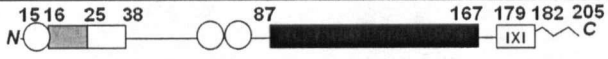	Smaller	Inactive	Similar
Δ1-24 	Smaller	Inactive	N/A
Δ29-35  (1)	Smaller	Increased	Faster

4.5 The role of the flexible C–terminal tail

The role of the C–terminal region of Hsp27 in self–association is less apparent than that of the N–terminus. The analytical ultracentrifugation data collected at 20 °C show that the 13 S peak, which is present in the sedimentation profile of the wild type protein, is not observed for the C–terminal deletion variant, but a new asymmetrical peak is present at higher S–value, and the percentage of small oligomers increases. Thus a flexible C–terminal region (Carver *et al.*, 1992; Carver *et al.*, 1995) is important for solubility, and in this case solubility is achieved by restricting the upper limit of oligomerization. On the other hand, the increase in percentage of small oligomers might indicate that this flexible extension is also involved in the oligomerization process. In both crystallographically–characterized sHsp (Hsp16.5 and Hsp16.9), subunits form critically important interactions with adjacent subunits in the assembly through the C–terminal sequences. Subunits in both of these proteins have shorter C–terminal extensions than does Hsp27, and these extensions are not flexible in the crystal structure (Kim *et al.*, 1998; van Montfort *et al.*, 2001). If the C–terminus of Hsp27 forms interactions similar to those formed by Hsp16.5 and Hsp16.9 subunits, then it should not be flexible, and it should not be observable by NMR spectroscopy. It is possible that the C–terminus forms interactions similar to those observed for Hsp16.5 and 16.9 and the tail is only flexible during intermediate states (*i.e.* dimer or tetramer), or on the other hand, it remains flexible when the Hsp27 is assembled and it interacts in a different manner than the one observed for the crystallized sHsps. It is also possible that, if this sequence remains flexible in the

oligomeric structure, it might restrict the upper limit of association by obstructing access to other monomers.

Sedimentation analysis of the Δ182–205 variant at 40 °C revealed a major peak (20–22 S) and a less prominent peak (3.5 S). This result is nearly identical to that obtained for this variant at 20 °C except that the peak at 20–22 S is more asymmetric and tails toward higher S values at lower temperature. Notably, the *c(s)* plots of this deletion variant and of the wild–type protein are virtually identical at 40 °C. Thus, the difference in self–association observed between this variant and the wild–type protein at 20 °C is abolished at 40 °C. This observation is consistent with the conclusion that for the wild–type protein, the C–terminal sequence inhibits formation of larger oligomers at 20 °C and that this inhibition is overcome simply by increasing temperature. In other words, at 20 °C the Δ182–205 Hsp27 variant is effectively locked in a larger oligomeric state that the wild–type protein can only form at 40 °C.

Deletion of the last 24 residues also severely affects chaperon activity. At 20 °C and in the presence of unfolding insulin, the Δ182–205 Hsp27 variant increases the amount of light scattered (increases precipitation) relative to unfolded insulin alone (Figure 3.29 p.91). It is not entirely clear why scattering increases because this variant alone does not precipitate in the presence of DTT. Perhaps Hsp27 lacking the C–terminal sequence binds to unfolding insulin but the Hsp27–insulin complex is not soluble. Alternatively, the Δ182–205 Hsp27 variant bound to insulin forms larger precipitates compared to insulin alone so light scattering increases. At 40 °C, the ΔC variant reduces scattering relative to a sample of insulin and DTT alone although the amount of scattering remains greater than

that observed in the presence of the wild–type protein at the same temperature. It seems that the chaperon activity of the ΔC variant is greater at 40 °C than at 20 °C. These results are in agreement with the analytical ultracentrifugation experiments in which Δ182–205 Hsp27 behaved more like the wild–type protein at 40 °C than at 20 °C. It is important to note that upon binding to the substrate, the C–terminal tail of murine Hsp25 remains flexible and observable by NMR spectroscopy (Lindner *et al.*, 2000).

FRET experiments indicate that although some energy transfer is observed upon mixing the AIAS– and LYI– modified C–terminal deletion variant, the effect is limited and is not induced by increased temperature. The absence of the C–terminal tail also increases the thermostability of Hsp27. Thus, oligomer size, subunit exchange and chaperon activity are highly influenced by the C–terminal tail, which could undergo conformational changes to accommodate different oligomers sizes.

The monomeric folds of the two small heat shock proteins that have been crystallized are similar to each other, but Hsp16.5 forms 24–mers, and the wheat protein is a dodecamer (Kim *et al.*, 1998; van Montfort *et al.*, 2001). The structural origin of this difference remains unknown, but there is increasing evidence that the C–terminal tail plays a critical role in stabilization of the assembly. The conserved IXI motif of both proteins forms similar interactions with the α–crystallin domain, but while the thermophilic Hsp forms these interactions with the C–terminus present in only one orientation, the C–terminal extension of the wheat protein exhibits two distinct conformations in which a hinge between the β9 and β10 strands allows the angle between the α–crystallin domain and the C–terminal tail to vary by 30 °C. A similar feature is observed in the viral VP1

protein from polyomavirus (Liddington *et al.*, 1991). VP1 is a pentameric protein that forms larger oligomers, the size and shape of which are mainly controlled by the C–terminal tail. Five tails, one from each monomer in the pentamer, interact with a subunit on an adjacent pentamer through conserved interactions. Similarly, domain swapping, which contributes to structural diversity in the lens βγ–crystallin family, is controlled by the C–terminal extensions (Bax *et al.*, 1990; Schlunegger *et al.*, 1997). Similar hinge mechanisms may contribute to the size and polydispersity observed for most sHsps (van Montfort *et al.*, 2001). Tsp36 lacks an extended C–terminal tail, and the IXI/V motif, which binds the hydrophobic groove at the β4–β8 interface, is present at the N–terminus (Ile^3, Pro^5). This situation indicates that the interaction of the IXI motif with the β4–β8 groove in the α–crystallin domain is important for assembly of higher order oligomers and that the C– and N–termini of small heat shock proteins are somehow flexible and interchangeable.

Cryo–EM studies of αB–crystallin show the presence of a large central cavity within the protein assembly, and the protein shell is observed at low resolution owing to weak density (Haley *et al.*, 1998). In that study a variable quaternary structure was observed in which each image represents a different conformation of the assembly rather than a different view of the same symmetrical assembly. The authors concluded that most of the variability is observed in the outer shell and results from the flexible and exposed C–terminal tail.

4.6 The use of histidine tag for small heat shock proteins

While the N–terminal His_6–tagged Hsp27 has no biological role, the ease with which this form of the protein can be purified makes it an appealing alternative to the true wild–type protein for use *in vitro*. As a result, it is important to determine whether this form of the protein is functionally equivalent to the wild–type protein or if the His_6 tag perturbs the behavior of Hsp27 significantly. The present analysis demonstrates clearly that introduction of the His_6 sequence at the N–terminus of either the wild–type protein or the S15D/S78D/S82D variant induces a far greater extent of oligomerization than observed for any other form of the protein. This observation presumably explains the extensive self–association reported for a 33 residue N–terminal deletion variant, which was expressed and studied with an N–terminal poly–His tag (Guo & Cooper, 2000).

4.7 Conclusions

An essential feature of the experimental approach used in this work has been the use of the *c(s)* analysis provided by the programs SEDFIT and SEDPHAT. The numerical analyses provided by these programs do not require initial guesses or information concerning the system under analysis other than the standard physical parameters (*e.g.*, temperature, buffer viscosity and density, and the protein amino acid sequence). Overall, the current results establish that human Hsp27 demonstrates considerable variability in the extent to which it can oligomerize in response to various solution conditions. Under all conditions studied, the wild–type protein and all variants are polydisperse and exhibit variable distribution between larger and smaller oligomeric forms.

Each domain of Hsp27 must be considered in regard to its role in self–association of Hsp27 in the absence of substrate but also in terms of its contribution to the chaperon activity of Hsp27. While these two properties of Hsp27 are related, they are not equivalent. The N– and C–termini as well as the sites of phosphorylation influence both properties. The following discussion proposes a model for Hsp27 self–association based on the current data as well as the three available small Hsp crystal structures: Hsp16.5, Hsp16.9 and Tsp36. The mechanism of Hsp27 chaperon activity is discussed subsequently.

4.7.1 Model for Hsp27 self–association

Introducing aspartic acid residues at position 15, 78 and 82 completely disrupts oligomerization, reducing Hsp27 to a mixture of monomers and covalently bound dimers with just a trace of large oligomers. While both Hsp16.5 and Hsp16.9 lack a cysteinyl residue, Hsp27 as well as Tsp36 have a single cysteine located in the β5–β7 loop. Although the structure of Tsp36 that has been solved is dimeric, and the dimers are not formed through this cysteinyl residue, Tsp36 tetramerizes under oxidizing conditions. Moreover, the position of the only cysteine residue is ideal for formation of a covalently bound tetramer (Figure 4.2 and Figure 1.7 p.13).

With charged amino acid residues at positions 15, 78, 82, the self–association equilibrium is clearly shifted toward the formation of smaller oligomers. At the same time, the ability to form covalently bound dimers is maintained, indicating that the interface for dimerization through disulfide bridge formation must be different from that influenced by the aspartic acid or phosphorylation *in vivo*. The presence of this cysteine and the ability to form covalently bound dimers despite phosphorylation may be important in regulating the

cellular glutathione level, a role that has been attributed to Hsp27 (Mehlen *et al.*, 1996). Moreover, for some biological functions of Hsp27, *e.g.* binding to cytochrome *c*, Cys^{137} is essential (Bruey *et al.*, 2000a). Another indication that the cysteinyl residue is not essential for oligomerization and chaperon activity derives from the observation that the C137S variant of Hsp27 forms large oligomers in a manner similar to the wild–type protein (data not shown) and that chaperon activity is measured in a large excess of DTT. Thus oxidizing conditions are not necessary for either properties of this protein.

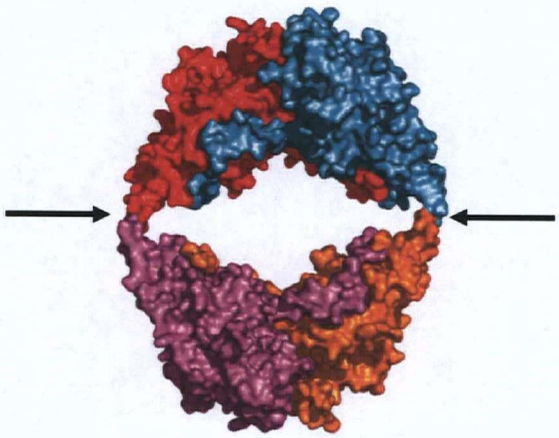

Figure 4.2 Model of Tsp36 tetramer. The dimer–dimer interaction was created by modeling a pair of disulphide bonds and assuming a 2–fold axis between dimers. The position of the cysteinyl residues is indicated with an arrow. (Modified from (Stamler *et al.*, 2005))

The structures of Hsp16.9 and Hsp16.5 both indicate that the N–terminus is involved in oligomerization and is directed towards the centre of the large oligomeric assembly. Moreover, Tsp36 forms tightly bound dimers through α–helices at its

N–terminus (Stamler *et al.*, 2005). Current and previously–reported experiments establish that this region of the protein is crucial for oligomerization.

Hsp27 and α–crystallin form oligomers of varying size, the range of which is diminished by selectively removing regions of the N–terminal sequence. This fact leads to the conclusion that the N–terminus acts as an amphiphilic protrusion of helices separated by prolyl residues (Figure 4.3) that helps control the size of Hsp27 oligomers. As this arm is reduced in length, the α–crystallin domains become closer to the core of the assembly, and fewer oligomeric states are accessible. Thus, the size of Hsp27 oligomers varies in the order wild–type > Δ1–14 variant > Δ1–24 variant and the Δ21–28 variant of α–crystallin is smaller than that of the corresponding wild–type protein. Nevertheless, although the oligomers formed by the Δ1–24 variant of Hsp27 are smaller than those formed by the wild–type protein, they are considerably larger than those formed by the S15D/S78D/S82D Hsp27 triple variant, consistent with retention of some interactions maintained by the α–crystallin domain. Moreover, removal of the 24 N–terminal residues in the Δ1–24/S78D/S82D Hsp27 variant restores the ability to form some larger oligomers. Evidently, the change in charge at residue 15 resulting from replacement of Ser with Asp has a greater effect on oligomerization than does removal of residues 1–24. Thus, in the absence of the S15D substitution in the Δ1–24/S78D/S82D variant, the remainder of the N–terminal sequence is sufficient to promote some oligomerization. The Asp residues at positions 78 and 82 promote dissociation at a different subunit interface. This model is consistent with the FRET experiments in which subunit exchange is observed for the

Δ1–14 Hsp27 variant, thereby demonstrating that the oligomers that are formed by this variant retain the ability to dissociate and re–associate in a highly dynamic manner.

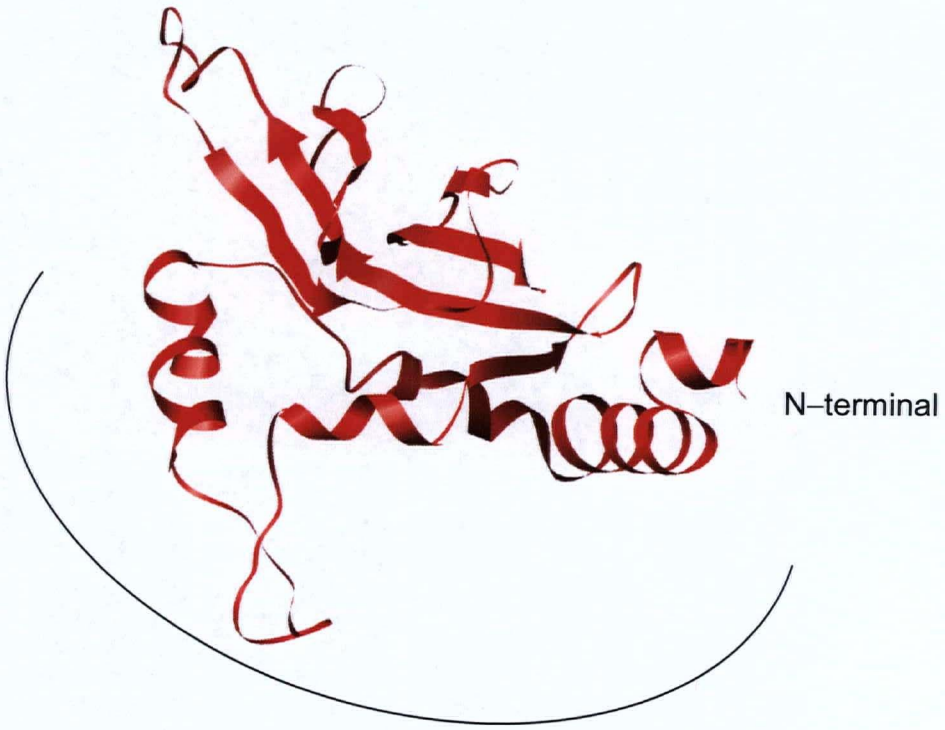

Figure 4.3 Model of Hsp27 based on the Tsp36 crystal structure (Stamler *et al.*, 2005) The model includes the residues 6–170 of wild–type Hsp27. The N–terminal region is labeled and indicated with a black line.

The role of the C–terminal 24 residues in oligomerization is more controversial. The flexible C–terminal tail that follows the conserved IXI region of Hsp27 is longer than the C–terminus of both Hsp16.5 and Hsp16.9. The IXI motif of Hsp16.9, for example, is followed by only 8 residues. Moreover, replacement of Pro^{182} with Leu, which is located at the hinge between the IXI motif and the last 24 residues, is the only known mutation outside of the α–crystallin domain that leads to a human disease (Evgrafov *et al.*, 2004).

The IXI/V motif is highly conserved amongst small heat shock proteins from protozoans to metazoans. Even Tsp36 which completely lacks a C–terminal tail has a PXI motif at its N–terminus that interacts with the C–terminal edge of the α–crystallin domain in the β4–β8 hydrophobic groove in a manner similar to that observed in the structures of Hsp16.5 and Hsp 16.9 (Kim *et al.*, 1998; Stamler *et al.*, 2005; van Montfort *et al.*, 2001) (Figure 4.4). It is tempting to speculate that the IXI motif of Hsp27 binds in a similar fashion, but two questions remain: what is the role of the following 24 residues (Pro^{182}–Lys^{205}) and to which subunit does each IXI motif bind? The first obvious role that can be attributed to the C–terminal tail is to increase solubility by coating the large assembly with a hydrophilic tail in a similar manner as hydrophilic heads would do in micellae. Cryo–EM as well as NMR experiments can confirm the flexibility of the C–terminal tail and its exposure to the solvent when the protein forms large assemblies.

The results presented so far suggest that this flexible tail does more than just render Hsp27 soluble. Lack of the C–terminus increases the thermal stability of the protein, indicating that a second role for this region is to initiate protein unfolding as a result of its mobility. In general, thermal instability of small heat shock proteins has been linked to

chaperon activity. The Δ21–28 α–crystallin variant, for example, has increased instability and increased chaperon activity relative to the wild–type protein (Pasta *et al.*, 2003).

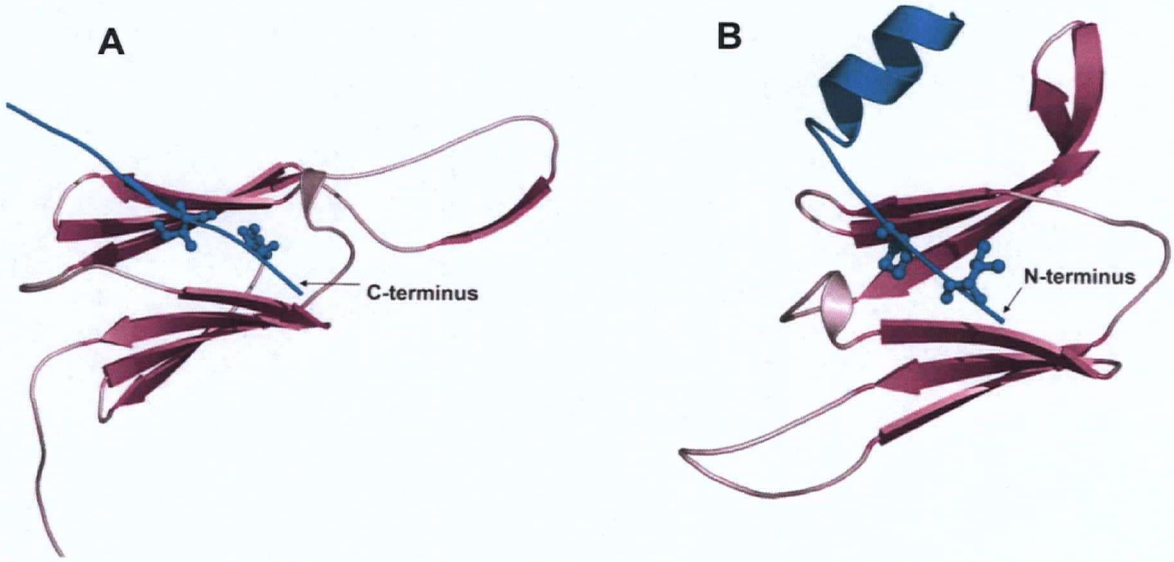

Figure 4.4 Interaction of the IXI motif with the C–terminal edge of the α–crystallin domain (β4–β8). A. Hsp16.9, α–crystallin of one molecule and IXI motif of a neighboring subunit (stick & ball representation). **B.** Tsp36 α–crystallin 1 with the N–terminal PXI of the dimeric partner (stick & ball representation). (Modified from (Stamler *et al.*, 2005))

Similarly, another α–crystallin variant with increased hydrophobicity at its C–terminus is less soluble, has diminished chaperon activity and a less flexibility tail as seen by NMR spectroscopy (Smulders *et al.*, 1996). It is possible that after heat shock the increased thermal energy induces greater conformational variation in the C–terminal tail that leads to dissociation of the large oligomers.

Finally, although the IXI motif binds to the β4–β8 groove of an α–crystallin domain, exactly to which domain within an oligomeric assembly will depend on a number of factors including the length of the N–terminal tail and the conformation of the C–terminal flexible region. In fact, the absence of the last 24 residues successfully locks the protein into a large assembly state compared to the wild–type protein. Moreover, the Δ182–205 Hsp27 variant, while it exchanges domains in a FRET experiment, exhibits a temperature independent rate of exchange. Interestingly in that conserved region, Hsp27 has more than one IXI/V motif, the amino acid sequence at the C–terminus is $\underline{I}^{179}T\underline{I}P\underline{V}$, it is possible that which IXI motif binds to another subunit depends on how large the oligomer is.

The mechanism of Hsp27 self–association is clearly complex. Nevertheless, the ability to form a vast number of oligomers in a thermally–regulated manner must depend on simple interactions. The model resulting from this work proposes that in addition to binding through the α–crystallin domain, N–terminal helices can form multiple interactions with similar regions of neighboring monomers, and the C–terminal tail can undergo temperature–dependent conformational changes that determine to which subunit the IXI motif will bind to.

Finally, the role of the α–crystallin domain is probably to mediate the basic subunit–subunit interactions, and it is possible that these interactions occur in more than one way as it is observed for the Hsp16.5, Hsp16.9 and Tsp36 proteins.

4.7.2 Model for Hsp27 chaperon activity

Hsp27 exhibits remarkable versatility in its ability to form oligomers of varying size, to bind a wide range of unfolding substrates, and to recognize specific, folded proteins. The present work is an effort to correlate the oligomeric state of the protein with its chaperon activity and to define the contributions made by specific domains or residues to both of these aspects of Hsp27 function.

Wild–type Hsp27 fully inhibits insulin unfolding at a ratio much smaller than 1:1 (insulin:Hsp27 subunit), and one Hsp27 oligomer can bind more than one molecule of insulin at a time. The crystal structures of Hsp16.9, Hsp16.5, and Tsp36 all indicate that upon formation of the large oligomer, an extensive hydrophobic surface of each monomer is buried in the final assembly. Repeated dissociation and re–association presumably expose similar hydrophobic patches on the surface of Hsp27 that result in recognition and interaction with unfolding peptides. Such interactions are expected to be relatively non–specific and to result in the involvement of several surface areas of Hsp27 in binding of insulin or other proteins of a variety of sizes.

If Hsp27 must dissociate prior to binding unfolding proteins, then an increased tendency to dissociate should increase chaperon activity. Such behavior was observed in the current studies insofar as increased temperature was found to result in an increased rate of Hsp27 subunit exchange (FRET experiments), an increase in Hsp27 oligomeric size (AUC experiments), and an increase in chaperon activity (activity measurements). The present results (Fig. 3.40; NMR unpublished) indicate that increased temperature also induces a conformational change and greater mobility in the C–terminal region of the protein that promotes faster subunit exchange and the formation of larger (possibly more

stable) oligomers. In the presence of unfolding proteins, greater accessibility of hydrophobic surfaces of Hsp27 afforded by elevated temperature should promote Hsp27–unfolding protein interaction.

While subunit exchange may be necessary for chaperon activity, it is not sufficient. The Δ1–14 Hsp27 variant exhibits no chaperon activity despite FRET behavior consistent with subunit exchange. This result can be attributed to a role for the 14 amino–terminal residues in binding to unfolding proteins and in the formation of larger oligomers. This conclusion is consistent with cryo–EM studies of Hsp25 and Hsp26 that indicate these proteins bind substrate to form complexes at least as large as those form by each protein in the absence of substrate (Stromer *et al.*, 2003).

The lack of a flexible C–terminal tail in the Δ182–205 variant inhibits chaperon activity only at low temperature (20 °C) while activity persists at heat shock temperature (40 °C). This observation is in agreement with the results of analytical ultracentrifugation studies in which behavior similar to that of the wild–type protein is observed at 40 °C but not at 20 °C. It is not entirely clear why this would occur, but it can be attributed to a lower solubility of this variant at 20 °C.

Interestingly, light scattering of unfolding insulin at 20 °C is greater in the presence of the Δ182–205 variant than in its absence, probably as a result of the formation of insoluble Δ182–205/insulin complexes that scatter light more than does unfolding insulin alone.

Surprisingly, the S15D/S78D/S82D triple variant retained a reasonable amount of chaperon activity despite an apparent lack of subunit exchange and minimal formation of larger oligomers. These observations would be expected if this variant forms larger

complexes upon binding the unfolding insulin and if the abundant, small oligomers formed by this variant occur in the "active," dissociated state. This interpretation could explain why the first cellular response to heat shock *in vivo* is phosphorylation of Hsp27. Phosphorylation of this protein would promote its dissociation and thereby increase access of unfolding proteins to the otherwise inaccessible hydrophobic surfaces through which Hsp27 is proposed to interact with such proteins. In this way, time is provided to permit synthesis of unphosphorylated Hsp27 and larger chaperones (*e.g.*, Hsp70) for a prolonged rescue response.

4.8 Future directions

The work described in this dissertation is an attempt to define the biophysical properties of the small Hsp27 and the role that conserved and non–conserved domains play in self–association and chaperon activity. Although small heat shock proteins are highly conserved in all organisms and great effort has been made to understand their function and behavior in solution, more work remains. It is also clear that despite many similar features each sHsp must be considered individually.

At least four directions for future studies of Hsp27 can be identified: a) further studies of the solution properties of Hsp27, b) further studies of Hsp27 chaperon activity and interaction with unfolding peptides, c) characterization of complexes formed by Hsp27 and specific native proteins and d) studies of the roles of Hsp27 in malignancies and its potential as a therapeutic target. Each possibility is considered below.

The hypothesis that the length of the N–terminal sequence regulates the size of the oligomers could be evaluated, by studies of variants of Hsp27 with longer rather than shorter N–terminal sequences in terms of oligomerization behavior and chaperon activity.

On the other hand, point mutation at the C–terminal tail, specifically in the IXI motif region, can be constructed to determine if this region acts as a hinge to regulate the sizes of the oligomers. Moreover, other deletion variants of Hsp27 with different length of C–terminus (Δ168–205 and Δ195–205 Hsp27), or deletion at both the N– and C–termini (Δ1–24+Δ165–205 Hsp27) have been already cloned in pET–30 vectors (B. L.–G. unpublished). These variants should be evaluated by analytical ultracentrifugation.

The proposal that phosphorylation of Hsp27 results in rapid exposure of hydrophobic surfaces to permit synthesis of more wild–type Hsp27 as a second wave of defense against cellular stress is appealing. Such a possibility makes it of interest to determine if a mixture of wild–type Hsp27 and the Hsp27 triple variant undergoes subunit exchange. Both analytical ultracentrifugation and FRET experiments would be suitable for this study.

It is clear that the polydispersity and structural dynamics of Hsp27 contribute to the difficulty in preparing crystals suitable for diffraction analysis. Although an attempt has been made to collect cryo–EM data, little useful information has been acquired other than the knowledge of the polydispersity of the sample (Haley *et al.*, 2000). The current results indicate that Hsp27 is extremely sensitive to temperature changes. Insight concerning this temperature dependence provided by the present study, might permit the design of new cryo–EM experiments in which, oligomerization of Hsp27 is tightly controlled with temperature prior to sample freezing.

Far more work is required to understand Hsp27 chaperon activity at a molecular level. One approach might be to purify the complexes formed by unfolding insulin and LYI– and AIAS–modified Hsp27 to evaluate the influence of peptide binding on subunit

exchange. The size and stoichiometry of the resulting purified complexes can be analyzed through the use of analytical ultracentrifugation. Moreover, if subunit exchange is observed between wild–type Hsp27 and the S15D/S78D/S82D variant, FRET experiments can be undertaken to evaluate interaction of phosphorylated variants bound to unfolding peptides and to wild–type Hsp27 free of substrate. Spectra of labeled Hsp27, either AIAS– or LYI–modified protein, mixed with free Hsp27 need to be recorded to control for light scattering. Sedimentation velocity experiments and chaperon activity measurements of the modified variants should be done to ensure that labeling has not changed the quaternary structure and activity of Hsp27. Moreover, it would be interesting to see if a peptide comprise of amino acids 1–24 of Hsp27 can inhibit self–association by competing for binding to the protein N–terminus.

Formation of an Hsp27–cytochrome *c* complex was not observed under any of the conditions tested although such complex has been reported in the literature (Bruey *et al.*, 2000a). This discrepancy could be explained by the requirement of an additional protein that would permit formation of a ternary complex. This possibility could be assessed by the use of mass spectrometry to determine the proteins present in an immunoprecipitate of Hsp27 bound to cytochrome *c* and/or cytochrome *c* bound to Hsp27 in an effort to identify other possible partners in the interaction. At the same time, Hsp27 has been reported to form specific complexes with actin and Daxx. Initial work succeeded in the preparation of a Hsp27–actin complex, and crystallization trails were initiated through a collaboration with Dr. Burtnick. Although these screens have yet to produce any crystals, it might be useful to study this complex in solution. The variants of Hsp27 already available could be

used to determine which domain of Hsp27 actin binds, while analytical ultracentrifugation could be used to determine the stoichiometry and association constant for the interaction.

Hsp27 synthesis is induced by cellular stress, and Hsp27 has been reported to reduce the chance of a successful chemotherapy when over–expressed in tumor cells (Rocchi *et al.*, 2005; Rocchi *et al.*, 2004). For this reason, inhibition of Hsp27 expression through the use of nucleotide–based therapies has been attempted (Kamada *et al.*, 2007). Alternatively, identification of small molecules that bind to Hsp27 and either inhibit dissociation of the oligomer or inhibit phosphorylation could lead to therapeutic inhibitors that reduce the chaperon activity of Hsp27 that can be used as adjuvant in chemotherapies. The chaperon assay presented in this work can be translated easily into a high throughput assay for inhibitor screening. If such a compound is found, it would open a new field of work concerning the mechanism(s) by which small molecules inhibit Hsp27 chaperon activity. Again, use of the variants reported in this dissertation in screens of this type could provide useful mechanistic insights. Finally, several point mutants of Hsp27 that induce pathological conditions have been reported (Benndorf & Welsh, 2004; Evgrafov *et al.*, 2004); the molecular mechanism(s) responsible for this pathological activity of these Hsp27 variants could be evaluated by methods employed in the current studies.

5. BIBLIOGRAPHY

Akhtar MW, Srinivas V, Raman B, Ramakrishna T, Inobe T, Maki K, Arai M, Kuwajima K and Rao Ch M. (2004). Oligomeric Hsp33 with enhanced chaperone activity: gel filtration, cross-linking, and small angle x-ray scattering (SAXS) analysis, *J. Biol. Chem.*, **279,** 55760-55769.

Aquino DA, Capello E, Weisstein J, Sanders V, Lopez C, Tourtellotte WW, Brosnan CF, Raine CS and Norton WT. (1997). Multiple sclerosis: altered expression of 70- and 27-kDa heat shock proteins in lesions and myelin, *J. Neuropathol. Exp. Neurol.*, **56,** 664-672.

Arrigo AP and Welch WJ. (1987). Characterization and purification of the small 28,000-dalton mammalian heat shock protein, *J. Biol. Chem.*, **262,** 15359-15369.

Ashburner M and Bonner JJ. (1979). The induction of gene activity in drosophilia by heat shock, *Cell*, **17,** 241-254.

Bax B, Lapatto R, Nalini V, Driessen H, Lindley PF, Mahadevan D, Blundell TL and Slingsby C. (1990). X-ray analysis of beta B2-crystallin and evolution of oligomeric lens proteins, *Nature*, **347,** 776-780.

Beaulieu JF, Arrigo AP and Tanguay RM. (1989). Interaction of Drosophila 27,000 Mr heat-shock protein with the nucleus of heat-shocked and ecdysone-stimulated culture cells, *J. Cell. Sci.*, **92 (Pt 1),** 29-36.

Bedard PA and Brandhorst BP. (1986). Translational activation of maternal mRNA encoding the heat-shock protein hsp90 during sea urchin embryogenesis, *Dev. Biol.*, **117,** 286-293.

Behlke J, Lutsch G, Gaestel M and Bielka H. (1991). Supramolecular structure of the recombinant murine small heat shock protein hsp25, *FEBS Lett.*, **288,** 119-122.

Benndorf R, Hayess K, Ryazantsev S, Wieske M, Behlke J and Lutsch G. (1994). Phosphorylation and supramolecular organization of murine small heat shock protein HSP25 abolish its actin polymerization-inhibiting activity, *J. Biol. Chem.*, **269,** 20780-20784.

Benndorf R, Sun X, Gilmont RR, Biederman KJ, Molloy MP, Goodmurphy CW, Cheng H, Andrews PC and Welsh MJ. (2001). HSP22, a new member of the small heat shock protein superfamily, interacts with mimic of phosphorylated HSP27 ((3D)HSP27), *J. Biol. Chem.*, **276,** 26753-26761.

Benndorf R and Welsh MJ. (2004). Shocking degeneration, *Nat. Genet.*, **36,** 547-548.

Bhat SP and Nagineni CN. (1989). alpha B subunit of lens-specific protein alpha-crystallin is present in other ocular and non-ocular tissues, *Biochem. Biophys. Res. Commun.*, **158,** 319-325.

Bienz M and Pelham HR. (1982). Expression of a Drosophila heat-shock protein in Xenopus oocytes: conserved and divergent regulatory signals, *Embo J.*, **1,** 1583-1588.

Bloemendal H. (1981). *Molecular and cellualar biology of the eye lens.* John Wiley and Sons: New York.

Boelens WC, Van Boekel MA and De Jong WW. (1998). HspB3, the most deviating of the six known human small heat shock proteins, *Biochim. Biophys. Acta*, **1388,** 513-516.

Bova MP, Ding LL, Horwitz J and Fung BK. (1997). Subunit exchange of alphaA-crystallin, *J. Biol. Chem.*, **272,** 29511-29517.

Bova MP, Huang Q, Ding L and Horwitz J. (2002). Subunit exchange, conformational stability, and chaperone-like function of the small heat shock protein 16.5 from Methanococcus jannaschii, *J. Biol. Chem.*, **277,** 38468-38475.

Bova MP, McHaourab HS, Han Y and Fung BK. (2000). Subunit exchange of small heat shock proteins. Analysis of oligomer formation of alphaA-crystallin and Hsp27 by fluorescence resonance energy transfer and site-directed truncations, *J. Biol. Chem.*, **275,** 1035-1042.

Brenner SL, Zlotnick A and Stafford WF, 3rd. (1990). RecA protein self-assembly. II. Analytical equilibrium ultracentrifugation studies of the entropy-driven self-association of RecA, *J. Mol. Biol.*, **216,** 949-964.

Bruey JM, Ducasse C, Bonniaud P, Ravagnan L, Susin SA, Diaz-Latoud C, Gurbuxani S, Arrigo AP, Kroemer G, Solary E and Garrido C. (2000a). Hsp27 negatively regulates cell death by interacting with cytochrome c, *Nat. Cell. Biol.*, **2,** 645-652.

Bruey JM, Paul C, Fromentin A, Hilpert S, Arrigo AP, Solary E and Garrido C. (2000b). Differential regulation of HSP27 oligomerization in tumor cells grown in vitro and in vivo, *Oncogene*, **19,** 4855-4863.

Cantor CR and Schimmel PR. (1980). *Biophysical Chemistry of Macromolecules, Pt. 3: The Behavior of Biological Macromolecules.* San Francisco: W. H. Freeman.

Carver JA, Aquilina JA, Truscott RJ and Ralston GB. (1992). Identification by ^{1}H NMR spectroscopy of flexible C-terminal extensions in bovine lens alpha-crystallin, *FEBS Lett.*, **311,** 143-149.

Carver JA, Esposito G, Schwedersky G and Gaestel M. (1995). ^{1}H NMR spectroscopy reveals that mouse Hsp25 has a flexible C-terminal extension of 18 amino acids, *FEBS Lett.*, **369,** 305-310.

Carver JA and Lindner RA. (1998). NMR spectroscopy of alpha-crystallin. Insights into the structure, interactions and chaperone action of small heat-shock proteins, *Int. J. Biol. Macromol.*, **22,** 197-209.

Caspers GJ, Leunissen JA and de Jong WW. (1995). The expanding small heat-shock protein family, and structure predictions of the conserved "alpha-crystallin domain", *J. Mol. Evol.*, **40,** 238-248.

Chadli A, Ladjimi MM, Baulieu EE and Catelli MG. (1999). Heat-induced oligomerization of the molecular chaperone Hsp90. Inhibition by ATP and geldanamycin and activation by transition metal oxyanions, *J. Biol. Chem.*, **274,** 4133-4139.

Charette SJ, Lavoie JN, Lambert H and Landry J. (2000). Inhibition of Daxx-mediated apoptosis by heat shock protein 27, *Mol. Cell. Biol.*, **20,** 7602-7612.

Chowdary TK, Raman B, Ramakrishna T and Rao CM. (2004). Mammalian Hsp22 is a heat-inducible small heat-shock protein with chaperone-like activity, *Biochem. J.*, **381,** 379-387.

Corces V, Pellicer A, Axel R and Meselson M. (1981). Integration, transcription, and control of a Drosophila heat shock gene in mouse cells, *Proc. Natl. Acad. Sci. U S A*, **78,** 7038-7042.

Cuff JA and Barton GJ. (2000). Application of multiple sequence alignment profiles to improve protein secondary structure prediction, *Proteins*, **40,** 502-511.

Dam J and Schuck P. (2005). Sedimentation velocity analysis of heterogeneous protein-protein interactions: sedimentation coefficient distributions c(s) and asymptotic boundary profiles from Gilbert-Jenkins theory, *Biophys. J.*, **89,** 651-666.

Dam J, Velikovsky CA, Mariuzza RA, Urbanke C and Schuck P. (2005). Sedimentation velocity analysis of heterogeneous protein-protein interactions: Lamm equation modeling and sedimentation coefficient distributions c(s), *Biophys. J.*, **89,** 619-634.

Darmon MC and Paulin DJ. (1985a). Translational activity of mRNA coding for cytoskeletal brain proteins in newborn and adult mice: a comparative study, *J. Neurochem.*, **44,** 1672-1678.

Darmon MC and Paulin DJ. (1985b). Translational activity of mRNA coding for cytoskeletal brain proteins in newborn and adult mice: a comparative study, *J Neurochem*, **44,** 1672-8.

de Jong WW, Leunissen JA, Leenen PJ, Zweers A and Versteeg M. (1988). Dogfish alpha-crystallin sequences. Comparison with small heat shock proteins and Schistosoma egg antigen, *J. Biol. Chem.*, **263,** 5141-5149.

Dudich IV, Zav'yalov VP, Pfeil W, Gaestel M, Zav'yalova GA, Denesyuk AI and Korpela T. (1995). Dimer structure as a minimum cooperative subunit of small heat-shock proteins, *Biochim. Biophys. Acta*, **1253,** 163-168.

Ehrnsperger M, Graber S, Gaestel M and Buchner J. (1997). Binding of non-native protein to Hsp25 during heat shock creates a reservoir of folding intermediates for reactivation, *Embo J.*, **16,** 221-229.

Ehrnsperger M, Lilie H, Gaestel M and Buchner J. (1999). The dynamics of Hsp25 quaternary structure. Structure and function of different oligomeric species, *J. Biol. Chem.*, **274,** 14867-14874.

Espenson JH. (1981). *Chemical kinetics and reaction mechanisms*. McGraw-Hill Book Company.

Evgrafov OV, Mersiyanova I, Irobi J, Van Den Bosch L, Dierick I, Leung CL, Schagina O, Verpoorten N, Van Impe K, Fedotov V, Dadali E, Auer-Grumbach M, Windpassinger C, Wagner K, Mitrovic Z, Hilton-Jones D, Talbot K, Martin JJ, Vasserman N, Tverskaya S, Polyakov A, Liem RK, Gettemans J, Robberecht W, De Jonghe P and Timmerman V. (2004). Mutant small heat-shock protein 27 causes axonal Charcot-Marie-Tooth disease and distal hereditary motor neuropathy, *Nat. Genet.*, **36,** 602-606.

Ewart AK, Morris CA, Atkinson D, Jin W, Sternes K, Spallone P, Stock AD, Leppert M and Keating MT. (1993). Hemizygosity at the elastin locus in a developmental disorder, Williams syndrome, *Nat. Genet.*, **5,** 11-6.

Farrelly FW and Finkelstein DB. (1984). Complete sequence of the heat shock-inducible HSP90 gene of Saccharomyces cerevisiae, *J Biol Chem*, **259,** 5745-51.

Fontaine JM, Rest JS, Welsh MJ and Benndorf R. (2003). The sperm outer dense fiber protein is the 10th member of the superfamily of mammalian small stress proteins, *Cell Stress Chaperones*, **8,** 62-69.

Förster T. (1948). Intermolecular energy migration and flurescence, *Ann. Phys.*, **2,** 55-75.

Franzmann TM, Wuhr M, Richter K, Walter S and Buchner J. (2005). The activation mechanism of Hsp26 does not require dissociation of the oligomer, *J. Mol. Biol.*, **350,** 1083-1093.

Frigon RP and Timasheff SN. (1975). Magnesium-induced self-association of calf brain tubulin. I. Stoichiometry, *Biochemistry*, **14,** 4559-4566.

Fu X, Liu C, Liu Y, Feng X, Gu L, Chen X and Chang Z. (2003). Small heat shock protein Hsp16.3 modulates its chaperone activity by adjusting the rate of oligomeric dissociation, *Biochem. Biophys. Res. Commun.*, **310,** 412-420.

Garrido C. (2002). Size matters: of the small HSP27 and its large oligomers, *Cell. Death Differ.*, **9,** 483-485.

Garrido C, Fromentin A, Bonnotte B, Favre N, Moutet M, Arrigo AP, Mehlen P and Solary E. (1998). Heat shock protein 27 enhances the tumorigenicity of immunogenic rat colon carcinoma cell clones, *Cancer Res.*, **58,** 5495-5499.

Garrido C, Gurbuxani S, Ravagnan L and Kroemer G. (2001). Heat shock proteins: endogenous modulators of apoptotic cell death, *Biochem. Biophys. Res. Commun.*, **286,** 433-442.

Garrido C and Solary E. (2003). A role of HSPs in apoptosis through "protein triage"? *Cell. Death Differ.*, **10,** 619-620.

Gasteiger E, Hoogland C, Gattiker A, Duvaud S, Wilkins MR, Appel RD and Bairoch A. (2005). *The Proteomics Protocols Handbook.* (Ed) Jmw (ed.). Humana Press, pp 571-607.

Giebeler R. (1992). *Analytical Ultracentrifugation in Biochemistry and Polymer Science.* S.E. Harding Ajr, and J.C. Horton (ed.). The Royal Society of Chemistry: Cambridge, U.K., pp 16-25.

Gill SC and von Hippel PH. (1989). Calculation of protein extinction coefficients from amino acid sequence data, *Anal. Biochem.*, **182,** 319-326.

Gough J, Karplus K, Hughey R and Chothia C. (2001). Assignment of homology to genome sequences using a library of hidden Markov models that represent all proteins of known structure, *J. Mol. Biol.*, **313,** 903-919.

Guo Z and Cooper LF. (2000). An N-terminal 33-amino-acid-deletion variant of hsp25 retains oligomerization and functional properties, *Biochem. Biophys. Res. Commun.*, **270,** 183-189.

Gusev NB, Bogatcheva NV and Marston SB. (2002). Structure and properties of small heat shock proteins (sHsp) and their interaction with cytoskeleton proteins, *Biochemistry (Mosc.)*, **67,** 511-519.

Haley DA, Bova MP, Huang QL, McHaourab HS and Stewart PL. (2000). Small heat-shock protein structures reveal a continuum from symmetric to variable assemblies, *J. Mol. Biol.*, **298,** 261-272.

Haley DA, Horwitz J and Stewart PL. (1998). The small heat-shock protein, alphaB-crystallin, has a variable quaternary structure, *J. Mol. Biol.*, **277,** 27-35.

Hanlon S, Lamers K, Lauterbach G, Johnson R and Schachman HK. (1962). Ultracentrifuge studies with absorption optics. I. An automatic photoelectric scanning absorption system, *Arch. Biochem. Biophys.*, **99,** 157-174.

Hartl FU and Hayer-Hartl M. (2002). Molecular chaperones in the cytosol: from nascent chain to folded protein, *Science*, **295,** 1852-1858.

Haslbeck M, Walke S, Stromer T, Ehrnsperger M, White HE, Chen S, Saibil HR and Buchner J. (1999). Hsp26: a temperature-regulated chaperone, *Embo J.*, **18,** 6744-6751.

Head MW, Corbin E and Goldman JE. (1993). Overexpression and abnormal modification of the stress proteins alpha B-crystallin and HSP27 in Alexander disease, *Am. J. Pathol.*, **143,** 1743-1753.

Hickey ED and Weber LA. (1982). Modulation of heat-shock polypeptide synthesis in HeLa cells during hyperthermia and recovery, *Biochemistry*, **21,** 1513-1521.

Hoffman E and Corces V. (1986). Sequences involved in temperature and ecdysterone-induced transcription are located in separate regions of a Drosophila melanogaster heat shock gene, *Mol. Cell. Biol.*, **6,** 663-673.

Howlett GJ, Minton AP and Rivas G. (2006). Analytical ultracentrifugation for the study of protein association and assembly, *Curr. Opin. Chem. Biol.*, **10,** 430-436.

Ingolia TD and Craig EA. (1982). Four small Drosophila heat shock proteins are related to each other and to mammalian alpha-crystallin, *Proc. Natl. Acad. Sci. U S A*, **79,** 2360-2364.

Iwaki A, Nagano T, Nakagawa M, Iwaki T and Fukumaki Y. (1997). Identification and characterization of the gene encoding a new member of the alpha-crystallin/small hsp family, closely linked to the alphaB-crystallin gene in a head-to-head manner, *Genomics*, **45,** 386-394.

Iwaki T, Iwaki A, Tateishi J, Sakaki Y and Goldman JE. (1993). Alpha B-crystallin and 27-kd heat shock protein are regulated by stress conditions in the central nervous system and accumulate in Rosenthal fibers, *Am. J. Pathol.*, **143,** 487-495.

Jakob U and Buchner J. (1994). Assisting spontaneity: the role of Hsp90 and small Hsps as molecular chaperones, *Trends Biochem. Sci.*, **19,** 205-211.

Jakob U, Gaestel M, Engel K and Buchner J. (1993). Small heat shock proteins are molecular chaperones, *J. Biol. Chem.*, **268,** 1517-1520.

Jeffrey L and Yphantis D. National Analytical Ultracentrifugation Facility, University of Connecticut, Storrs,CT.

Jiang C and Chang JY. (2005). Unfolding and breakdown of insulin in the presence of endogenous thiols, *FEBS Lett.*, **579,** 3927-3931.

Jiao W, Qian M, Li P, Zhao L and Chang Z. (2005). The essential role of the flexible termini in the temperature-responsiveness of the oligomeric state and chaperone-like activity for the polydisperse small heat shock protein IbpB from Escherichia coli, *J. Mol. Biol.*, **347,** 871-884.

Johnson ML, Correia JJ, Yphantis DA and Halvorson HR. (1981). Analysis of data from the analytical ultracentrifuge by nonlinear least-squares techniques, *Biophys. J.*, **36,** 575-588.

Kamada M, So A, Muramaki M, Rocchi P, Beraldi E and Gleave M. (2007). Hsp27 knockdown using nucleotide-based therapies inhibit tumor growth and enhance chemotherapy in human bladder cancer cells, *Mol. Cancer Ther.*, **6,** 299-308.

Kappe G, Aquilina JA, Wunderink L, Kamps B, Robinson CV, Garate T, Boelens WC and de Jong WW. (2004). Tsp36, a tapeworm small heat-shock protein with a duplicated alpha-crystallin domain, forms dimers and tetramers with good chaperone-like activity, *Proteins*, **57,** 109-117.

Kappe G, Verschuure P, Philipsen RL, Staalduinen AA, Van de Boogaart P, Boelens WC and De Jong WW. (2001). Characterization of two novel human small heat shock proteins: protein kinase-related HspB8 and testis-specific HspB9, *Biochim Biophys Acta*, **1520,** 1-6.

Kato K, Goto S, Inaguma Y, Hasegawa K, Morishita R and Asano T. (1994a). Purification and characterization of a 20-kDa protein that is highly homologous to alpha B crystallin, *J. Biol. Chem.*, **269,** 15302-15309.

Kato K, Hasegawa K, Goto S and Inaguma Y. (1994b). Dissociation as a result of phosphorylation of an aggregated form of the small stress protein, hsp27, *J. Biol. Chem.*, **269,** 11274-11278.

Kato S, Hirano A, Umahara T, Llena JF, Herz F and Ohama E. (1992). Ultrastructural and immunohistochemical studies on ballooned cortical neurons in Creutzfeldt-Jakob disease: expression of alpha B-crystallin, ubiquitin and stress-response protein 27, *Acta Neuropathol. (Berl)*, **84,** 443-448.

Kelley PM and Schlesinger MJ. (1978). The effect of amino acid analogues and heat shock on gene expression in chicken embryo fibroblasts, *Cell*, **15,** 1277-86.

Kim KK, Kim R and Kim SH. (1998). Crystal structure of a small heat-shock protein, *Nature*, **394,** 595-599.

Kim SJ, Jeong DG, Chi SW, Lee JS and Ryu SE. (2001). Crystal structure of proteolytic fragments of the redox-sensitive Hsp33 with constitutive chaperone activity, *Nat. Struct. Biol.*, **8,** 459-466.

Klemenz R, Frohli E, Steiger RH, Schafer R and Aoyama A. (1991). Alpha B-crystallin is a small heat shock protein, *Proc. Natl. Acad. Sci. USA*, **88,** 3652-3656.

Krief S, Faivre JF, Robert P, Le Douarin B, Brument-Larignon N, Lefrere I, Bouzyk MM, Anderson KM, Greller LD, Tobin FL, Souchet M and Bril A. (1999). Identification and characterization of cvHsp. A novel human small stress protein selectively expressed in cardiovascular and insulin-sensitive tissues, *J. Biol. Chem.*, **274,** 36592-36600.

Lambert H, Charette SJ, Bernier AF, Guimond A and Landry J. (1999). HSP27 multimerization mediated by phosphorylation-sensitive intermolecular interactions at the amino terminus, *J. Biol. Chem.*, **274,** 9378-9385.

Lamm O. (1929). Die Differentialgleichung derl Ultrazentrifugierung, *Ark. Mat. Astr. Fys*, **21B,** 1-4.

Laue TM, Shah BD, Ridgeway TM and Pelletier SL. (1992). Harding S, Rowe A and Horton J (eds). Royal Society of Chemistry, Cambridge, pp 90-125.

Lavoie JN, Lambert H, Hickey E, Weber LA and Landry J. (1995). Modulation of cellular thermoresistance and actin filament stability accompanies phosphorylation-induced changes in the oligomeric structure of heat shock protein 27, *Mol. Cell. Biol.*, **15,** 505-516.

Lebowitz J, Lewis MS and Schuck P. (2002). Modern analytical ultracentrifugation in protein science: a tutorial review, *Protein Sci.*, **11,** 2067-2079.

Lelj-Garolla B and Mauk AG. (2005). Self-association of a small heat shock protein, *J. Mol. Biol.*, **345,** 631-642.

Lelj-Garolla B and Mauk AG. (2006). Self-association and chaperone activity of Hsp27 are thermally activated, *J. Biol. Chem.*, **281,** 8169-8174.

Lentze N, Aquilina JA, Lindbauer M, Robinson CV and Narberhaus F. (2004). Temperature and concentration-controlled dynamics of rhizobial small heat shock proteins, *Eur. J. Biochem.*, **271,** 2494-2503.

Leroux MR, Melki R, Gordon B, Batelier G and Candido EP. (1997). Structure-function studies on small heat shock protein oligomeric assembly and interaction with unfolded polypeptides, *J. Biol. Chem.*, **272,** 24646-24656.

Liddington RC, Yan Y, Moulai J, Sahli R, Benjamin TL and Harrison SC. (1991). Structure of simian virus 40 at 3.8-A resolution, *Nature*, **354,** 278-284.

Lindner RA, Carver JA, Ehrnsperger M, Buchner J, Esposito G, Behlke J, Lutsch G, Kotlyarov A and Gaestel M. (2000). Mouse Hsp25, a small shock protein. The role of its C-terminal extension in oligomerization and chaperone action, *Eur. J. Biochem.*, **267,** 1923-1932.

MacRae TH. (2000). Structure and function of small heat shock/alpha-crystallin proteins: established concepts and emerging ideas, *Cell. Mol. Life Sci.*, **57,** 899-913.

Mazzarella RA and Green M. (1987). ERp99, an abundant, conserved glycoprotein of the endoplasmic reticulum, is homologous to the 90-kDa heat shock protein (hsp90) and the 94-kDa glucose regulated protein (GRP94), *J. Biol. Chem.*, **262,** 8875-83.

Mehlen P, Kretz-Remy C, Preville X and Arrigo AP. (1996). Human hsp27, Drosophila hsp27 and human alphaB-crystallin expression-mediated increase in glutathione is essential for the protective activity of these proteins against TNFalpha-induced cell death, *Embo J.*, **15,** 2695-2706.

Merck KB, Groenen PJ, Voorter CE, de Haard-Hoekman WA, Horwitz J, Bloemendal H and de Jong WW. (1993). Structural and functional similarities of bovine alpha-crystallin and mouse small heat-shock protein. A family of chaperones, *J. Biol. Chem.*, **268,** 1046-1052.

Minton AP. (2000). Quantitative characterization of reversible macromolecular associations via sedimentation equilibrium: an introduction, *Exp. Mol. Med.*, **32,** 1-5.

Mörner C. (1894). Untersuchung der Proteinsubstanzen in den lichtbrechenden Medien des Auges., *Hoppe Seyler's Z Physiol. Chem.*, **18,** 61-106.

Munchbach M, Nocker A and Narberhaus F. (1999). Multiple small heat shock proteins in rhizobia, *J. Bacteriol.*, **181,** 83-90.

Nocker A, Krstulovic NP, Perret X and Narberhaus F. (2001). ROSE elements occur in disparate rhizobia and are functionally interchangeable between species, *Arch. Microbiol.*, **176,** 44-51.

Pandey P, Farber R, Nakazawa A, Kumar S, Bharti A, Nalin C, Weichselbaum R, Kufe D and Kharbanda S. (2000). Hsp27 functions as a negative regulator of cytochrome c-dependent activation of procaspase-3, *Oncogene*, **19,** 1975-1981.

Parcellier A, Schmitt E, Gurbuxani S, Seigneurin-Berny D, Pance A, Chantome A, Plenchette S, Khochbin S, Solary E and Garrido C. (2003). HSP27 is a ubiquitin-binding protein involved in I-kappaBalpha proteasomal degradation, *Mol. Cell. Biol.*, **23,** 5790-5802.

Pasta SY, Raman B, Ramakrishna T and Rao Ch M. (2003). Role of the conserved SRLFDQFFG region of alpha-crystallin, a small heat shock protein. Effect on oligomeric size, subunit exchange, and chaperone-like activity, *J. Biol. Chem.*, **278,** 51159-51166.

Pauli D, Tonka CH, Tissieres A and Arrigo AP. (1990). Tissue-specific expression of the heat shock protein HSP27 during Drosophila melanogaster development, *J. Cell. Biol.*, **111,** 817-828.

Pelham HR and Bienz M. (1982). A synthetic heat-shock promoter element confers heat-inducibility on the herpes simplex virus thymidine kinase gene, *Embo J.*, **1,** 1473-1477.

Peterson NS, Moller G and Mitchell HK. (1979). Genetic mapping of the coding regions for three heat-shock proteins in Drosophila melanogaster, *Genetics*, **92,** 891-902.

Pettersen EF, Goddard TD, Huang CC, Couch GS, Greenblatt DM, Meng EC and Ferrin TE. (2004). UCSF Chimera--a visualization system for exploratory research and analysis, *J Comput Chem*, **25,** 1605-12.

Philo JS. (2006). Is any measurement method optimal for all aggregate sizes and types? *Aaps J.*, **8,** E564-571.

Raman B, Ramakrishna T and Rao CM. (1995a). Temperature dependent chaperone-like activity of alpha-crystallin, *FEBS Lett*, **365,** 133-136.

Raman B and Rao CM. (1994). Chaperone-like activity and quaternary structure of alpha-crystallin, *J Biol Chem*, **269,** 27264-27268.

Raman B and Rao CM. (1997). Chaperone-like activity and temperature-induced structural changes of alpha-crystallin, *J. Biol. Chem.*, **272,** 23559-23564.

Raman CS, Allen MJ and Nall BT. (1995b). Enthalpy of antibody--cytochrome c binding, *Biochemistry*, **34,** 5831-5838.

Renkawek K, Stege GJ and Bosman GJ. (1999). Dementia, gliosis and expression of the small heat shock proteins hsp27 and alpha B-crystallin in Parkinson's disease, *Neuroreport*, **10,** 2273-6.

Ritossa P. (1962). [Problems of prophylactic vaccinations of infants.], *Riv. Ist. Sieroter. Ital.*, **37,** 79-108.

Rocchi P, Beraldi E, Ettinger S, Fazli L, Vessella RL, Nelson C and Gleave M. (2005). Increased Hsp27 after androgen ablation facilitates androgen-independent progression in prostate cancer via signal transducers and activators of transcription 3-mediated suppression of apoptosis, *Cancer Res.*, **65,** 11083-11093.

Rocchi P, So A, Kojima S, Signaevsky M, Beraldi E, Fazli L, Hurtado-Coll A, Yamanaka K and Gleave M. (2004). Heat shock protein 27 increases after androgen ablation and plays a cytoprotective role in hormone-refractory prostate cancer, *Cancer Res.*, **64,** 6595-6602.

Rogalla T, Ehrnsperger M, Preville X, Kotlyarov A, Lutsch G, Ducasse C, Paul C, Wieske M, Arrigo AP, Buchner J and Gaestel M. (1999). Regulation of Hsp27 oligomerization, chaperone function, and protective activity against oxidative stress/tumor necrosis factor alpha by phosphorylation, *J. Biol. Chem.*, **274,** 18947-18956.

Rost B and Sander C. (1993). Prediction of protein secondary structure at better than 70% accuracy, *J. Mol. Biol.*, **232,** 584-599.

Schachman HK. (1959). *Ultracentrifuge in Biochemistry*. Academic Press: New York.

Schachman HK, Gropper L, Hanlon S and Putney F. (1962). Ultracentrifuge studies with absorption optics. II. Incorporation of a monochromator and its application to the study of proteins and interacting systems, *Arch. Biochem. Biophys.*, **99,** 175-190.

Schlunegger MP, Bennett MJ and Eisenberg D. (1997). Oligomer formation by 3D domain swapping: a model for protein assembly and misassembly, *Adv.Protein. Chem.*, **50,** 61-122.

Schmitt E, Gehrmann M, Brunet M, Multhoff G and Garrido C. (2007). Intracellular and extracellular functions of heat shock proteins: repercussions in cancer therapy, *J. Leukoc. Biol.*, **81,** 15-27.

Schuck P. (1998). Sedimentation analysis of noninteracting and self-associating solutes using numerical solutions to the Lamm equation, *Biophys. J.*, **75,** 1503-1512.

Schuck P. (2003). On the analysis of protein self-association by sedimentation velocity analytical ultracentrifugation, *Anal. Biochem.*, **320,** 104-124.

Schuck P, Perugini MA, Gonzales NR, Howlett GJ and Schubert D. (2002). Size-distribution analysis of proteins by analytical ultracentrifugation: strategies and application to model systems, *Biophys. J.*, **82,** 1096-1111.

Schuck P and Rossmanith P. (2000). Determination of the sedimentation coefficient distribution by least-squares boundary modeling, *Biopolymers*, **54,** 328-341.

Schuster TM and Toedt JM. (1996). New revolutions in the evolution of analytical ultracentrifugation, *Curr. Opin. Struct. Biol.*, **6,** 650-658.

Siezen RJ, Bindels JG and Hoenders HJ. (1980). The quaternary structure of bovine alpha-crystallin. Effects of variation in alkaline pH, ionic strength, temperature and calcium ion concentration, *Eur. J. Biochem.*, **111,** 435-444.

Smulders R, Carver JA, Lindner RA, van Boekel MA, Bloemendal H and de Jong WW. (1996). Immobilization of the C-terminal extension of bovine alphaA-crystallin reduces chaperone-like activity, *J. Biol. Chem.*, **271,** 29060-29066.

Stamler R, Kappe G, Boelens W and Slingsby C. (2005). Wrapping the alpha-crystallin domain fold in a chaperone assembly, *J. Mol. Biol.*, **353,** 68-79.

Stege GJ, Renkawek K, Overkamp PS, Verschuure P, van Rijk AF, Reijnen-Aalbers A, Boelens WC, Bosman GJ and de Jong WW. (1999). The molecular chaperone alphaB-crystallin enhances amyloid beta neurotoxicity, *Biochem Biophys Res Commun*, **262,** 152-6.

Stock AD, Spallone PA, Dennis TR, Netski D, Morris CA, Mervis CB and Hobart HH. (2003). Heat shock protein 27 gene: chromosomal and molecular location and relationship to Williams syndrome, *Am. J. Med. Genet. A*, **120,** 320-325.

Stokoe D, Engel K, Campbell DG, Cohen P and Gaestel M. (1992). Identification of MAPKAP kinase 2 as a major enzyme responsible for the phosphorylation of the small mammalian heat shock proteins, *FEBS Lett.*, **313,** 307-313.

Stromer T, Ehrnsperger M, Gaestel M and Buchner J. (2003). Analysis of the interaction of small heat shock proteins with unfolding proteins, *J. Biol. Chem.*, **278,** 18015-18021.

Stromer T, Fischer E, Richter K, Haslbeck M and Buchner J. (2004a). Analysis of the regulation of the molecular chaperone Hsp26 by temperature-induced dissociation: the N-terminal domail is important for oligomer assembly and the binding of unfolding proteins, *J. Biol. Chem.*, **279,** 11222-11228.

Stromer T, Fischer E, Richter K, Haslbeck M and Buchner J. (2004b). Analysis of the regulation of the molecular chaperone Hsp26 by temperature-induced dissociation: the N-terminal domain is important for oligomer assembly and the binding of unfolding proteins, *J. Biol. Chem.*, **279,** 11222-11228.

Studer S and Narberhaus F. (2000). Chaperone activity and homo- and hetero-oligomer formation of bacterial small heat shock proteins, *J. Biol. Chem.*, **275,** 37212-37218.

Sugiyama Y, Suzuki A, Kishikawa M, Akutsu R, Hirose T, Waye MM, Tsui SK, Yoshida S and Ohno S. (2000). Muscle develops a specific form of small heat shock protein complex composed of MKBP/HSPB2 and HSPB3 during myogenic differentiation, *J. Biol. Chem.*, **275,** 1095-1104.

Sun TX and Liang JJ. (1998). Intermolecular exchange and stabilization of recombinant human alphaA- and alphaB-crystallin, *J. Biol. Chem.*, **273,** 286-290.

Sun X, Fontaine JM, Rest JS, Shelden EA, Welsh MJ and Benndorf R. (2004). Interaction of human HSP22 (HSPB8) with other small heat shock proteins, *J. Biol. Chem.*, **279,** 2394-2402.

Svedberg T and Pedersen KO. (1940). *The Ultracentrifuge*. Oxford Univeristy Press: London, UK.

Theriault JR, Lambert H, Chavez-Zobel AT, Charest G, Lavigne P and Landry J. (2004). Essential role of the NH2-terminal WD/EPF motif in the phosphorylation-activated protective function of mammalian Hsp27, *J. Biol. Chem.*, **279,** 23463-23471.

Thomson JA and Augusteyn RC. (1983). alpha m-Crystallin: the native form of the protein? *Exp. Eye Res.*, **37,** 367-377.

Thorne ME and McQuade KL. (2004). Heat-induced oligomerization of gp96 occurs via a site distinct from substrate binding and is regulated by ATP, *Biochem. Biophys. Res. Commun.*, **323,** 1163-1171.

Usui K, Hatipoglu OF, Ishii N and Yohda M. (2004a). Role of the N-terminal region of the crenarchaeal sHsp, StHsp14.0, in thermal-induced disassembly of the complex and molecular chaperone activity, *Biochem. Biophys. Res. Commun.*, **315,** 113-118.

Usui K, Ishii N, Kawarabayasi Y and Yohda M. (2004b). Expression and biochemical characterization of two small heat shock proteins from the thermoacidophilic crenarchaeon Sulfolobus tokodaii strain 7, *Protein Sci.*, **13,** 134-144.

van Montfort RL, Basha E, Friedrich KL, Slingsby C and Vierling E. (2001). Crystal structure and assembly of a eukaryotic small heat shock protein, *Nat. Struct. Biol.*, **8,** 1025-1030.

Vanhoudt J, Aerts T, Abgar S and Clauwaert J. (1998). Quaternary structure of bovine alpha-crystallin: influence of temperature, *Int. J. Biol. Macromol.*, **22,** 229-237.

Vijayalakshmi J, Mukhergee MK, Graumann J, Jakob U and Saper MA. (2001). The 2.2 A crystal structure of Hsp33: a heat shock protein with redox-regulated chaperone activity, *Structure (Camb)*, **9,** 367-375.

Wang K and Spector A. (2001). ATP causes small heat shock proteins to release denatured protein, *Eur. J. Biochem.*, **268,** 6335-6345.

Wang X and Pielak GJ. (1999). Equilibrium thermodynamics of a physiologically-relevant heme-protein complex, *Biochemistry*, **38,** 16876-16881.

Yphantis D, Lary JW, Stafford WF, Liu S, Holsen PH, Hayes DB, Moody TP, Ridgeway TM, Lyons DA and Laue TM. (1994). *Modern Analytical Ultracentfuge*. Laue Tmsatm (ed.). Birkhäuser: Boston, MA, pp 209-226.

Zantema A, Verlaan-De Vries M, Maasdam D, Bol S and van der Eb A. (1992). Heat shock protein 27 and alpha B-crystallin can form a complex, which dissociates by heat shock, *J Biol Chem*, **267,** 12936-41.